SANDIA NATIONAL LABORATORIES
WASTE ISOLATION PILOT PLANT

ANALYSIS REPORT FOR ACTINIDE MOBILIZATION AND SALADO TRANSPORT IN THE 2026 COMPLIANCE RECERTIFICATION APPLICATION PERFORMANCE ASSESSMENT: INTERIM STATE REPOSITORY

REVISION 0

PAUL DOCHERTY
(Affiliate)

Digitally signed by PAUL DOCHERTY
(Affiliate)
Date: 2025.11.06 10:08:20 -07'00'

Authentication

Author:	Paul Docherty	Org.	8881
Author:	Sungtae Kim	Org.	8881
Technical Reviewer:	Sarah Brunell	Org.	8881
QA Reviewer:	Shelly R. Nielsen	Org.	8883
Management Reviewer:	Steve Wagner	Org.	8881

NOVEMBER 2025

Information Only

Executive Summary

The Waste Isolation Pilot Plant (WIPP) was initially certified as a repository consisting of 10 panels, which were excavated for the long-term storage and placement of transuranic waste (U.S. EPA 1998). However, due to operational constraints, the entire volume of the 10 panels is no longer available for waste disposal. In March 2024, the U.S. Department of Energy (DOE) submitted the Replacement Panels Planned Change Request (RPPCR) to the U.S. Environmental Protection Agency (EPA) for approval of waste emplacement in two new panels. These panels, referred to as replacement panels, are located to the west of the existing operations area. The RPPCR received EPA approval in July 2025.

The addition of the two replacement panels is not expected to provide adequate space for the disposal of the allowable waste volume designated for WIPP under the Land Withdrawal Act; thus, the 12-panel configuration is regarded as an interim state of the repository. The DOE may pursue approval for waste disposal in seven additional panels to accommodate the full allowable volume of waste. This hypothetical 19-panel configuration is considered the anticipated final state of the repository.

The DOE demonstrates compliance with containment requirements as outlined in the Certification Criteria of Title 40 CFR Part 191.13 through performance assessment (PA). PA calculations estimate the probability and consequences of potential radionuclide releases from the repository to the accessible environment over a regulatory period of 10,000 years following facility closure. WIPP PA models are utilized to support the periodic recertification of WIPP.

The 2026 Compliance Recertification Application (CRA-2026) represents the fifth recertification application submitted to the EPA. A PA has been carried out by Sandia National Laboratories to support the DOE's submission of the CRA-2026. The results presented in the CRA-2026 PA are compared to those from the RPPCR PA, the most recent regulatory submission.

This analysis report documents the actinide mobilization and Salado transport component of the CRA-2026 PA for the interim state repository, named the CRA26_IS PA. Radionuclide concentrations used in the determination of direct brine releases increase in the CRA26_IS in comparison to the RPPCR due to increases in inventory, baseline solubilities, and colloid-related concentration parameters. Radionuclide releases to the Culebra are mostly reduced in the CRA26_IS compared to the RPCCR, a consequence of reduced brine flow up the borehole. In both the CRA26_IS and the RPPCR, radionuclide releases to the Culebra are two orders of magnitude, or more, less than in the CRA-2019.

Information Only

TABLE OF CONTENTS

EXECUTIVE SUMMARY II

1.0 INTRODUCTION 8

2.0 CHANGES SINCE THE RPPCR 9

2.1 Repository Design 9
2.2 Parameters Related to Repository Dimensions 11
2.3 Updates to the Salado Flow and Transport Computational Grid 11
2.4 Waste Inventory 12
2.5 Baseline Actinide Solubilities 12
2.6 Solubility Uncertainty Distributions 13
2.7 Colloidal Enhancement Parameters 13
2.8 Minimum Brine Volume Needed for a DBR 13
2.9 Parameters Not Updated as Anticipated in Analysis Plan AP-214 14

3.0 BRIEF OVERVIEW OF PANEL 15

3.1 Concentrations 15
3.1.1 Element mobile concentration limits 16
3.1.2 Actinide solubility: baseline and uncertainty factor 17
3.1.3 Colloid concentrations 19
3.1.4 Mobile concentration limits of the secondary elements 20
3.1.5 Radionuclide mobile concentration limits 20
3.1.6 Radionuclide concentrations for DBRs 20
3.1.7 Conversion to EPA Units 21
3.1.8 Total concentration for DBRs 21
3.1.9 Lumped radionuclides 22
3.1.10 Lumped radionuclide mobile concentration limits 22
3.2 Decay and ingrowth 23
3.3 E2E1 transport 25
3.3.1 Radionuclide concentrations for E2E1 25
3.3.2 Time shifting 26
3.3.3 Brine volume extrapolation 26
3.3.4 E2E1 *to Culebra* releases 26
3.3.5 Fractional contributions to the element concentration limit 26

Information Only

3.4 PANEL summary 27

4.0 BRIEF OVERVIEW OF NUTS 29

4.1 NUTS operation modes 29

4.2 Concentrations of lumped radionuclides 31

4.3 Decay of lumped radionuclides 31

4.4 NUTS *to Culebra* releases 31

4.5 NUTS summary 32

5.0 RESULTS 33

5.1 Inventory 33

5.2 PANEL: Radionuclide mobilization 38

5.2.1 Baseline solubility 38

5.2.2 Uncertainty factor 40

5.2.3 Actinide solubility 44

5.2.4 Colloid enhancement parameters 47

5.2.5 Element mobile concentration limits 49

5.2.6 Mobile concentration limits of the lumped radionuclides 54

5.2.7 Radionuclide concentrations for DBRs as a function of time 56

5.3 NUTS and PANEL: radionuclide transport 65

5.3.1 Brine flow to the Culebra 65

5.3.2 NUTS vector screening 66

5.3.3 Radionuclide releases through the marker beds and up the shaft 68

5.3.4 Radionuclide *to Culebra* releases 69

5.3.5 Radionuclide *to Culebra* release histories 72

6.0 SUMMARY 79

7.0 REFERENCES 80

LIST OF FIGURES

Figure 1. Interim State Repository Layout 10

Figure 2. CRA26_IS Salado Flow and Transport Computational Grid 12

Figure 3. Abridged decay chains in PANEL 24

Figure 4. Top-level view of PANEL and NUTS 28

Information Only

Figure 5. Decay chains modeled in NUTS 31
Figure 6. Largest contributors (in curies) to inventory at closure....34
Figure 7. Relative inventory at closure 34
Figure 8. Largest contributors (in curies) to inventory at closure in the waste area....35
Figure 9. Mole fractions of isotopes of Pu, U, Th and Am at closure 36
Figure 10. Mole fractions for PU238L, U234L and TH230L....37
Figure 11. Lumped inventory at closure in the waste area (in curies)....37
Figure 12. Relative inventory of lumped radionuclides at closure 38
Figure 13. Baseline solubilities for GWB brine....40
Figure 14. Baseline solubilities for ERDA-6 brine....40
Figure 15. Cumulative probability distributions for SOLMOD3:SOLVAR 42
Figure 16. Histograms of SOLMOD3:SOLVAR sample values....42
Figure 17. Cumulative probability distributions for SOLMOD4:SOLVAR 43
Figure 18. Histograms of SOLMOD4:SOLVAR sample values....43
Figure 19. Log_{10} of solubility (Replicate 1, ERDA-6, b = 1) 45
Figure 20. Log_{10} of solubility (Replicate 1, GWB, b = 1) 46
Figure 21. Histograms of Log_{10} of the element mobile concentration limit (Replicate 1, ERDA-6 brine, b = 1)....51
Figure 22. Fractional contributions to the element mobile concentration limit (Replicate 1, ERDA-6 brine, b = 1, low oxidation state for Pu, U and Np)....52
Figure 23. Fractional contributions to the element mobile concentration limit (Replicate 1, ERDA-6 brine, b = 1, high oxidation state for Pu, U and Np)....53
Figure 24. Histograms of Log_{10} of the lumped radionuclide mobile concentration limit (Replicate 1, ERDA-6, b = 1)....55
Figure 25. RPPCR mean concentrations versus time (Replicate 1, ERDA-6, b = 1)....58
Figure 26. CRA26_IS mean concentrations versus time (Rep. 1, ERDA-6, b = 1) 58
Figure 27. Comparison of mean concentrations (Replicate 1, ERDA-6, b = 1)....59
Figure 28. Comparison of mean concentrations (Replicate 1, ERDA-6, b = 5)....59
Figure 29. Radionuclide mobile concentration limit bounds and inventory limit (Replicate 1, ERDA-6, b = 1)....60
Figure 30. Concentration versus time, all vectors (Replicate 1, ERDA-6, b = 1) 61
Figure 31. DBR concentration versus time, all vectors (Replicate 1, ERDA-6, b = 1)....62

Information Only

Figure 32. AM241 concentration vs time (Replicate 1, ERDA-6, b = 1) 63
Figure 33. PU239 concentration vs time (Replicate 1, ERDA-6, b = 1) 63
Figure 34. PU240 concentration vs time (Replicate 1, ERDA-6, b = 1) 64
Figure 35. DBR concentration vs time (Replicate 1, ERDA-6, b = 1) 64
Figure 36. Cumulative brine discharge up the borehole (Replicate 1) 65
Figure 37. Cumulative tracer releases to the Culebra in kg at 10,000 years (Replicate 1) 67
Figure 38. Total cumulative releases through marker beds and shaft at 10,000 years 68
Figure 39. Cumulative lumped radionuclide discharge (Replicate 1) 70
Figure 40. Lumped radionuclide concentrations at the Culebra (Replicate 1) 71
Figure 41. Lumped radionuclide concentrations in the waste (Replicate 1) 71
Figure 42. Cumulative radionuclide discharges for Replicate 1 of Scenario 2 vs time 73
Figure 43. Cumulative radionuclide discharges for Replicate 1 of Scenario 3 vs time 74
Figure 44. Cumulative radionuclide discharges for Replicate 1 of Scenario 4 vs time 75
Figure 45. Cumulative radionuclide discharges for Replicate 1 of Scenario 5 vs time 76
Figure 46. Cumulative radionuclide discharges for Replicate 1 of Scenario 6 vs time 77
Figure 47. Total cumulative radionuclide discharges for Replicate 1 vs time 78

LIST OF TABLES

Table 1. Changed Repository Parameters 11
Table 2. Updated Minimum Brine Volume Parameter 13
Table 3. Primary actinide oxidation states in WIPP brines 18
Table 4. Lumped radionuclide constituents 22
Table 5. BRAGFLO, NUTS, and PANEL intrusions (times in years following repository closure) 30
Table 6. Predicted Baseline Solubilities (mol/L) 39
Table 7. Mean solubility in mol/L (Replicate 1, b = 1) 47
Table 8. PROPMIC (dimensionless) and CAPMIC (mol/L) for the RPPCR 47
Table 9. PROPMIC (dimensionless) and CAPMIC (mol/L) for the CRA26_IS 48
Table 10. PHUMSIM and PHUMCIM (dimensionless) for the RPPCR and the CRA26_IS* 48
Table 11. CONCMIN, CONCINT, and CAPHUM (mol/L) for the RPPCR and the CRA26_IS 48
Table 12. Mean element mobile concentration limits in mol/L (Replicate 1, b = 1) 53

Information Only

Table 13. Mean values of lumped radionuclide mobile concentration limit in mol/L (Replicate 1, b = 1) 56

Table 14. Mean, maximum and median cumulative brine discharge up the borehole at 10,000 years (Replicate 1) 66

Table 15. Mean, maximum and median cumulative tracer releases through a borehole to the Culebra at 10,000 years (Replicate 1) 67

Table 16. Number of screened-in vectors 68

Table 17. Mean cumulative lumped radionuclides discharges through a borehole to the Culebra at 10,000 years (EPA units, Replicate 1) 71

Table 18. Maximum cumulative lumped radionuclide discharges through a borehole to the Culebra at 10,000 years (EPA units, Replicate 1) 72

Information Only

1.0 INTRODUCTION

The Waste Isolation Pilot Plant (WIPP), located in southeastern New Mexico, has been developed by the U.S. Department of Energy (DOE) for the geologic disposal of transuranic (TRU) waste. The containment of TRU waste at WIPP is regulated by the U.S. Environmental Protection Agency (EPA) under Title 40 of the Code of Federal Regulations (CFR), Part 191.

The DOE demonstrates compliance with the containment requirements of 40 CFR 191.13 by means of performance assessment (PA) as described in the Certification Criteria of Title 40 CFR Part 194. Sandia National Laboratories (SNL) conducts PAs at the request of the DOE. The PA calculations estimate the probability and consequences of potential radionuclide releases from the repository to the accessible environment over a regulatory period of 10,000 years following facility closure. The PA models are continuously maintained and updated with new information, which typically leads to refinements and modifications in both the models and their parameters. Additionally, planned changes to the repository and its components necessitate updates to the WIPP PA models.

All previous WIPP certifications have been based on a repository consisting of 10 panels. In March 2024, the DOE submitted the Replacement Panels Planned Change Request (RPPCR) to seek EPA approval for waste emplacement in two new panels, referred to as replacement panels, located to the west of the existing operations area (Bollinger 2024). The EPA approved the RPPCR in July 2025.

The addition of the two replacement panels is not expected to provide sufficient space for the disposal of the allowable waste volume designated for WIPP under the Land Withdrawal Act (LWA). The 12-panel configuration is thus regarded as an interim state of the repository. The DOE may seek approval for waste disposal in up to seven additional panels to accommodate the full allowable volume of waste. This 19-panel configuration is considered the anticipated final state of the repository.

The CRA-2026 is the fifth recertification application for the WIPP submitted by the DOE for EPA approval. As described in AP-214 (Hansen et al. 2025), the CRA-2026 includes two PA calculations, one for the interim state repository and one for the expected final state repository. The interim state repository calculation is named CRA26_IS, while the final state repository calculation is named CRA26_FS. This analysis report will focus on the actinide mobilization and Salado transport results for the CRA26_IS PA.

Information Only

2.0 CHANGES SINCE THE RPPCR

Several changes are incorporated in the CRA-2026 PA relative to the RPPCR that may impact the actinide mobilization and Salado transport results. These changes include:

- The repository design.
- Parameters related to repository dimensions.
- The waste inventory.
- Baseline actinide solubilities.
- Solubility uncertainty distributions.
- Colloid enhancement parameters for humic and microbial colloids.
- The Salado flow and transport computational grid.
- The minimum brine volume needed for a DBR.

Changes listed above are discussed in more detail in the sections that follow.

2.1 Repository Design

This analysis represents the 12-panel interim state repository consisting of ten original and two replacement panels. Figure 1 depicts the interim state repository. The RPPCR considered the anticipated final repository state, which included a total of 19 waste panels and the entire allowable inventory volume.

Information Only

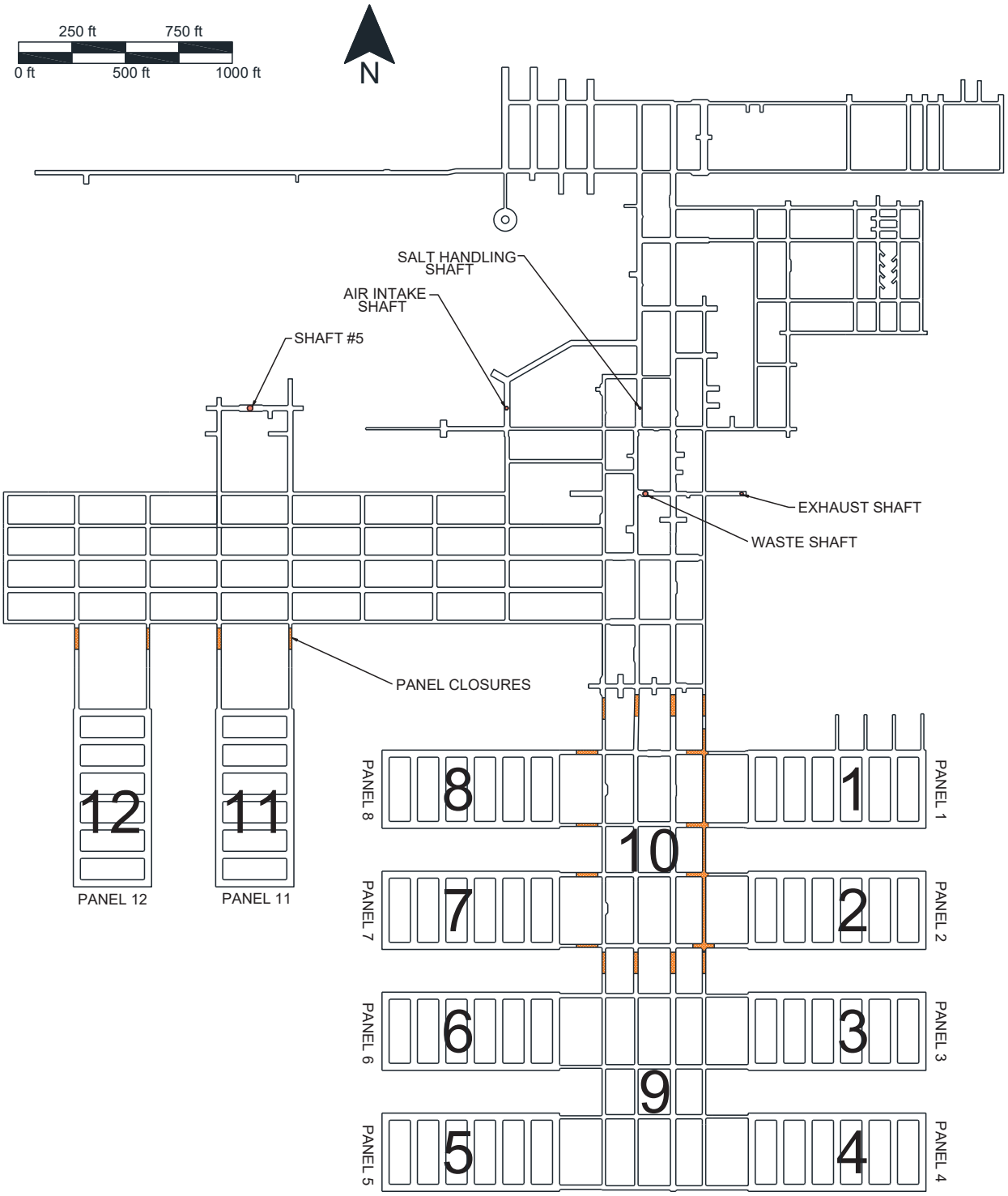


Figure 1. Interim State Repository Layout

Information Only

2.2 Parameters Related to Repository Dimensions

The repository design (Section 2.1) requires changes to several parameters describing repository dimensions. Brunell (2025) revises four parameters to align with the dimensions used in the development of the Salado flow and transport grid (Section 2.3). The parameters include:

- the waste storage volume (REFCON:VREPOS).
- the area of the berm placed over the waste panels (REFCON:ABERM).
- the area allocated for contact-handled (CH) waste disposal (REFCON:AREA_CH).
- the fraction of the repository volume occupied by CH waste (REFCON:FVW).

Although not listed in AP-214 as an anticipated change (Hansen et al. 2025), the area for emplaced remote-handled (RH) waste (REFCON:AREA_RH) is revised by King (2025) due to the reduced inventory volume used in the CRA26_IS PA calculation (see Section 2.24). The updated values are provided in Table 1.

Table 1. Changed Repository Parameters

Material	Property	RPPCR Value	CRA26_IS Value	Units
REFCON	VREPOS	853,284.89	560,722.29	m^3
REFCON	ABERM	1,268,303	750,000	m^2
REFCON	AREA_CH	216,952	141,511	m^2
REFCON	FVW	0.197	0.279	—
REFCON	AREA_RH	15,760	3,528	m^2

2.3 Updates to the Salado Flow and Transport Computational Grid

Dimensions in the computational grid for the Salado flow (BRAGFLO) and transport (NUTS) calculation are changed to be consistent with the interim state repository dimensions (Section 2.1). Day (2025) modifies the computational grid based on as-built excavation footprint dimensions within the existing repository, plans for future excavations, and the planned change for alternative panel closure locations for Panels 1 and 2 (Knerr 2020). The Salado flow and transport computational grid is shown in Figure 2.

Information Only

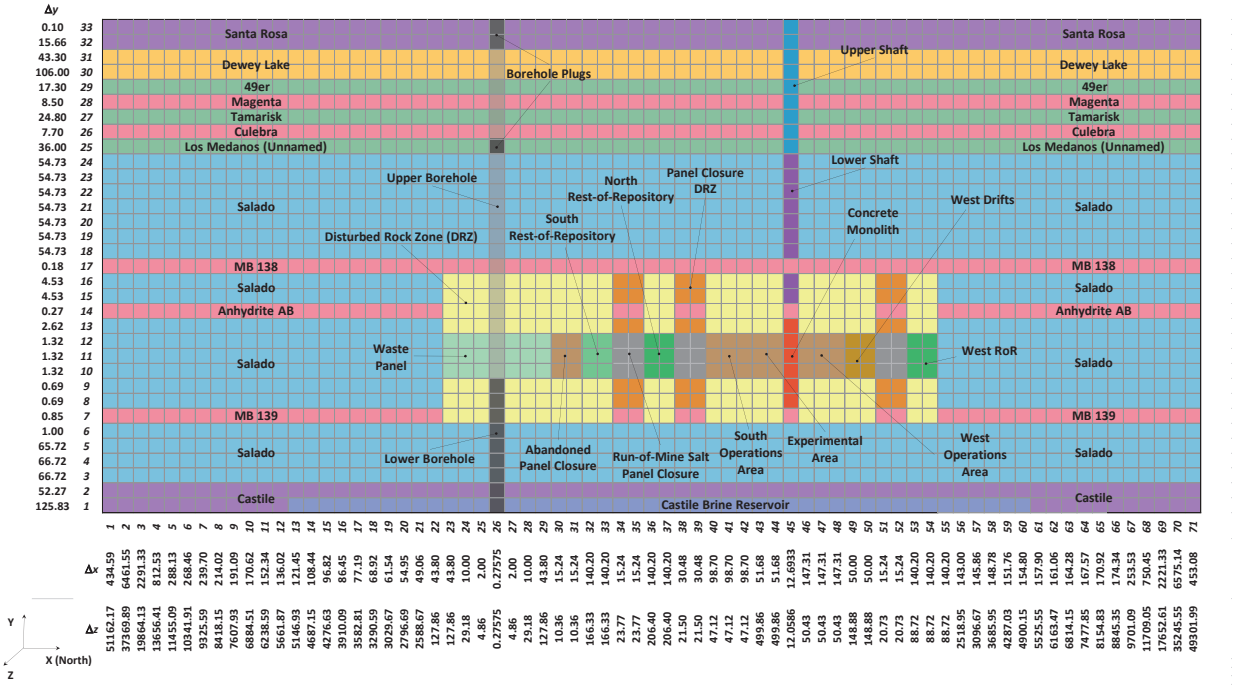


Figure 2. CRA26_IS Salado Flow and Transport Computational Grid

2.4 Waste Inventory

The LWA establishes a statutory limit on the volume of waste that can be disposed of in the WIPP repository, set at 175,564 m^3 (6,200,000 ft^3). Current assessments indicate that the interim state repository will accommodate less waste than the LWA volume. Ward (2025) provided an assessment of the projected waste storage capacity at 157,831.92 m^3, which includes 156,247.12 m^3 of Contact-Handled (CH) waste and 1,584.80 m^3 of Remote-Handled (RH) waste. Based on information collected up to December 31, 2023, the Interim State Performance Assessment Inventory Report-2024 (Van Soest 2025), or ISPAIR-2024, offers an inventory estimate scaled to the waste volume specified by Ward. Kicker (2025) conducted a screening analysis of the inventory estimates for the ISPAIR-2024 to define the inventory-related input parameters for the PA calculations.

2.5 Baseline Actinide Solubilities

Thermodynamic calculations are used to compute the baseline solubilities for actinides in the +III, +IV, and +V oxidation states in GWB and ERDA-6 brines for five multiples of the minimum brine volume for a DBR event. These baseline solubility calculations account for inventory components and thus are updated to be consistent with inventory estimates. Domski (2025a) reports the baseline solubility values based on the CRA26_IS inventory.

Currently there is no thermodynamic model for WIPP actinides in the +VI oxidation state. The Los Alamos National Laboratory Actinide Chemistry and Repository Science Program (LANL-

Information Only

ACRSP) has performed experimental investigations on U(VI) solubility under WIPP-relevant conditions. Based on this experimental work, Kaplan et al. (2025) recommends a solubility of 3×10^{-6} moles/liter (mol/L) for actinides in the +VI oxidation state in both Salado and Castile brines.

2.6 Solubility Uncertainty Distributions

Actinide solubility uncertainty distributions, which are independent of the repository inventory, are updated for CRA-2026_IS, as documented in Domski (2025b). A literature review was conducted to identify relevant studies published prior to the CRA-2026_IS cutoff date. Based on this review, the uncertainty distribution for +III actinide solubilities is updated. No new literature was found for +IV actinide solubilities; therefore, no update to the +IV solubility uncertainty distribution is made.

2.7 Colloidal Enhancement Parameters

Based on updates to the thermodynamic model and baseline solubility values, Mariner (2025) reevaluated the proportionality constant for humic colloids. Mariner recommends updated values for radionuclides in the +III oxidation state for both Castile and Salado brines (PHUMOX3:PHUMCIM and PHUMOX3:PHUMSIM) and an updated value for radionuclides in the +IV oxidation state for Salado brine (PHUMOX4:PHUMSIM).

In previous WIPP PA calculations, microbial colloid enhancement parameters (PROPMIC and CAPMIC) have been specified for each element (parameter materials AM, NP, PU, TH, and U). For the CRA-2026 PA, the microbial enhancement parameters have been specified for each element-oxidation state (materials AM+3, NP+4, NP+5, PU+3, PU+4, U+4, U+6, and TH+4), to more closely align to the experimental data used to derive the parameter values. Kaplan et al. (2025) recommends the microbial colloid parameter values for the CRA-2026_IS PA.

2.8 Minimum Brine Volume Needed for a DBR

The parameter representing minimum brine volume required for a direct brine release (DBR), GLOBAL:DBRMINBV, is revised (Brunell 2025) to be consistent with geomechanical modeling that predicts repository porosity and with the repository geometry described in Section 2.1. The value used in the CRA-2026 IS PA is presented in Table 2.

Table 2. Updated Minimum Brine Volume Parameter

Material	Property	RPPCR Value	CRA26_IS Value	Units
GLOBAL	DBRMINBV	33,804	6,314	m^3

Information Only

2.9 Parameters Not Updated as Anticipated in Analysis Plan AP-214

AP-214 (Hansen et al. 2025) indicates that several parameters were expected to be updated for CRA-2026_IS. Specifically, the parameter specifying the likelihood of low or high oxidation state for an actinide (property OXCUTOFF for materials NP, PU, and U) and the parameters related to mineral and intrinsic colloids (properties CONCMIN and CONCINT for materials AM, NP, PU, TH, and U) were anticipated to undergo revisions. Kaplan et al. (2025) re-examines the basis for these parameter values and recommends the continued use of the RPPCR values. As a result, no changes were made to these parameters for CRA-2026_IS.

Information Only

3.0 BRIEF OVERVIEW OF PANEL

PANEL has three roles in PA. First, it determines radionuclide concentrations as a function of time for use in calculating DBRs. Second, it calculates radionuclide transport releases to the Culebra for the E2E1 scenario, which involves a borehole intrusion into the repository followed by a borehole intrusion into a hypothetical pressurized brine reservoir beneath the repository. Third, PANEL determines the mobile concentration limits of five lumped radionuclides, and the fractions of these limits associated with dissolution and attachment to colloids.

Kicker (2025) reports a total of 168 radionuclides in the repository for the CRA-2026_IS. PANEL models decay and ingrowth for 30 of the radionuclides; and, for 26 of the 30, PANEL determines both concentrations and E2E1 transport releases. Kim et al. (2024) estimate, for the RPPCR, that the radionuclides included in PA account for more than 99% of the DBRs and more than 90% of the transport releases predicted to occur using the total inventory of the repository.

PANEL has three separate modes of execution: Decay mode, which tracks radionuclide decay and ingrowth; Concentration mode for determining mobile concentration limits and instantaneous concentrations; and Intrusion mode, which computes E2E1 transport releases to the Culebra.[1] In the following sections, concentrations are considered first in some detail, then decay and E2E1 releases are briefly described.

3.1 Concentrations

The 26 radionuclides selected for concentration calculations in PANEL are ^{241}Am, ^{243}Am, ^{252}Cf, ^{243}Cm, ^{244}Cm, ^{245}Cm, ^{248}Cm, ^{137}Cs, ^{237}Np, ^{231}Pa, ^{147}Pm, ^{238}Pu, ^{239}Pu, ^{240}Pu, ^{241}Pu, ^{242}Pu, ^{244}Pu, ^{90}Sr, ^{229}Th, ^{230}Th, ^{232}Th, ^{233}U, ^{234}U, ^{235}U, ^{236}U and ^{238}U. Key quantities related to concentrations in this report are defined in Box 1, where indices k and j denote elements and isotopes, respectively. Except where noted, units of concentration and concentration limits are mol/L and brine volume is measured in liters. For brevity, only variation with time is indicated.

[1] Intrusion mode is also referred to as Standard mode in the PANEL code documentation (Kim, 2022a).

Information Only

Box 1: Key quantities for concentrations

b	integer brine volume multiplier
$c_{DBR}(t)$	concentration for determining DBR at time t (EPA units/L)
$c_{k,j}(t)$	concentration of isotope j of element k at time t
$I_{k,j}(t)$	number of moles of isotope j of element k at time t in the waste area
S_k	mobile concentration limit for element k
$S_{k,j}(t)$	mobile concentration limit for isotope j of element k at time t
$S_{k,j}^L$	mobile concentration limit of lumped radionuclide
$S_{k,dissolved}$	element k solubility; sometimes called "dissolved solubility" in PA
$S_{k,humic}$	concentration of element k associated with humic colloids
$S_{k,intrinsic}$	concentration of element k associated with intrinsic colloids
$S_{k,microbial}$	concentration of element k associated with microbial colloids
$S_{k,mineral}$	concentration of element k associated with mineral fragment colloids
V_{min}	minimum brine volume in the waste area for a DBR to occur
$X_{k,j}(t)$	mole fraction of isotope j of element k at time t
$X_{k,j}^L$	mole fraction of lumped radionuclide

PANEL determines radionuclide concentrations differently for use with DBRs and E2E1 transport. For DBRs (Section 3.1.6), fixed volumes of brine are used; whereas for E2E1 transport (Section 3.3.1), an instantaneous volume of brine in the waste area[2] is considered. In both cases, radionuclide concentrations are constrained by radionuclide mobile concentration limits, which are determined from element mobile concentration limits.

3.1.1 Element mobile concentration limits

The 26 radionuclides for which PANEL determines concentrations are isotopes of 11 elements, namely Am, Cf, Cm, Cs, Np, Pa, Pm, Pu, Sr, Th, and U. In PANEL, elements Pu, U, Np, Am, and Th are referred to as the primary actinides. In the following, Cf, Cm, Cs, Pa, Pm, and Sr will be referred to as the secondary elements. PANEL determines the mobile concentration limits of the primary actinides first, then uses these, or just a constant, to set values for the secondary elements.

For primary actinide k, the mobile concentration limit, S_k, is made up of solubility, $S_{k,dissolved}$, added to the concentrations of actinide ionic species attached to four different types of dispersed

[2] The waste area is five waste panels, as described in Section 5.1.

Information Only

colloid forms. The four colloid forms considered are mineral fragments, intrinsic colloids, humic colloids, and microbial colloids. The equation for S_k is

$$S_k = S_{k,dissolved} + S_{k,mineral} + S_{k,intrinsic} + S_{k,humic} + S_{k,microbial} \quad . \tag{1}$$

Since the WIPP chemical conditions remain consistent throughout the regulatory period of 10,000 years, chemical equilibrium is maintained for all chemical reactions, making the terms on the right side of Eq. 1 time-independent. Consequently, S_k does not depend on time and can be determined just once in a PANEL simulation.

3.1.2 Actinide solubility: baseline and uncertainty factor

Solubility, $S_{k,dissolved}$, is obtained in PA by multiplying a baseline solubility, $S_{k,baseline}$, by the number 10^{u_k}, where u_k is called the solubility uncertainty factor:

$$S_{k,dissolved} = S_{k,baseline} \times 10^{u_k} \quad , \quad with$$

$$S_{k,baseline} = SOLMOD\{v_k\}{:}SOL\{f\}OH\{b\} \quad , \quad and \tag{2}$$

$$u_k = SOLMOD\{v_k\}{:}SOLVAR \quad .$$

In Eq. 2, v_k is the oxidation state of actinide k in the current simulation. Oxidation states of the primary actinides present in WIPP brine are listed in Table 3. As indicated, Pu, U and Np exist in two oxidation states within the brine. The variable f in Eq. 2 denotes the type of brine in the repository by designating the formation in which the brine originates. The value of f is either C for Castile, or S for Salado. The variable b in Eq. 2, termed the brine volume multiplier, is an integer that can take on values from one to five. Baseline solubility is estimated for five multiples of the minimum volume of brine in the repository for a DBR to occur, that is, five multiples of parameter GLOBAL:DBRMINBV, or just DBRMINBV.

Values of v_k, f, and b are inserted[3] inside the curly braces on the right-hand sides of Eq. 2 to yield the name either of a constant set in PA code, a constant retrieved from the PA database ParamDB, or a PA sampled value. As an example, consider an actinide with a +III oxidation state, Castile brine, and brine volume multiplier equal to four. Baseline solubility is assigned to the constant parameter SOLMOD3:SOLCOH4; while u_k is assigned to the sampled parameter SOLMOD3:SOLVAR.[4] PA sampled parameter values are generated by code LHS before PANEL is run. PA sampled parameter values are the elements of PA parameter vectors.

[3] Except for the case b=1, where no value of b is inserted.

[4] Integers replace roman numerals in parameter names.

Information Only

Table 3. Primary actinide oxidation states in WIPP brines

Primary Actinide	PU	U	NP	AM	TH
Oxidation State	III or IV	IV or VI	IV or V	III	IV
OXCUTOFF	0.25	0.5	0.5	—	—

PA uses the parameters PU:OXCUTOFF, U:OXCUTOFF, and NP:OXCUTOFF, to represent the likelihood of selecting the lower oxidation state for Pu, U and Np in each realization (Table 3). For both the RPPCR and the CRA26_IS, Pu has oxidation state +III with probability 0.25 and state +IV with probability 0.75; U is assigned state +IV or state +VI with equal probability; and Np takes on state +IV or state +V, also with equal probability. PA realizes these probabilities as follows. First, LHS uses Latin hypercube sampling to draw a sample, once for each parameter vector, from the distribution GLOBAL:OXSTAT, which is a uniform distribution on [0, 1]. Next, PANEL checks the vector element assigned to GLOBAL:OXSTAT against the OXCUTOFF values, setting the oxidation states of Pu, U and Np accordingly. For example, consider a parameter vector with a value 0.3 for GLOBAL:OXSTAT. Since GLOBAL:OXSTAT is greater than 0.25, PANEL assigns oxidation state +IV to Pu. Similarly, with GLOBAL:OXSTAT less than 0.5 for this vector, PANEL assigns oxidation state +IV to U and oxidation state +IV to Np.

Formation identifier f in Eq. 2 is not a parameter in PA but depends on the intrusion scenario in the simulation. If a simulation involves a penetration into a hypothetical pressurized brine reservoir in the Castile, then f is set to C and the chemical properties of a synthetic brine known as ERDA-6 are used in the determination of the baseline solubility. ERDA-6 synthetic brine is representative of brine at the ERDA-6 well, which encountered pressurized brine in the Castile (Popielak et al. 1983). If a simulation does not penetrate pressurized brine in the Castile, then f is set to S and the properties of a synthetic brine known as Generic Weep Brine (GWB) are used. GWB is representative of brines in the Salado formation at the depth of the repository.

The full inventory of organic ligands in the repository is considered to dissolve completely in the available brine volume, establishing constant organic ligand concentrations. Non-radioactive materials affect the interactions of the primary actinide ionic species with organic ligands. Organic ligand concentrations, non-radioactive materials, DBRMINBV, and the brine volume multiplier b (Eq. 2), are input to thermodynamic model calculations to determine $S_{k,baseline}$ for Np(V), Am(III) and Th(IV) (Domski 2025a). Thermodynamic modeling in both the RPPCR and the CRA26_IS uses code EQ3/6 and the WIPP thermodynamic database DATA0.FM6, or FM6 (Domski 2023a). The thermodynamic calculations are carried out for the five values of b and for both ERDA-6 and GWB brines, giving a total of ten thermodynamic calculation runs. Baseline solubilities determined for Th(IV) are used for Pu(IV), U(IV), and Np(IV). Baseline solubilities determined for Am(III) are used for Pu(III). Due to an absence of literature and experimental data measured under WIPP-relevant conditions, a model has not been developed for U(VI). The RPPCR uses 1×10^{-3} mol/L for the baseline solubility of U(VI), a value specified by the EPA (U.S. EPA 2006) and in use since the CRA-2004 PABC. The CRA26_IS updates the baseline solubility for U(VI)

Information Only

to 3×10^{-6} mol/L, as recommended by Kaplan et al. (2025). U(VI) baseline solubility does not depend on brine type.

Uncertainty in the thermodynamic model predictions is expressed using the solubility uncertainty factor, u_k, in Eq. 2. Uncertainty has been estimated for actinides with oxidation states +III and +IV. Domski (2025b) gives a description of the procedure. Briefly, peer-reviewed laboratory experiments are emulated using EQ3/6 and FM6; differences between $\log_{10}$ of measured solubility and $\log_{10}$ of predicted solubility are computed; and cumulative probability distributions of the differences are formed. SOLMOD3:SOLVAR is the sampled parameter defined by the cumulative probability distribution for actinides with oxidation state +III. SOLMOD4:SOLVAR is the sampled parameter defined by the cumulative distribution for actinides with oxidation state +IV. Code LHS samples the two distributions for each parameter vector (the sampled values reside in two separate vector elements). Where PANEL determines an actinide oxidation state of +III or +IV, the corresponding distribution's sampled value is used for u_k in Eq. 2. Uncertainty factors are not calculated for actinides with oxidation states +V and +VI in Table 3. The reasons are: (i) a thermodynamic model has not been developed for U(VI); and (ii) it has been predicted that the contribution of +V actinides to total releases at the WIPP is insignificant (Brush and Garner, 2005). SOLVAR parameters for oxidation states +V and +VI are set to zero. The result is an uncertainty multiplier of 1.0 for these two oxidation states.

3.1.3 Colloid concentrations

The colloid contributions to S_k in Eq. 1 are specified using so-called colloid enhancement parameters, which have been derived from literature reviews and from WIPP-specific experiments dating as far back as the CCA (Reed et al. 2013). The colloid contributions to S_k are

$$S_{k,mineral} = \{a_k\}\text{:}\,CONCMIN \quad ,$$

$$S_{k,intrinsic} = \{a_k\}\text{:}\,CONCINT \quad ,$$

$$S_{k,humic} = min\left(S_{k,dissolved} \times PHUMOX\{v_k\}\text{:}\,PHUM\{f\}IM, \{a_k\}\text{:}\,CAPHUM\right) \quad , \tag{3}$$

$$S_{k,microbial} = min\left(S_{k,dissolved} \times \{a_k\}\text{:}\,PROPMIC, \{a_k\}\text{:}\,CAPMIC\right) \quad , for\ the\ RPPCR, and$$

$$S_{k,microbial} = min\left(S_{k,dissolved} \times \{a_k\}+\{v_k\}\text{:}\,PROPMIC, \{a_k\}+\{v_k\}\text{:}\,CAPMIC\right), for\ the\ CRA26_IS.$$

Colloid enhancement parameters appear on the right-hand sides of Eq. 3, where curly braces indicate a substitution is to be made. The quantity a_k in Eq. 3 is the element symbol (letters capitalized) of a primary actinide, that is, a_k is either PU, U, NP, AM, or TH. Oxidation state v_k and brine identifier f fill out the colloid enhancement parameter names. From Eq. 3, mineral-fragment and intrinsic colloid-associated concentration limits are constant for an actinide, while humic and microbial limits are proportional to solubility, up to a cap value. A significant change for the CRA26_IS is that the proportionality constant and the cap for microbial colloids depend on the actinide *and* its oxidation state (Kaplan et al. 2025). Colloid enhancement parameters are discussed in detail in Appendix SOTERM of U.S. DOE (2019) and in Reed et al. (2013).

Information Only

3.1.4 Mobile concentration limits of the secondary elements

PANEL sets the mobile concentration limits of the secondary elements as follows:

(i) the mobile concentration limits of Cm, Cf, and Pm are set equal to the mobile concentration limit of Am,

(ii) the mobile concentration limit of Pa is set equal to the mobile concentration limit of Np, and

(iii) the mobile concentration limits of Cs and Sr are set equal to 1.0 mol/L (Kim 2022a).

3.1.5 Radionuclide mobile concentration limits

The mobile concentration limit, $S_{k,j}(t)$, of isotope j of element k at time t is determined as a fraction of element k's mobile concentration limit:

$$S_{k,j}(t) = S_k X_{k,j}(t) \quad . \tag{4}$$

The fraction, $X_{k,j}(t)$, is the number of moles, $I_{k,j}(t)$, of isotope j of element k, in the waste area at time t, divided by the number of moles for all isotopes of element k tracked by PANEL in the waste area at time t:

$$X_{k,j}(t) = \frac{I_{k,j}(t)}{\sum_j I_{k,j}(t)} \quad . \tag{5}$$

$I_{k,j}(t)$ is a product of PANEL's decay calculations. At any time t, the sum of isotope mobile concentration limits equals the element mobile concentration limit: $\sum_j S_{k,j}(t) = S_k$.

3.1.6 Radionuclide concentrations for DBRs

For DBRs, PANEL determines the concentration, $c_{k,j}(t)$, of isotope j of element k at time t as

$$c_{k,j}(t) = Min\left(S_{k,j}(t), \frac{I_{k,j}(t)}{b\, V_{min}}\right) \quad , \quad b = 1, \ldots, 5 \quad , \tag{6}$$

where V_{min} is the minimum volume of brine in the waste area necessary for a DBR to occur.[5] Concentration $c_{k,j}(t)$ is said to be solubility limited if $S_{k,j}(t)$ is the minimum in Eq. 6 and inventory limited if $I_{k,j}(t)/b\, V_{min}$ is the minimum.

For each vector of sampled parameters, PANEL reports concentrations determined using Eq. 6, as functions of time, for six separate intrusion scenarios and, for each scenario, for five brine volume multipliers.[6] PANEL also reports the sum of the individual radionuclide concentrations as a function of time. The sum is used in determining DBRs (Section 3.1.8).

[5] The difference between V_{min} and DBRMINBV is described in Section 5.1.

[6] There is redundancy in the PANEL output. Concentrations are identical for scenarios that involve the same type of brine; namely, GWB in scenarios 1, 4, and 5, and ERDA-6 in scenarios 2, 3, and 6.

Information Only

3.1.7 Conversion to EPA Units

Factors to convert from curies to EPA units and from moles to EPA units are provided here. Conversion to EPA units is possible only for regulated radionuclides.

First, introduce f_w, the Waste Unit Factor or WUF, given by

$$f_w = \frac{W}{\mu} \quad , \tag{7}$$

where W is the total inventory in curies, at closure, of alpha-emitting transuranic radionuclides with half-lives greater than 20 years. The quantity μ in Eq. 7 is a constant equal to 10^6 curies, making f_w dimensionless.

Next, note that a regulated radionuclide is one that has been assigned an EPA release limit in 40 CFR 191 (U.S. DOE 1996). If $L_{k,j}$ is the EPA release limit for regulated isotope j of element k, then the factor, $e^c_{k,j}$, that converts curies to EPA units is simply

$$e^c_{k,j} = 1/\left(f_w\, L_{k,j}\right) \quad . \tag{8}$$

Moles can be converted to EPA units by first converting to curies and then using Eq. 8. The factor, $e^m_{k,j}$, that converts moles to EPA units is

$$e^m_{k,j} = \left(\frac{A \ln(2)}{B\left(t_{1/2}\right)_{k,j}}\right) \times e^c_{k,j} \quad . \tag{9}$$

In Eq. 9, A is Avogadro's number, B converts curies to becquerels, and $\left(t_{1/2}\right)_{k,j}$ is half-life in seconds of isotope j of element k.[7]

3.1.8 Total concentration for DBRs

PANEL determines a sum of concentrations, $c_{DBR}(t)$, for use by code CCDFGF in determining DBRS:

$$c_{DBR}(t) = \sum_{k,j} c_{k,j}(t) \times e^m_{k,j} \quad , \tag{10}$$

where $c_{k,j}(t)$ is the radionuclide concentration from Eq. 6 and $e^m_{k,j}$ converts moles to EPA units (Eq. 9).[8] All 26 radionuclides tracked by PANEL for concentrations are included in the sum; however, a difficulty arises because four of the radionuclides, namely ^{252}Cf, ^{244}Cm, ^{147}Pm and ^{241}Pu, are unregulated. PANEL sets the release limits (Eq. 8) of the unregulated radionuclides to

[7] A=6.02×10^{23}; B=3.7×10^{10}.

[8] PANEL reports $c_{DBR}(t)$ as the quantity CNETOTAL in EPA units/m^3 (Kim 2022a). The units of $c_{DBR}(t)$ in Eq. 10 are EPA units/L.

Information Only

1.0×10^{30} (Table 5-5, Kim 2022a); in effect, eliminating them from the sum. Note, however, that decay products (Section 3.2) of the four unregulated radionuclides will contribute to $c_{DBR}(t)$.

3.1.9 Lumped radionuclides

Ten of the 26 radionuclides used in the PANEL concentration calculations are combined to produce five so-called lumped radionuclides. The lumped radionuclides and their constituents are shown in Table 4. The ten constituent radionuclides account for more than 99% of total inventory in EPA units at the time of repository closure in the CRA26_IS (Kicker, 2025).

Table 4. Lumped radionuclide constituents

Lumped Radionuclide	Constituent Radionuclides
AM241L	^{241}Am, ^{241}Pu
PU239L	^{239}Pu, ^{240}Pu, ^{242}Pu
PU238L	^{238}Pu
U234L	^{233}U, ^{234}U
TH230L	^{229}Th, ^{230}Th

Helton et al. (1998), Leigh and Trone (2005), and Fox et al. (2009) describe how the constituent radionuclides are combined. The main idea is that radionuclides of the same element will transport at the same rate since they have the same chemical properties but slightly different weights. Radionuclides are lumped together either on a curie or mole basis; that is, either the inventory in curies is added directly, or the curies are converted to moles, the moles are added, and the result is converted back to curies. The method that results in the largest number of curies is chosen. An exception to this strategy is that moles of ^{241}Pu are added to moles ^{241}Am to get AM241L (Helton et al. 1998, Section 4.3.2).

PANEL forms both lumped radionuclide concentrations and lumped E2E1 releases (Section 3.3.4) at each time step in a simulation. PANEL reports the lumped concentrations, but they are not used further in PA. PANEL's lumped E2E1 releases are used by code CCDFGF in the calculation of transport releases through the Culebra. PANEL also determines mobile concentration limits of the lumped radionuclides, as discussed next.

3.1.10 Lumped radionuclide mobile concentration limits

PANEL calculates the lumped radionuclide mole fraction, $X^L_{k,j}$, as

$$X^L_{k,j} = \begin{cases} max\left(\dfrac{\sum_{l(k)} I_{k,l}(t)}{\sum_j I_{k,j}(t)}\right), & for\ \ PU238L, U234L, and\ TH230L, \\ 1.0, & for\ \ PU239L\ and\ AM241L. \end{cases} \quad (11)$$

The fraction in Eq. 11 is the mole count of the isotopes being lumped together for element k – picked out by index $l(k)$ – divided by the mole count of all isotopes of element k tracked by

Information Only

PANEL. The maximum in the equation is taken over time. $X^L_{k,j}$ is constant for all simulations in an analysis.[9]

PANEL uses $X^L_{k,j}$ to determine the mobile concentration limit, $S^L_{k,j}$, of a lumped radionuclide:

$$S^L_{k,j} = S_k(b{=}1)\ X^L_{k,j} \quad . \tag{12}$$

Here, element k's mobile concentration limit at the minimum brine volume has been used. $S^L_{k,j}$ is not a function of time but does vary by simulation. Code NUTS uses $S^L_{k,j}$ in its determination of lumped radionuclide concentrations. $S^L_{k,j}$ is the *only* PANEL result used by NUTS.

3.2 Decay and ingrowth

In Decay mode, PANEL models decay and ingrowth for the following 30 radionuclides: ^{241}Am, ^{243}Am, ^{252}Cf, ^{243}Cm, ^{244}Cm, ^{245}Cm, ^{248}Cm, ^{137}Cs, ^{237}Np, ^{231}Pa, ^{210}Pb, ^{147}Pm, ^{238}Pu, ^{239}Pu, ^{240}Pu, ^{241}Pu, ^{242}Pu, ^{244}Pu, ^{226}Ra, ^{228}Ra, ^{147}Sm, ^{90}Sr, ^{229}Th, ^{230}Th, ^{232}Th, ^{233}U, ^{234}U, ^{235}U, ^{236}U and ^{238}U. This list is made up of the 26 radionuclides for which PANEL determines concentrations plus ^{210}Pb, ^{226}Ra, ^{228}Ra, and ^{147}Sm.[10] PANEL models decay and ingrowth to obtain the remaining radionuclide inventory ($I_{k,j}(t)$ in Eq. 5), as well as the remaining inventory of lumped radionuclides (used in Eq. 11). PANEL's Decay mode does not consider radionuclide transport.

[9] PANEL reports a quantity it calls LSOLDIFF, which is negative $\log_{10}$ of $X^L_{k,j}$.

[10] Kim et al. (2024) describe rationales for which radionuclides are included in PA. ^{210}Pb, ^{226}Ra, ^{228}Ra, and ^{147}Sm were identified in the CCA as potentially contributing to releases and continue to be tracked by PANEL for decay.

Information Only

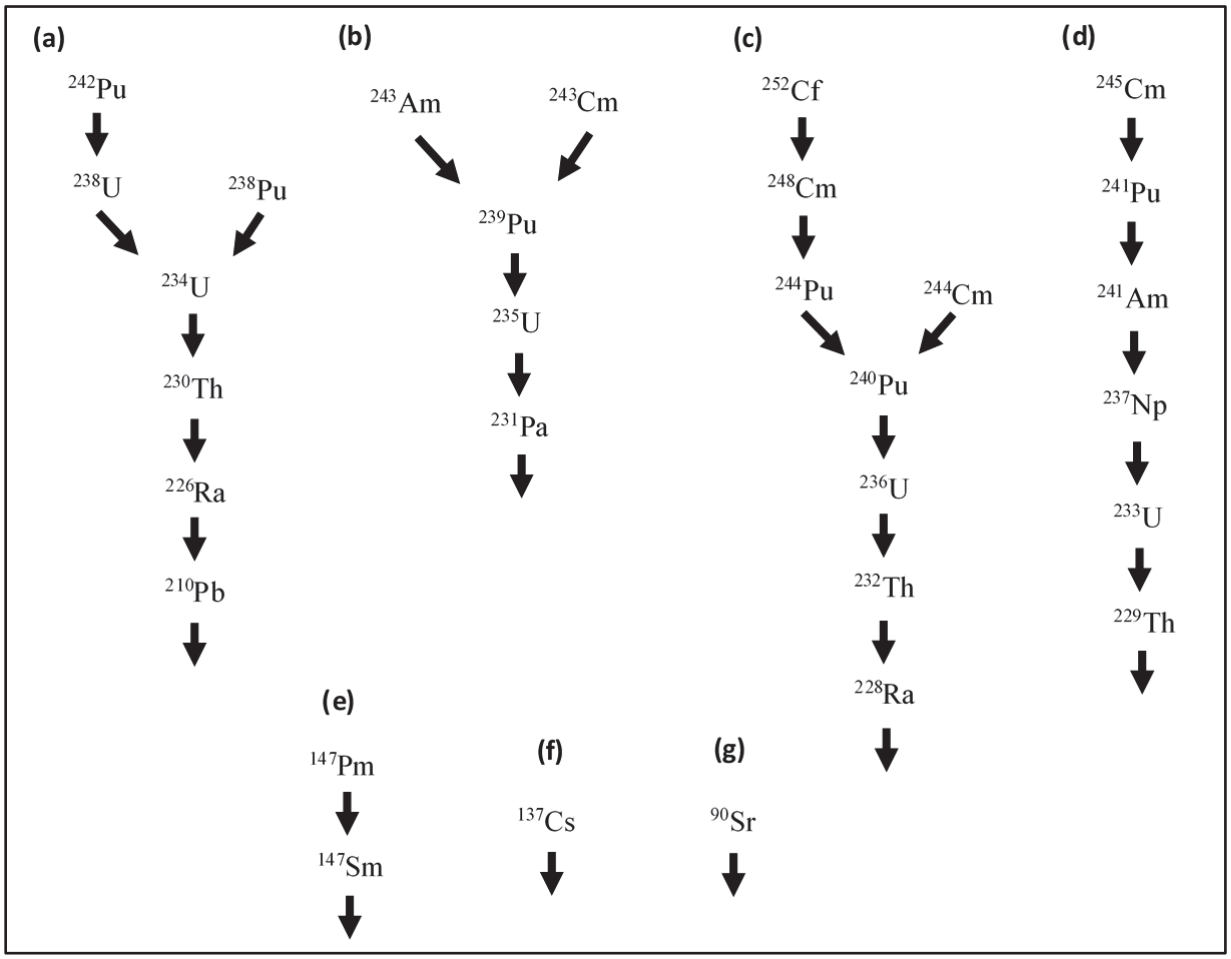


Figure 3. Abridged decay chains in PANEL

The 30 radionuclides belong to the abridged decay chains shown in Figure 3, where the last radionuclide in each chain decays into a radionuclide not tracked by PANEL. Chains (a)-(d) in the figure correspond to the Uranium, Actinium, Thorium, and Neptunium series (Sarathi 2019; Kim 2023a).

The abridged decay chains were originally formulated to include radionuclides called out in Title 40 CFR Part 191 Appendix A. These radionuclides have half-lives longer than 20 years and are deemed potentially significant to releases based on criteria set forth in Appendix-WCA of the CCA (U.S. DOE 1996). Historically, some radionuclides with half-lives longer than 20 years have been screened out due to a small initial inventory and a small potential for ingrowth during the 10,000-year regulatory period (Appendix WCA, U.S. DOE 1996; Kicker and Zeitler 2013; Kicker 2025). Conversely, certain radionuclides with half-lives shorter than 20 years are included if their inventories are significant and their decay leads to radionuclides with half-lives longer than 20 years; one example is ^{241}Pu. Radionuclides with very short half-lives – less than 2 years – are excluded from the abridged chains; in these cases, PANEL assumes that the parent decays directly to the next long-lived radionuclide. Stable radionuclides are not tracked.

Information Only

3.3 E2E1 transport

PANEL determines radionuclide releases up the borehole in the E2E1 scenario for each of the 26 radionuclides listed at the beginning of Section 3.1. The releases are assumed to flow into the Culebra member of the Rustler formation and are called *to Culebra* releases in PA.[11] Unlike code NUTS, PANEL does not determine releases through anhydrite marker beds to the Land Withdrawal Boundary (LWB) or to the Culebra via the repository's shaft.

3.3.1 Radionuclide concentrations for E2E1

PANEL accounts for brine flow out of the repository, in addition to decay and ingrowth, when calculating radionuclide concentrations for the E2E1 scenario. Treating the waste area as a whole and writing $A_{k,j}(t)$ for the amount (number of moles) of isotope j of element k at time t, PANEL solves the equation (Helton et al. 1998):

$$\frac{dA_{k,j}(t)}{dt} = -q'_{BF}(\mathbf{x}_{\mathrm{MB}}, t)\, c_{k,j}(t) - \lambda_{k,j}\, A_{k,j}(t) + \sum_{(l,m)\in P(k,j)} \lambda_{l,m}\, A_{l,m}(t) \quad , \tag{13}$$

where concentration $c_{k,j}(t)$ is subject to the constraint

$$c_{k,j}(t) = Min\left(S_{k,j}(t, b{=}1), \frac{A_{k,j}(t)}{V'(t)}\right) \quad , \quad for\ E2E1\ transport. \tag{14}$$

BRAGFLO determines a brine flow rate everywhere on its computational grid. In its transport calculations, PANEL takes brine flow out of the repository to be brine flow up the borehole at $\mathbf{x}_{\mathrm{MB}}{=}(x_{\mathrm{MB}}, y_{\mathrm{MB}})$, the location where the borehole intersects MB138. PANEL may also time shift the brine flow, as described in the next section. Brine flow rate up through a cell at location $\mathbf{x}{=}(x, y)$, inside the borehole, is designated $q_{BF}(\mathbf{x}, t)$ in this report. The quantity $q'_{BF}(\mathbf{x}_{\mathrm{MB}}, t)$ in Eq. 13 is time-shifted brine flow rate at $\mathbf{x}_{\mathrm{MB}}$. Note also that PANEL receives cumulative brine flow up the borehole at $\mathbf{x}_{\mathrm{MB}}$ as input; a time derivative is taken to get brine flow rate.

The other quantities in Eq. 13 are the decay constant, $\lambda_{k,j}$, and the parents, $P(k,j)$, of element k, isotope j. (^{234}U, ^{239}Pu and ^{240}Pu each have two parents. See Figure 3.) The three terms on the right side of Eq. 13 thus describe loss of inventory due to brine discharge, loss of inventory due to radionuclide decay, and gain of inventory due to radionuclide ingrowth.

The volume of brine in the waste area, $V(t)$, at time t is calculated as

$$V(t) = \sum_{\mathbf{x}\,\in\, waste\ area} \phi_{BF}(\mathbf{x}, t)\, s_{BF}(\mathbf{x}, t)\, \Delta\mathbf{x} \quad , \tag{15}$$

where $\phi_{BF}(\mathbf{x}, t)$ and $s_{BF}(\mathbf{x}, t)$ are BRAGFLO porosity and brine saturation at $\mathbf{x}$ and time t, and $\Delta\mathbf{x} = \Delta x \Delta y \Delta z$ is the volume of a grid cell with thickness Δz. Volume $V(t)$ is an input to PANEL. As with brine flow rate, PANEL may time shift $V(t)$: this is $V'(t)$ in Eq. 14.

[11] Radionuclides entering the Culebra are not releases in terms of WIPP regulatory compliance.

Information Only

3.3.2 Time shifting

PANEL considers a series of times for the occurrence of the E1 intrusion (Table 5, Section 4.1). BRAGFLO's scenario 6, or S6-BF, on the other hand, simulates E2E1 only with time 1,000 years for the E2 intrusion and time 2,000 years for the E1. Time shifting is used to accommodate the additional intrusion times. If t_{BFI} is the BRAGFLO E1 intrusion time and t_I is the PANEL E1 time, then the time-shifted brine flow rate $q'_{BF}(\mathbf{x},t)$ and waste area brine volume $V'(t)$ are determined as

$$q'_{BF}(\mathbf{x},t) = q_{BF}(\mathbf{x}, t_{BFI} + t - t_I) \quad , \qquad (16)$$

and

$$V'(t) = V(t_{BFI} + t - t_I) \quad .$$

No time shifting occurs if t_{BFI} and t_I are equal. Note that by using S6-BF results, an E2 intrusion, in effect, always precedes an E1 by 1,000 years in a PANEL E2E1 scenario.

3.3.3 Brine volume extrapolation

Where $t_I < t_{BF1}$ it is necessary to extrapolate brine flow and brine volume to times beyond 10,000 years – the maximum BRAGFLO simulation time – for later times *t*. Linear extrapolation is used. Kim (2023b) reported that the extrapolation can lead to negative values being generated by PANEL for $V'(t)$. This issue did not impact the results of previous analyses and has not been observed with the NUTS code. The CRA26_IS uses PANEL version 5.03, in which linear extrapolation is still employed except that brine volume is not allowed to fall below a minimum of 1,000 m^3 (Kim 2024).

3.3.4 E2E1 *to Culebra* releases

PANEL takes the brine discharge through the borehole at the Culebra to be the same as the brine discharge at MB138; that is, $q'_{BF}(\mathbf{x}_C,t) = q'_{BF}(\mathbf{x}_{MB},t)$, with $\mathbf{x}_C = (x_C, y_C)$ the location where borehole and Culebra intersect. PANEL then determines cumulative *to Culebra* releases, $R_{k,j}(\mathbf{x}_C,t)$, for isotope *j* of element *k,* at time *t*, as

$$R_{k,j}(\mathbf{x}_C,t) = \int_0^t q'_{BF}(\mathbf{x}_C,\tau)\, c_{k,j}(\tau)\, d\tau \quad , \quad for\ the\ E2E1\ scenario, \qquad (17)$$

where $c_{k,j}(t)$ is the concentration from Eq. 14. Using the approach described in Section 3.1.9, PANEL combines individual radionuclide releases, at each time *t*, to form five lumped radionuclide *to Culebra* releases, $R^L_{k,j}(\mathbf{x}_C,t)$. PANEL reports both $R_{k,j}(\mathbf{x}_C,t)$ and $R^L_{k,j}(\mathbf{x}_C,t)$, but only lumped releases are used further in PA.

3.3.5 Fractional contributions to the element concentration limit

In addition to the element concentration limit, S_k, PANEL reports dissolved and colloidal fractional components of S_k. Dividing both sides of Eq. 1 by S_k gives the fractional components:

Information Only

$$1 = \frac{1}{S_k}\left(S_{k,dissolved} + S_{k,mineral} + S_{k,intrinsic} + S_{k,humic} + S_{k,microbial}\right)$$
$$= F_{k,dissolved} + F_{k,mineral} + F_{k,intrinsic} + F_{k,humic} + F_{k,microbial} \quad . \qquad (18)$$

PA assumes that mineral fragment, intrinsic, and microbial colloids are not transported through the Culebra. CCDFGF forms fractional *to Culebra* releases, $r^L_{k,j}(\mathbf{x}_C, t)$ say, where

$$r^L_{k,j}(\mathbf{x}_C, t) = \left(1 - F_{k,mineral} - F_{k,intrinsic} - F_{k,microbial}\right) \times R^L_{k,j}(\mathbf{x}_C, t) \quad . \qquad (19)$$

CCDFGF convolves the time derivative of $r^L_{k,j}(\mathbf{x}_C, t)$ with the response, determined by PA code SECOTP2D, of a unit impulsive radionuclide source in the Culebra. The result of the convolution is *from Culebra* releases at the LWB.

3.4 PANEL summary

In summary, PANEL determines radionuclide concentrations for use in DBRs; *to Culebra* releases for the E2E1 intrusion scenario; and concentration limits for five lumped radionuclides, including fractions associated with dissolved and colloidal contributions. PANEL has three separate modes of execution:

(1) Decay Mode, yielding $I_{k,j}(t)$,
(2) Concentration Mode, yielding S_k and its fractional components, $c_{k,j}(t)$, $c_{DBR}(t)$, $S^L_{k,j}$, and
(3) Intrusion Mode, yielding $R_{k,j}(\mathbf{x}_C, t)$ and $R^L_{k,j}(\mathbf{x}_C, t)$.

Figure 4 sketches the PANEL and NUTS contributions to releases. Cumulative brine discharge up the borehole and waste area brine volume inputs to PANEL are determined by an instance of PA code ALGEBRACDB using output from BRAGFLO. Brine flow, brine saturation, and porosity at each cell in the modeling grid are input to NUTS directly from BRAGFLO. NUTS uses $S^L_{k,j}$ in its determination of lumped concentrations. Code CCDFGF uses $c_{DBR}(t)$ to determine DBRs, and $R^L_{k,j}(\mathbf{x}_C, t)$ and the fractional components of S_k to compute *from Culebra* releases.[12]

[12] CCDFGF determines *from Culebra* releases only for AM241L, PU239L, U234L, and TH230L.

Information Only

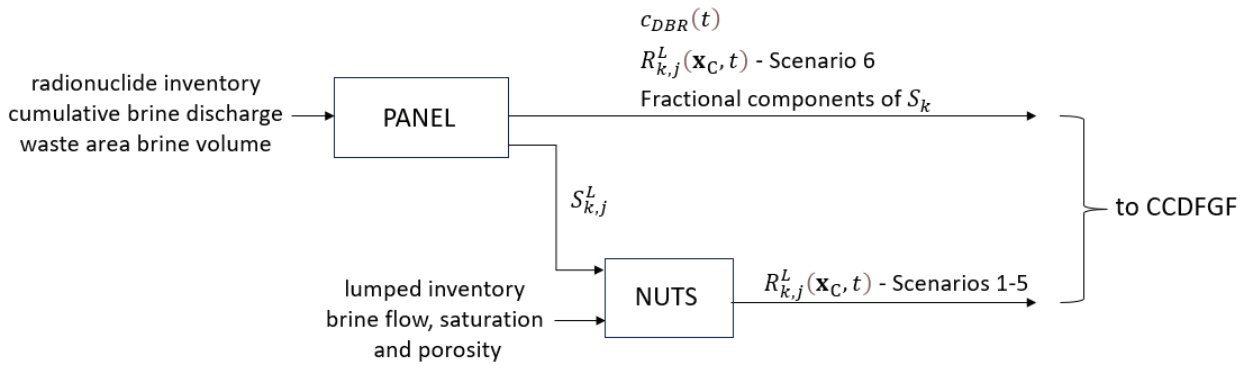


Figure 4. Top-level view of PANEL and NUTS

Information Only

4.0 BRIEF OVERVIEW OF NUTS

The NUTS code simulates the transport of lumped radionuclides in the Salado formation for BRAGFLO intrusion scenarios 1-5. The NUTS transport model accounts for contaminant advection in the aqueous phase, dissolution and precipitation, and radioactive decay (Shinta 1997; Kim 2022b; Helton et al. 1998). The transport equations are solved on the same two-dimensional computational grid used by BRAGFLO. Additionally, NUTS relies on BRAGFLO for values of brine flow rate, brine saturation, and porosity, all of which are functions of space and time.

NUTS considers three pathways for potentially significant transport releases: (i) along anhydrite marker beds to the LWB; (ii) up the repository shaft[13] to the Culebra; and (iii) up through an intruding borehole to the Culebra. Releases up the borehole to the Culebra are the NUTS contribution to *to Culebra* releases.

4.1 NUTS operation modes

NUTS has three modes of operation. SCN (Screening) mode identifies vectors with the potential for significant releases; ISO (Isotopes) mode computes transport releases for the undisturbed and single intrusion BRAGFLO scenarios; and INT (Intrusion) mode computes releases for single intrusions at times shifted from the BRAGFLO intrusion times.

Table 5 shows the BRAGFLO scenarios and corresponding NUTS simulations. Each NUTS simulation has at most one intrusion. The four INT mode intrusion times for S3-BF and S5-BF are accommodated with separate simulations. The bottom row of Table 5 describes BRAGFLO's S6-BF, or E2E1, scenario. E2E1 transport is handled by PANEL. A dash in the table signifies that a simulation is not run.

[13] The five WIPP repository shafts – intake, exhaust, salt, waste, and the new Safety Significant Confinement Ventilation System (SSCVS) shaft – are conceptually combined into one shaft in the BRAGFLO and NUTS computational grids.

Information Only

Table 5. BRAGFLO, NUTS, and PANEL intrusions (times in years following repository closure)

BRAGFLO Scenario	BRAGLO Intrusions	NUTS SCN Intrusions	NUTS ISO Intrusions	NUTS INT Intrusions	PANEL Intrusions
S1-BF	none	none	none	—	—
S2-BF	E1 at 350	E1 at 350	E1 at 350	E1 at 100	—
S3-BF	E1 at 1000	E1 at 1000	E1 at 1000	E1 at 3000, 5000, 7000, 9000	—
S4-BF	E2 at 350	E2 at 350	E2 at 350	E2 at 100	—
S5-BF	E2 at 1000	E2 at 1000	E2 at 1000	E2 at 3000, 5000, 7000, 9000	—
S6-BF	E2 at 1000 and E1 at 2000	—	—	—	E1 at 100, 350, 1000, 2000, 4000, 6000, 9000*

*Time-shifted S6-BF results simulate the effects of an E2 intrusion occurring 1,000 years before each of these E1s.

NUTS SCN mode employs a hypothetical wholly-passive, non-decaying, non-sorbing tracer (Stockman et al. 1996). A fixed tracer concentration of 1 kg/m^3 is assigned to any brine leaving the waste areas of the repository. NUTS monitors the amount of tracer reaching the LWB (via the marker beds) or reaching the Culebra (through the shaft and borehole). In a given scenario, if a cumulative tracer mass of 10^{-7} kg is observed crossing the LWB or entering the Culebra, then the parameter vector is designated as screened-in for the scenario; if a lesser amount of tracer is accumulated then the parameter vector is designated screened-out for the scenario. Different scenarios may have different numbers of screened-in vectors. An exception to this strategy is that a vector screened in for any of scenarios S2-BF through S5-BF is automatically screened in for scenario S1-BF.[14] Only screened-in vectors take part in NUTS ISO and INT simulations.

If the NUTS transport equations were solved for all individual radionuclides, the computational load – even after screening – could be very high. NUTS ISO and INT modes reduce the load significantly by working only with the five lumped radionuclides described in Section 3.1.9. The lumped radionuclide inventories at the time of repository closure are read from the PA database.

NUTS INT mode uses the approach described in Sec 3.3.2 to time shift BRAGFLO data to INT mode intrusion times. Time-shifted brine flow is obtained using the first equation in Eq. 16, with BRAGFLO intrusion times, t_{BFI}, and NUTS intrusion times, t_I, from Table 5. Time-shifted BRAGFLO brine saturation and porosity are similarly obtained.

[14] This is because INT mode uses results from NUTS undisturbed simulations (Kim 2013).

Information Only

4.2 Concentrations of lumped radionuclides

NUTS solves its transport equations for lumped radionuclide concentration, $c^L_{k,j}(\mathbf{x},t)$, at location **x** and time *t*. At the end of each time step, $c^L_{k,j}(\mathbf{x},t)$ is constrained to be no greater than the lumped radionuclide mobile concentration limit. Writing $A^L_{k,j}(\mathbf{x},t)$ for the number of moles of lumped radionuclide per unit volume (mol/L) in the grid cell at location **x** and at time *t,* the constraint is

$$c^L_{k,j}(\mathbf{x},t) \;=\; Min\left(S^L_{k,j}, \frac{A^L_{k,j}(\mathbf{x},t)}{\phi'_{BF}(\mathbf{x},t)\; s'_{BF}(\mathbf{x},t)}\right) , \tag{20}$$

where $S^L_{k,j}$ is defined in Eq. 12. Quantities $\phi'_{BF}(\mathbf{x},t)$ and $s'_{BF}(\mathbf{x},t)$ in Eq. 20 are BRAGFLO porosity and brine saturation, time shifted in INT mode.[15] If $c^L_{k,j}(\mathbf{x},t)$ falls below $S^L_{k,j}$, NUTS dissolves precipitate to restore the concentration limit, assuming precipitate is available. NUTS adds to the precipitate if $c^L_{k,j}(\mathbf{x},t)$ exceeds $S^L_{k,j}$.

4.3 Decay of lumped radionuclides

In ISO and INT modes, NUTS models lumped radionuclide decay in both solid and liquid phases using the three reduced decay chains shown in Figure 5. Decay is implemented using the atomic properties of the named lumped radionuclide. The last radionuclide in each chain decays into one not tracked by NUTS. There is no decay of the tracer in NUTS SCN mode.

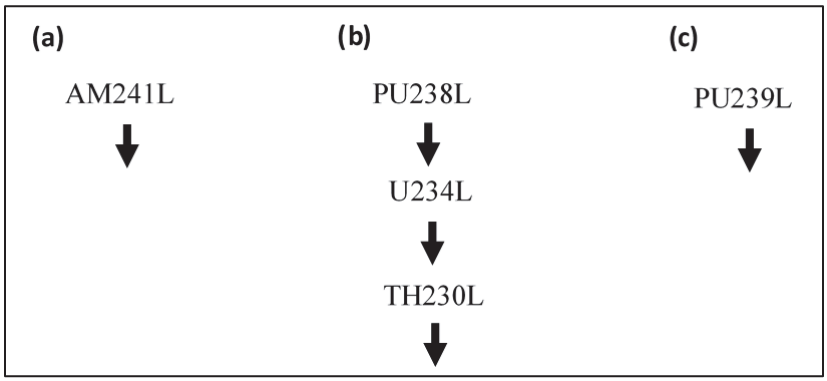


Figure 5. Decay chains modeled in NUTS

4.4 NUTS *to Culebra* releases

Results from vector screening (Section 5.3.2) indicate that the only route for significant transport release is up through an intruding borehole to the Culebra. NUTS determines cumulative *to Culebra* releases, $R^L_{k,j}(\mathbf{x}_C,t)$, for the lumped radionuclides as

[15] Multiplying numerator and denominator of the fraction on the right side of Eq. 20 by the grid cell volume in liters would give number of moles in the cell divided by liters of brine in the cell.

Information Only

$$R^{L}_{k,j}(\mathbf{x}_C, t) = \int_0^t q'_{BF}(\mathbf{x}_C, \tau)\, c^{L}_{k,j}(\mathbf{x}_C, \tau)\, d\tau \quad , \quad for\ scenarios\ 1\text{-}5. \tag{21}$$

Here, $\mathbf{x}_C$ is the location where an intruding borehole intersects the Culebra, $c^{L}_{k,j}(\mathbf{x}_C, t)$ is the lumped radionuclide concentration (Eq. 20) at $\mathbf{x}_C$, and $q'_{BF}(\mathbf{x}_C, t)$ is the BRAGFLO rate of brine flowing up the borehole through the grid cell at $\mathbf{x}_C$, time shifted in INT mode. As described in Section 3.3.5 for the E2E1 scenario, code CCDFGF forms fractional *to Culebra* releases (Eq. 19) when determining transport through the Culebra.

4.5 NUTS summary

NUTS determines long-term transport releases through Marker Beds to the LWB; through a shaft to the Culebra; and through a borehole to the Culebra. Only the last of these – NUTS *to Culebra* releases – tend to contribute significantly to total releases. For efficiency, NUTS works only with lumped radionuclides. NUTS models decay of the lumped radionuclides and solves its transport equations for lumped radionuclide concentrations as functions of space and time. NUTS has three modes of execution:

(1) Screening mode, identifying parameter vectors for which full transport calculations are to be carried out,
(2) Isotope mode, yielding cumulative lumped radionuclide releases for the screened-in parameter vectors in BRAGFO's S1-BF through S5-BF scenarios, and
(3) Intrusion mode, yielding cumulative lumped radionuclide releases for screened-in parameter vectors in BRAGFLO's S2-BF through S5-BF scenarios, but with shifted intrusion times.

NUTS *to Culebra* radionuclide releases are used by CCDFGF, along with results from PA code SECOT2PD, to calculate *from Culebra* radionuclide releases at the LWB.

Information Only

5.0 RESULTS

Results from the CRA26_IS actinide mobilization and transport simulations are presented in the following sections and compared to the RPPCR. A brief overview of radionuclide inventory is given first, including a description of the waste area as opposed to a waste panel. Next, PANEL results are discussed; namely, solubility and its components, colloid contributions to concentrations, element mobile concentration limits, and radionuclide concentrations as a function of time. Mobile concentration limits for the lumped radionuclides are also shown. NUTS results for tracer discharge and radionuclide releases through the marker beds and shaft are then given. Lastly, NUTS and PANEL results for releases to the Culebra are presented together.

5.1 Inventory

A new radionuclide inventory for the CRA26_IS is provided by ISPAIR-2024 (Van Soest 2025), which is based on the ATWIR-2024 report (U.S. DOE 2024). Kicker (2025) describes the new inventory and compares it to the RPPCR. The key changes since the RPPCR are:

(i) the waste storage capacity has decreased from 175,564 m^3 in the RPPCR to 157,832 m^3 (Ward, 2025),
(ii) the total activity at repository closure has increased from a total activity of 6.51×10^6 Ci in the RPPCR to 8.05×10^6 Ci for the CRA26_IS,
(iii) the transuranic inventory of alpha-emitting radionuclides with half-lives greater than 20 years at repository closure has risen from 5.59×10^6 Ci in the RPPCR to 7.37×10^6 Ci for the CRA26_IS, and
(iv) the WUF (Eq. 7) has increased from 5.59 in the RPPCR to 7.37 in the CRA26_IS.

Waste stream volumes of contact-handled (CH) waste are counted based on internal container volume for both analyses. It is important to note that the larger WUF for the CRA26_IS means that one EPA unit of waste in the CRA26_IS represents more curies of activity than one EPA unit of waste in the RPPCR.

Figure 6 illustrates the twelve largest contributors to total activity in the RPPCR and the CRA26_IS, based on curies at closure, of the 30 radionuclides considered by PANEL. The five largest contributors in order, in both analyses, are ^{239}Pu, ^{241}Am, ^{238}Pu, ^{240}Pu, and ^{241}Pu. The inventory of each of these radionuclides has increased in the CRA26_IS. The significant increase in ^{239}Pu in the CRA26_IS is due to the addition of waste stream SR-KAC-PuOx-2 (Van Soest 2025), which includes ^{239}Pu activity of 1.74×10^6 curies. Figure 7 compares relative contributions to the total inventory at closure, in curies, of the 30 radionuclides considered by PANEL. The five dominant radionuclides account for more than 97% of the total in the RPPCR and more than 99% in the CRA26_IS.

Information Only

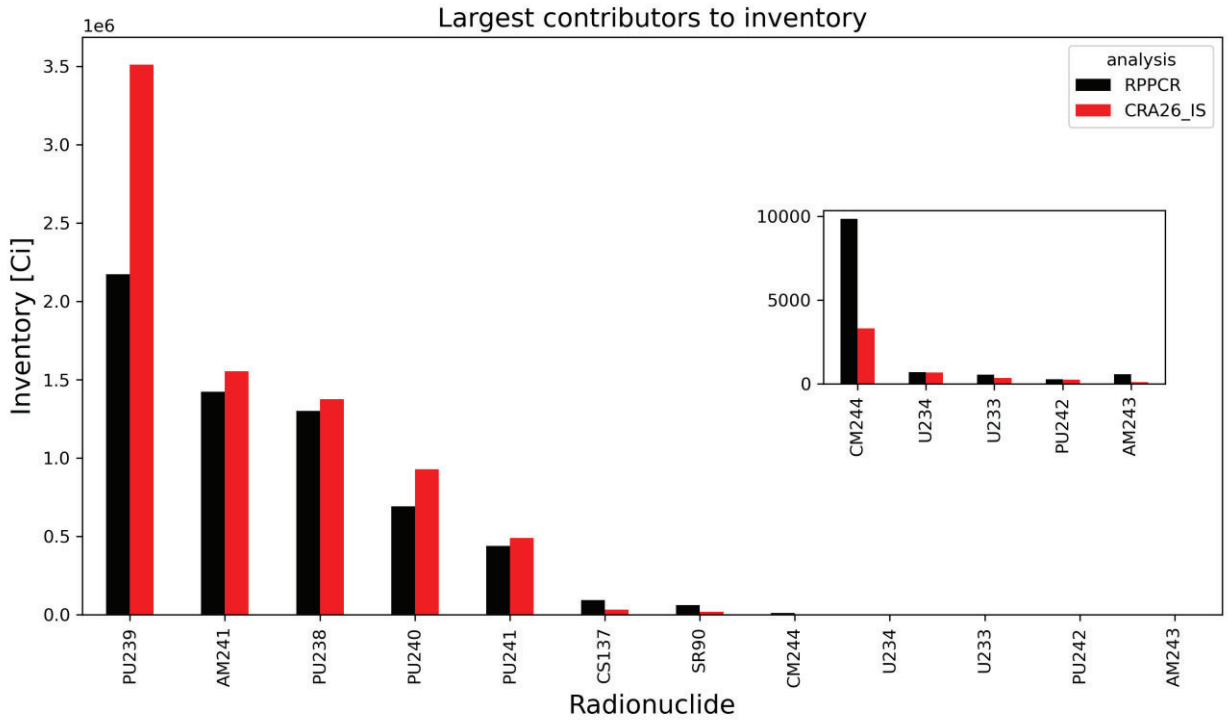


Figure 6. Largest contributors (in curies) to inventory at closure

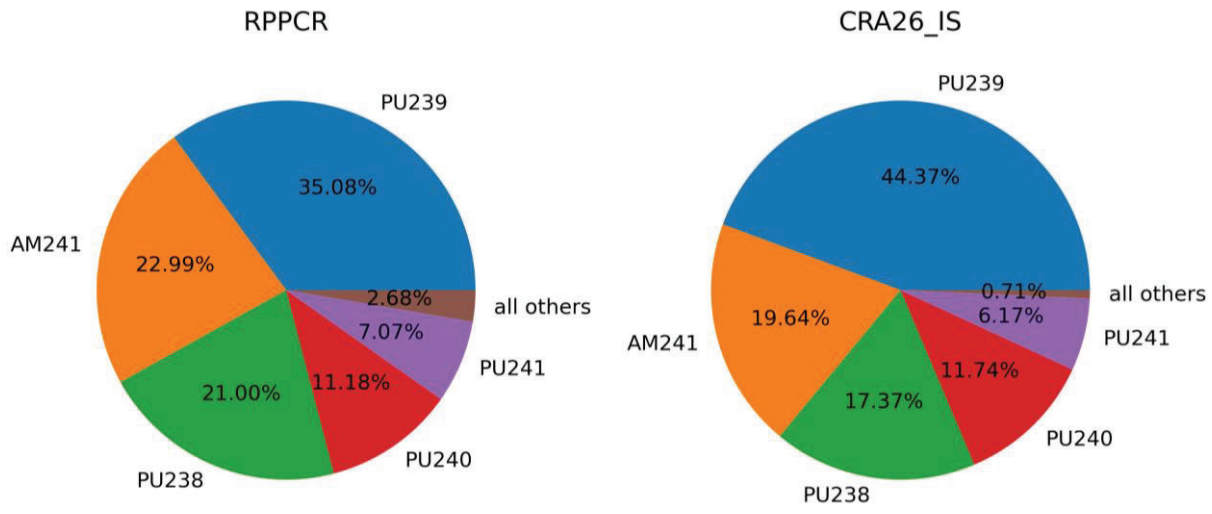


Figure 7. Relative inventory at closure

Information Only

For the CCA, the PANEL code set the fraction of the total inventory contained in one standard waste panel for regulatory PANEL runs (Appendix PANEL, US DOE 1996). The fraction was obtained as the volume of one standard panel divided by the volume of the repository. Waste Panel 5 was used as the standard panel. Following the temporary closure of the WIPP repository in February 2014 and its later reopening, the planned installation of run-of-mine salt panel closure systems in Panels 3, 4, 5, and 6 was no longer possible; in addition, further access to Panel 9 was prohibited (Appendix PA, U.S. DOE 2019). Unchecked communication between these panels affects transport since a borehole intrusion would lead to the draining of five panels rather than the draining of just one. For this reason, code PANEL was changed to model a group of five interconnected waste panels, designated as the *waste area*, assuming homogeneous loading of all panels. While PANEL's calculations of concentrations and concentration limits are not affected by the change from one to five panels (inventory and brine volume scale equally), for simplicity all PANEL calculations have been done based on the waste area since, and including, the CRA-2019.

Waste area inventory is obtained from total inventory by multiplying by the factor 5×REFCON: VPANLEX/REFCON: VREPOS; that is, by five times the volume of one panel, divided by the volume of the repository.[16] Waste area minimum volume of brine for a DBR to occur, V_{min} in Eq. 6, is obtained by multiplying parameter DBRMINBV by the same factor. For the RPPCR the factor is 0.270; for the CRA26_IS it is 0.411. Figure 8 compares waste area inventories for the RPPCR and the CRA26_IS.

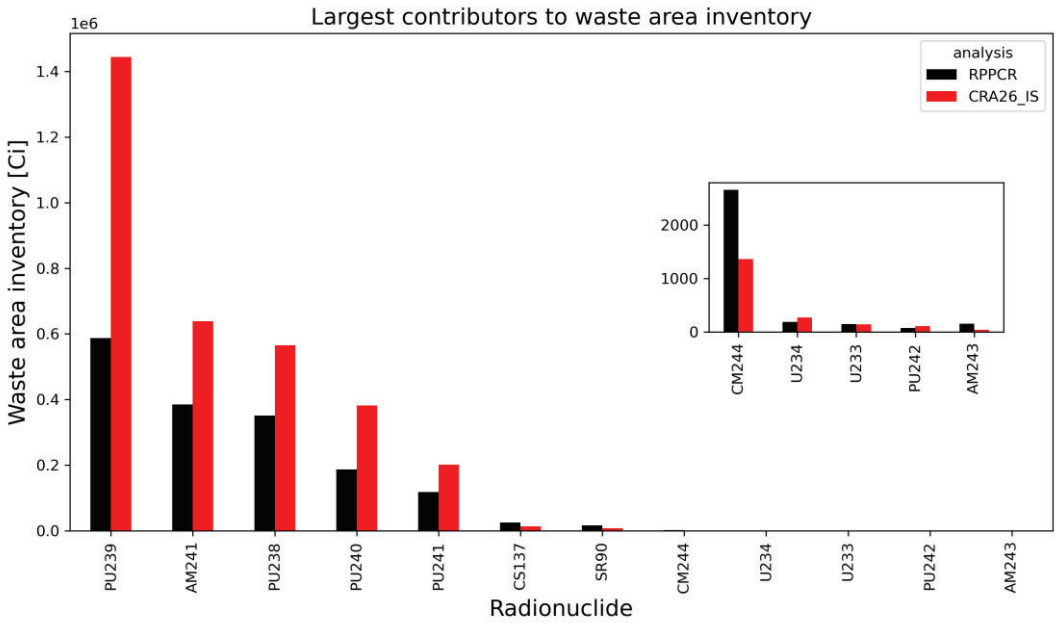


Figure 8. Largest contributors (in curies) to inventory at closure in the waste area

The radionuclide mobile concentration limit, $S_{k,j}(t)$, of isotope j of element k is the product of the element mobile concentration limit, S_k, and the mole fraction $X_{k,j}(t)$ (Eq. 4). S_k is constant in a

[16] Table 1 gives repository volumes. Panel volume is 46,097.65 m^3 in both analyses.

Information Only

simulation because chemical conditions are assumed constant for the 10,000-year regulatory period. Changes through time to $S_{k,j}(t)$ are thus brought about by changes to $X_{k,j}(t)$, that is, by decay and ingrowth of tracked isotopes of element k. Note that $X_{k,j}(t)$ depends entirely on inventory: it is the same for all vectors in an analysis. Figure 9 shows initial mole fractions for the isotopes of Pu, U, Th, and Am tracked by PANEL. Initial mole fractions of ^{239}Pu, ^{238}U, ^{232}Th, and ^{241}Am are approximately one in both the RPPCR and the CRA26_IS.

Lumped radionuclide mole fraction, $X^L_{k,j}$ (Eq. 11), is plotted in Figure 10 for PU238L, U234L, and TH230L. $X^L_{k,j}$ is constant for an analysis. As described by Eq. 12, $X^L_{k,j}$ modifies the element mobile concentration limit (for minimum brine volume) to give the lumped radionuclide mobile concentration limit. Figure 10 does not show mole fractions for PU239L and AM241L; PANEL sets these values to 1.0 (Eq. 11).

Waste area inventory at closure of the lumped radionuclides is shown in Figure 11. The dominant lumped radionuclides are PU239L, AM241L, and PU238L; all have increased inventories in the CRA26_IS. Figure 12 plots relative inventory of the lumped radionuclides. (TH230L has a waste area inventory between 2 and 3 curies and a relative inventory around 0.0001% in both analyses; it is not shown in Figure 12.)

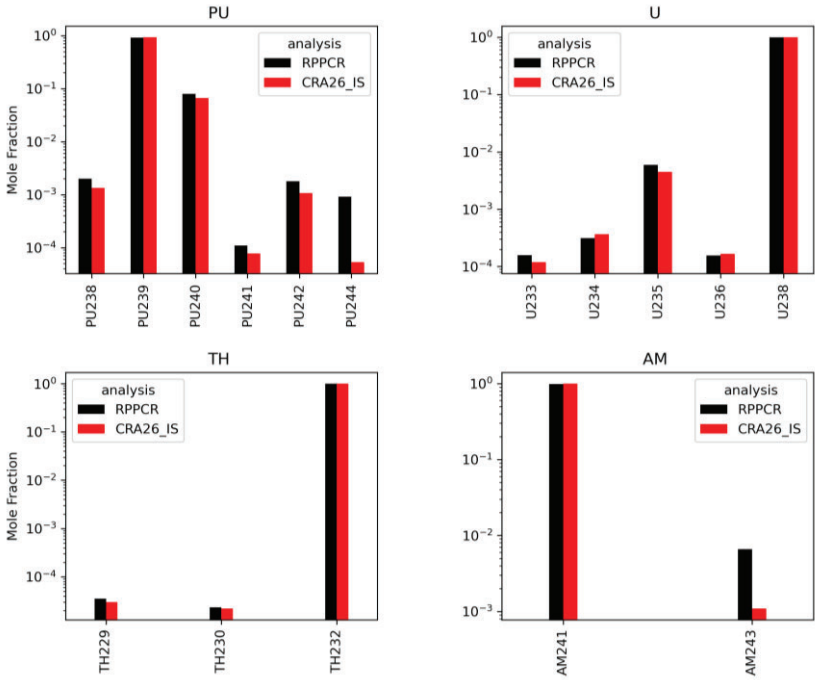


Figure 9. Mole fractions of isotopes of Pu, U, Th and Am at closure

Information Only

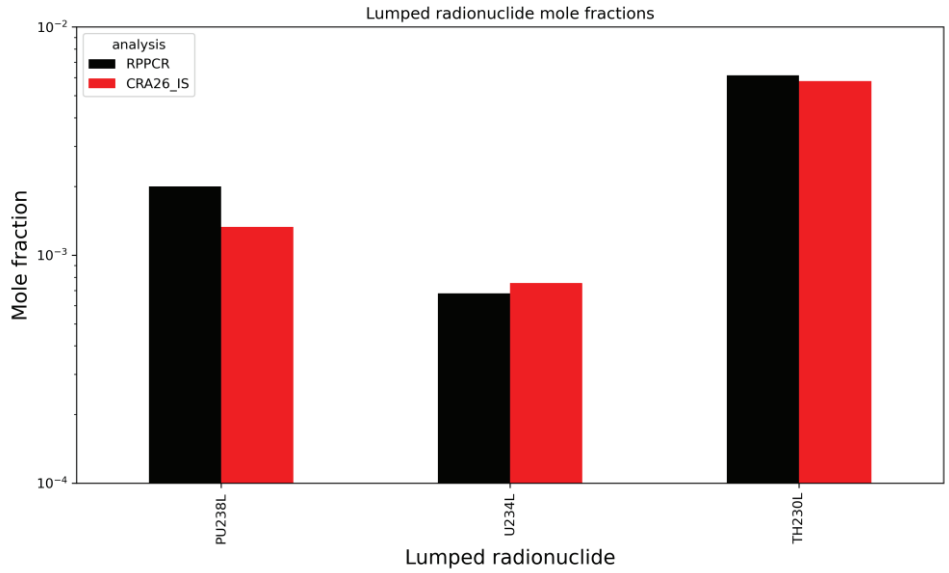


Figure 10. Mole fractions for PU238L, U234L and TH230L

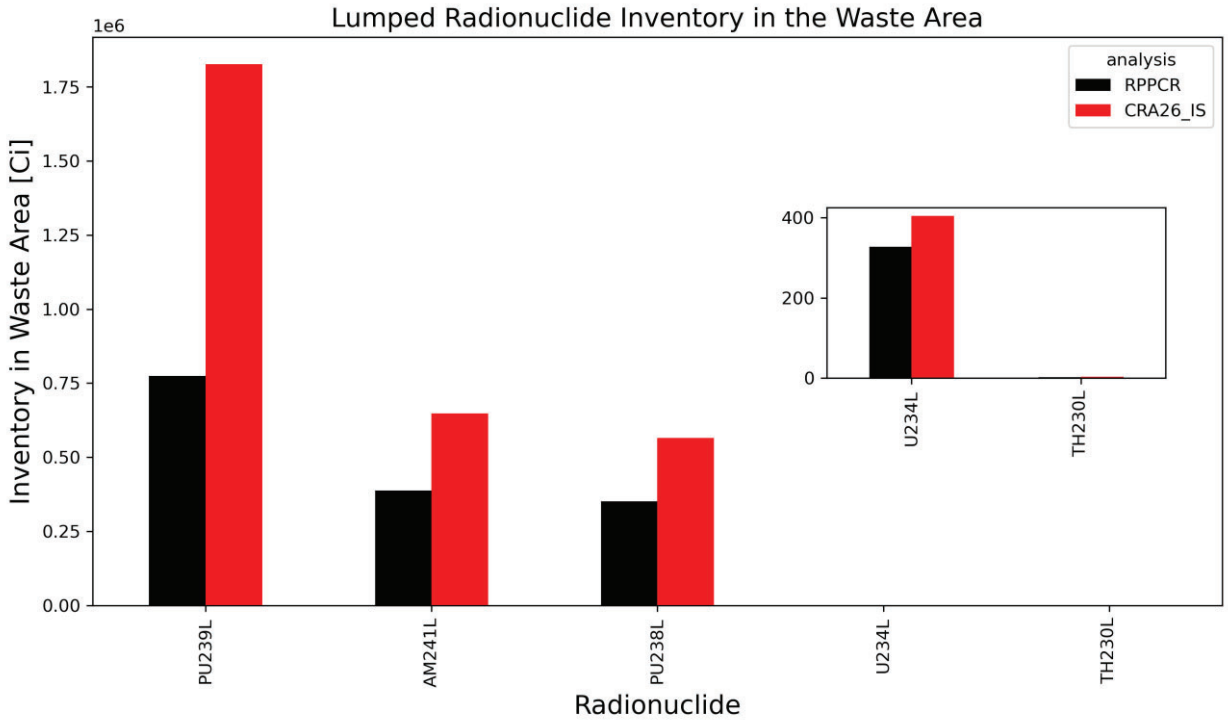


Figure 11. Lumped inventory at closure in the waste area (in curies)

Information Only

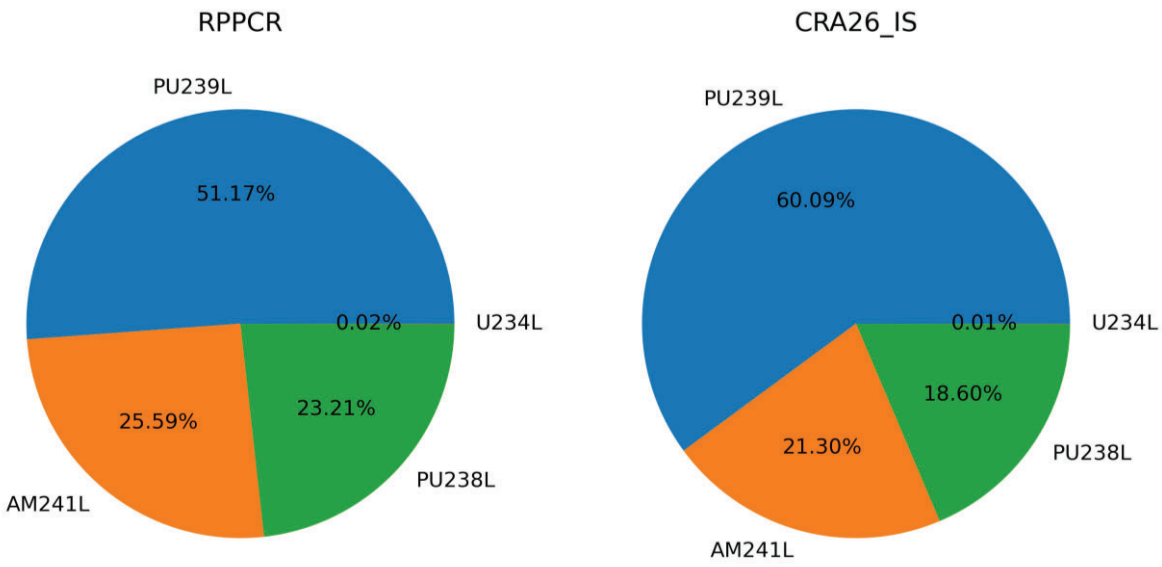


Figure 12. Relative inventory of lumped radionuclides at closure

5.2 PANEL: Radionuclide mobilization

PANEL accounts for the dissolution of an element in a specific oxidation state within the mobilization model, as well as the colloidal suspension of this element in the waste area brine. Consequently, PANEL defines the element mobile concentration limit, S_k, as the thermodynamic measure, in moles/liter, of element *k* in a specific oxidation state that can be mobilized in the brine. The mobile concentration limit of an isotope of element *k* in the specific oxidation state is obtained as a fraction of S_k (Eq. 4).

Five components – actinide solubility plus actinide ionic species sorbed to four types of colloids – make up S_k (Eq. 1). Actinide solubility is the product of a baseline solubility, $S_{k,baseline}$, and the number 10^{u_k}, where u_k is the solubility uncertainty factor (Eq. 2). In PA, the solubility uncertainty factor is a sampled parameter for actinides in the +III and +IV oxidation states. For the CRA26_IS, changes were made to the baseline solubilities and, for the +III state, to the probability distribution from which u_k is drawn. Humic colloid enhancement parameters (Eq. 3) are also updated for the CRA26_IS, and microbial parameters are both updated and made element-oxidation state specific. The following sections describe these changes and their combined effects on radionuclide mobilization.

5.2.1 Baseline solubility

As discussed in Section 3.1.2, both the RPPCR and CRA26_IS use code EQ3/6 and the WIPP thermodynamic database FM6 (Domski 2023a) to predict the baseline solubilities of Am(III), Th(IV) and Np(V), which serve as analogs for other actinides with the +III, +IV, and +V oxidation

Information Only

states. Baseline solubilities are estimated for two types of brine – ERDA-6 and GWB – and for five brine volumes. There are two differences between the RPPCR and CRA26_IS baseline solubility models (Domski 2025a):

(i) A new inventory for CRA26_IS (Section 5.1), and
(ii) DBRMINBV is reduced from 33,804 m^3 in the RPPCR to 6,314 m^3 in the CRA26_IS, consistent with new geomechanical modeling (Brunell 2025).

A thermodynamic model for U(VI) has not been developed due to lack of experimental data. U(VI) baseline solubility is reduced from 1×10^{-3} mol/L in the RPPCR to 3×10^{-6} mol/L for the CRA26_IS, as recommended by Kaplan et al. (2025).

Baseline solubilities for the RPPCR and the CRA26_IS are listed in Table 6 and compared using bar charts in Figure 14. The brine volume multiplier, b in Eq. 2, labels the columns of solubility values in the table and is the x-axis in the bar charts. The +III, +IV, and +V values are from Domski (2023b) and Domski (2025a).

Table 6. Predicted Baseline Solubilities (mol/L)

Brine	Analysis	An species	1x	2x	3x	4x	5x
GWB	RPPCR	An(+III)	3.40E-06	1.86E-06	1.33E-06	1.07E-06	9.09E-07
GWB	RPPCR	An(+IV)	5.34E-08	5.34E-08	5.34E-08	5.34E-08	5.34E-08
GWB	RPPCR	An(+V)	4.95E-07	4.21E-07	3.96E-07	3.84E-07	3.76E-07
GWB	RPPCR	An(+VI)	1.00E-03	1.00E-03	1.00E-03	1.00E-03	1.00E-03
GWB	CRA26_IS	An(+III)	1.45E-05	7.88E-06	5.45E-06	4.20E-06	3.43E-06
GWB	CRA26_IS	An(+IV)	5.34E-08	5.34E-08	5.33E-08	5.34E-08	5.34E-08
GWB	CRA26_IS	An(+V)	9.75E-07	6.88E-07	5.81E-07	5.24E-07	4.90E-07
GWB	CRA26_IS	An(+VI)	3.00E-06	3.00E-06	3.00E-06	3.00E-06	3.00E-06
ERDA-6	RPPCR	An(+III)	3.51E-06	1.93E-06	1.39E-06	1.13E-06	9.59E-07
ERDA-6	RPPCR	An(+IV)	5.73E-08	5.74E-08	5.75E-08	5.75E-08	5.75E-08
ERDA-6	RPPCR	An(+V)	1.80E-06	1.50E-06	1.41E-06	1.36E-06	1.33E-06
ERDA-6	RPPCR	An(+VI)	1.00E-03	1.00E-03	1.00E-03	1.00E-03	1.00E-03
ERDA-6	CRA26_IS	An(+III)	1.44E-05	8.02E-06	5.59E-06	4.32E-06	3.54E-06
ERDA-6	CRA26_IS	An(+IV)	5.63E-08	5.69E-08	5.71E-08	5.72E-08	5.73E-08
ERDA-6	CRA26_IS	An(+V)	4.01E-06	2.64E-06	2.17E-06	1.93E-06	1.79E-06
ERDA-6	CRA26_IS	An(+VI)	3.00E-06	3.00E-06	3.00E-06	3.00E-06	3.00E-06

For both types of brine: An(III) baseline solubilities are about 4 times larger in the CRA26_IS than in the RPPCR; An(IV) baseline solubilities are similar in the two analyses; and An(V) baseline solubilities show a modest increase in the CRA26_IS. Domski (2025a) notes that the total moles of organic ligands are nearly the same in the two analyses, so that decreasing the minimum brine volume (DBRMINBV) in the CRA26_IS increases organic ligand concentrations.

Organic ligands are the aqueous species that react with the ionic species of An(III) and An(V). Consequently, the concentrations of the aqueous phases of An(III) and An(V) are increased, leading to higher baseline solubilities for these actinides. In contrast, the baseline solubilities of An(IV) in both analyses remain comparable because the ionic species of An(IV) preferentially react with hydroxide (OH^-) and carbonate (CO_3^{2-}), rather than with organic ligands. As a result, changes in organic ligand concentrations have little effect on the baseline solubility of An(IV).

Information Only

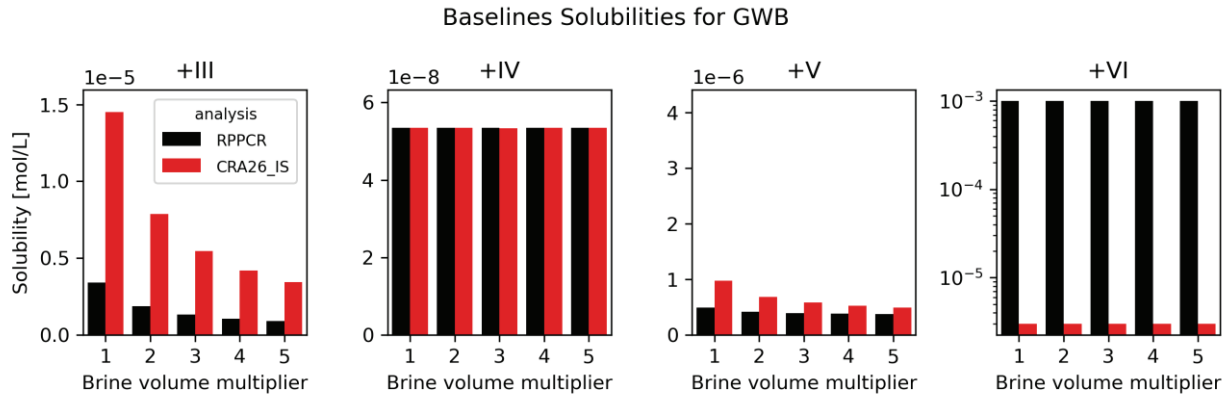


Figure 13. Baseline solubilities for GWB brine

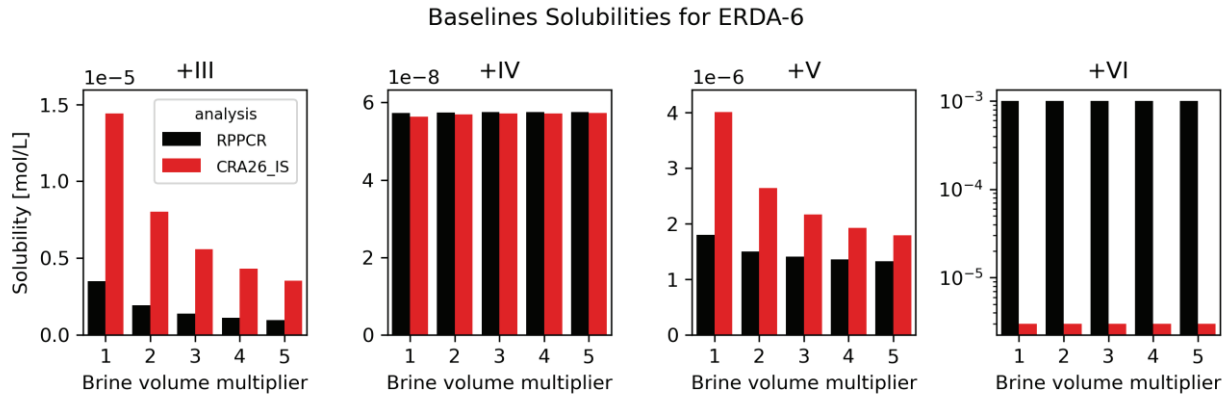


Figure 14. Baseline solubilities for ERDA-6 brine

5.2.2 Uncertainty factor

Solubility uncertainty factors for An(III) and An(IV) are PA's sampled parameters SOLMOD3:SOLVAR and SOLMOD4:SOLVAR. For the CRA26_IS, the cumulative probability distribution from which the SOLMOD3:SOLVAR samples are drawn is updated using data from one new solubility study in the literature that satisfied screening requirements.

Figure 15 plots the new An (III) distribution alongside the version used for the RPPCR. Histograms of SOLMOD3:SOLVAR sampled values for Replicate 1 are plotted in Figure 16.[17] No new studies were found for An(IV) and the RPPCR distribution from which SOLMOD4:SOLVAR samples are drawn is not updated for the CRA26_IS. Figure 17 shows the cumulative distributions for

[17] In this report, the left edge of the first bar in a histogram occurs at the minimum of the data. Width of a bar is 0.4 (no units) in all histograms shown.

Information Only

An(IV) and Figure 18 plots the histograms of SOLMOD4:SOLVAR Replicate 1 samples. SOLMOD4 distributions, sampled values, and histograms are identical in the two analyses. Sampled values of SOLMOD3:SOLVAR and SOLMOD4:SOLVAR are mostly negative, indicating the FM6 database overpredicts An(III) and An(IV) solubilities (Eq. 2).

Information Only

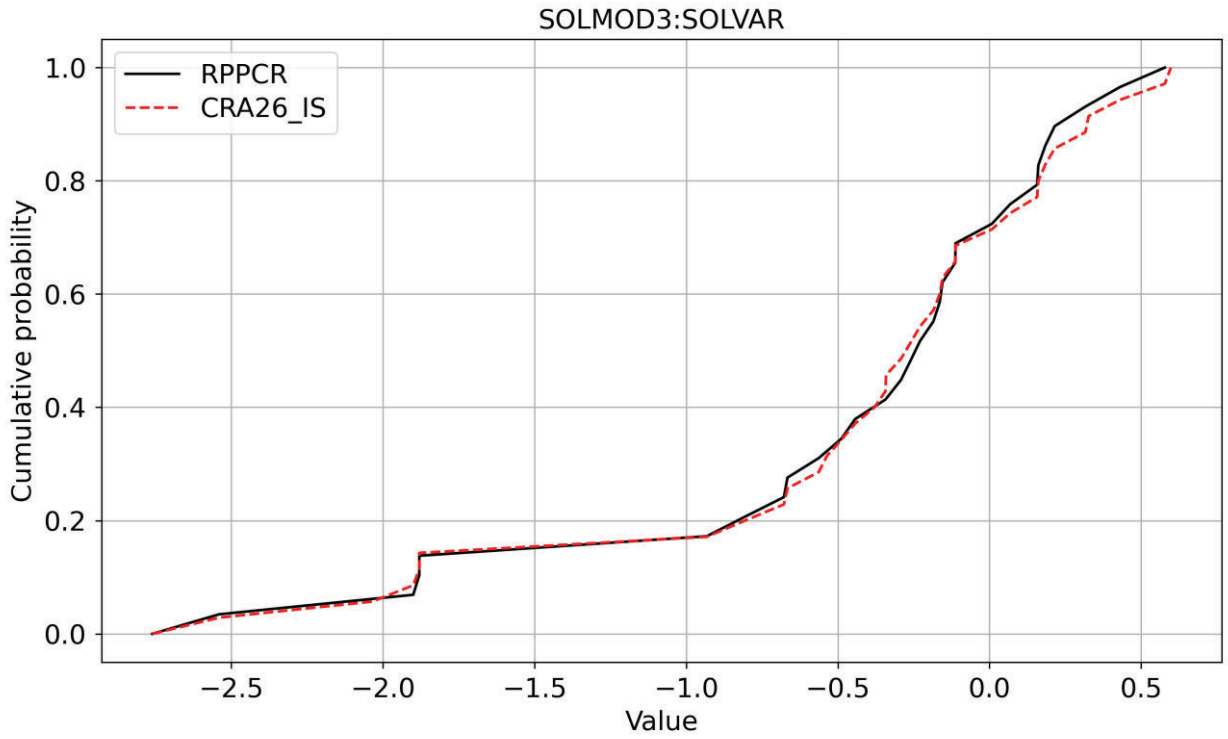


Figure 15. Cumulative probability distributions for SOLMOD3:SOLVAR

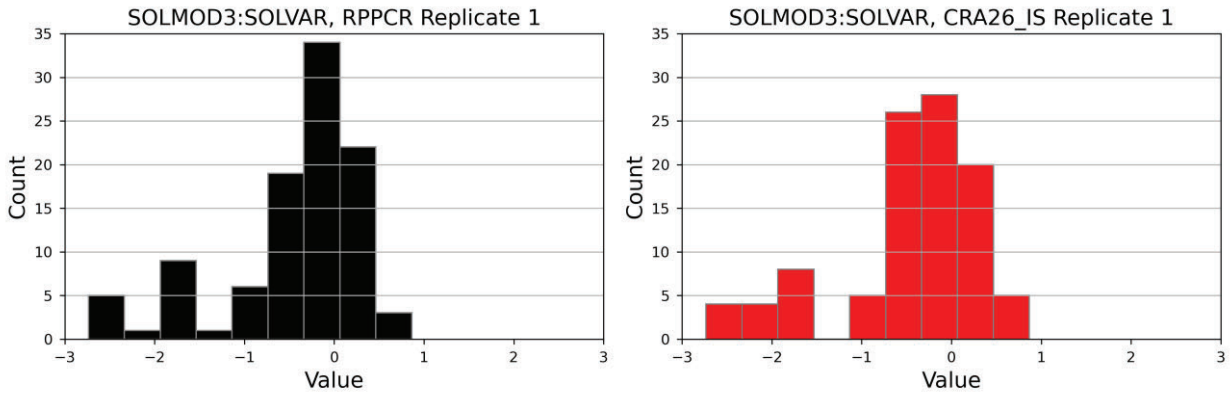


Figure 16. Histograms of SOLMOD3:SOLVAR sample values

Information Only

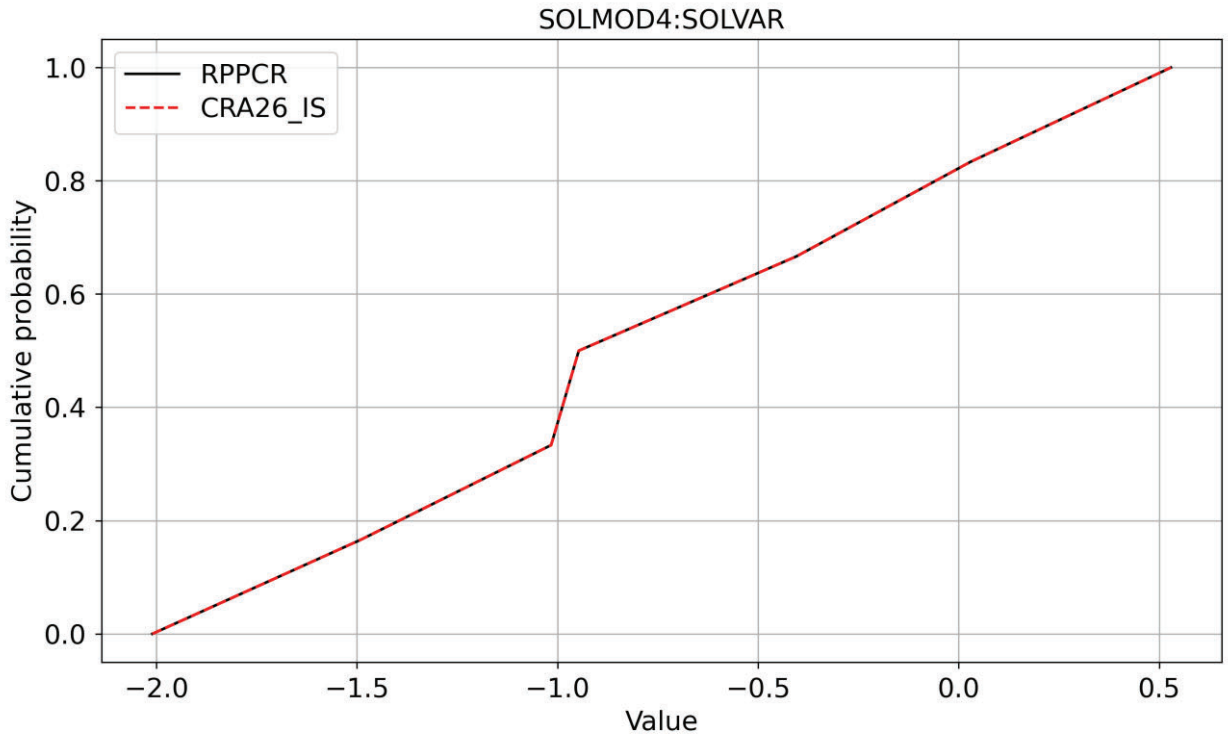


Figure 17. Cumulative probability distributions for SOLMOD4:SOLVAR

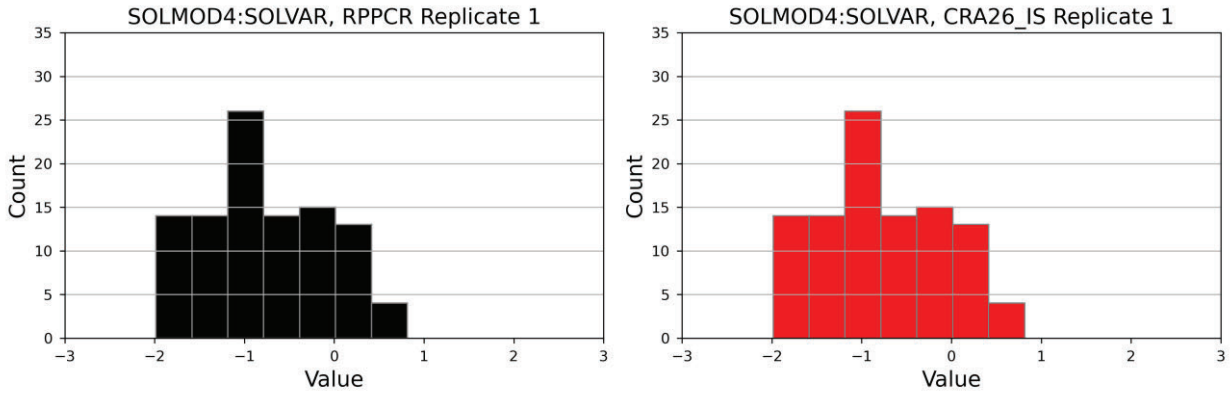


Figure 18. Histograms of SOLMOD4:SOLVAR sample values

Information Only

5.2.3 Actinide solubility

Solubility, $S_{k,dissolved}$, of actinide k in a specific oxidation state is described by Eq. 2 as the product of its baseline solubility, $S_{k,baseline}$, and 10^{u_k}, where u_k is the solubility uncertainty factor. Taking $\log_{10}$ of each side of the equation[18]:

$$log_{10}(S_{k,dissolved}) = log_{10}(S_{k,baseline}) + u_k \quad . \tag{22}$$

Figure 19 compares histograms of $\log_{10}$ of solubility for vectors in Replicate 1 of the RPPCR and the CRA26_IS. Values are determined for each of the primary actinides dissolved in ERDA-6 brine. The brine volume used for the figure is the smallest of the five volumes, that is, baseline solubility values in the "1x" column of Table 6 are used. For Pu, U, and Np, lighter colors indicate counts in the high oxidation state.

Histograms for Am and Th – actinides with a single oxidation state in PA – are the SOLMOD3:SOLVAR and SOLMOD4:SOLVAR histograms (Figure 16 and Figure 18) shifted by $\log_{10}$ of the baseline solubility. For Am the shift is -5.5 for the RPPCR and -4.8 for the CRA26_IS (see 1x values for ERDA-6 and An(III) in Table 6). For Th the shift is -7.2 for the RPPCR and -7.2 for the CRA26_IS.

Pu, with stability for oxidation states +III and +IV, obtains its solubility uncertainty factor as samples of both SOLMOD3:SOLVAR and SOLMOD4:SOLVAR. The RPPCR and CRA26_IS each have PU:OXCUTOFF=0.25, so that 25 values in Replicate 1 are SOLMOD3:SOLVAR samples and 75 are SOLMOD4:SOLVAR samples. The largest values of solubility for Pu occur for oxidation state +III in both analyses, largely a consequence of the much greater baseline solubility of An(III) compared to An(IV) (Table 6).

For U and Np in the high oxidation state, the uncertainty factor is zero making solubility equal to baseline solubility. For both U and Np, the high state is set for half of the vectors in a replicate in both analyses. In their low (+IV) state, U and Np draw samples from SOLMOD4:SOLVAR's distribution. Solubility of U and Np is greatest in the high oxidation state

Changing the brine type from ERDA-6 to GWB results in the histograms in Figure 20. A comparison with Figure 19 indicates that brine type tends to have a small effect on solubility. An exception is the solubility of Np: baseline solubility for An(V) decreases by a factor of more than three in GWB brine (Table 6).

Table 7 gives mean solubility of the primary actinides in ERDA-6 and GWB brines.

[18] Units are removed before taking a logarithm. In the case of Eq. 22, both sides are divided by one mol/L.

Information Only

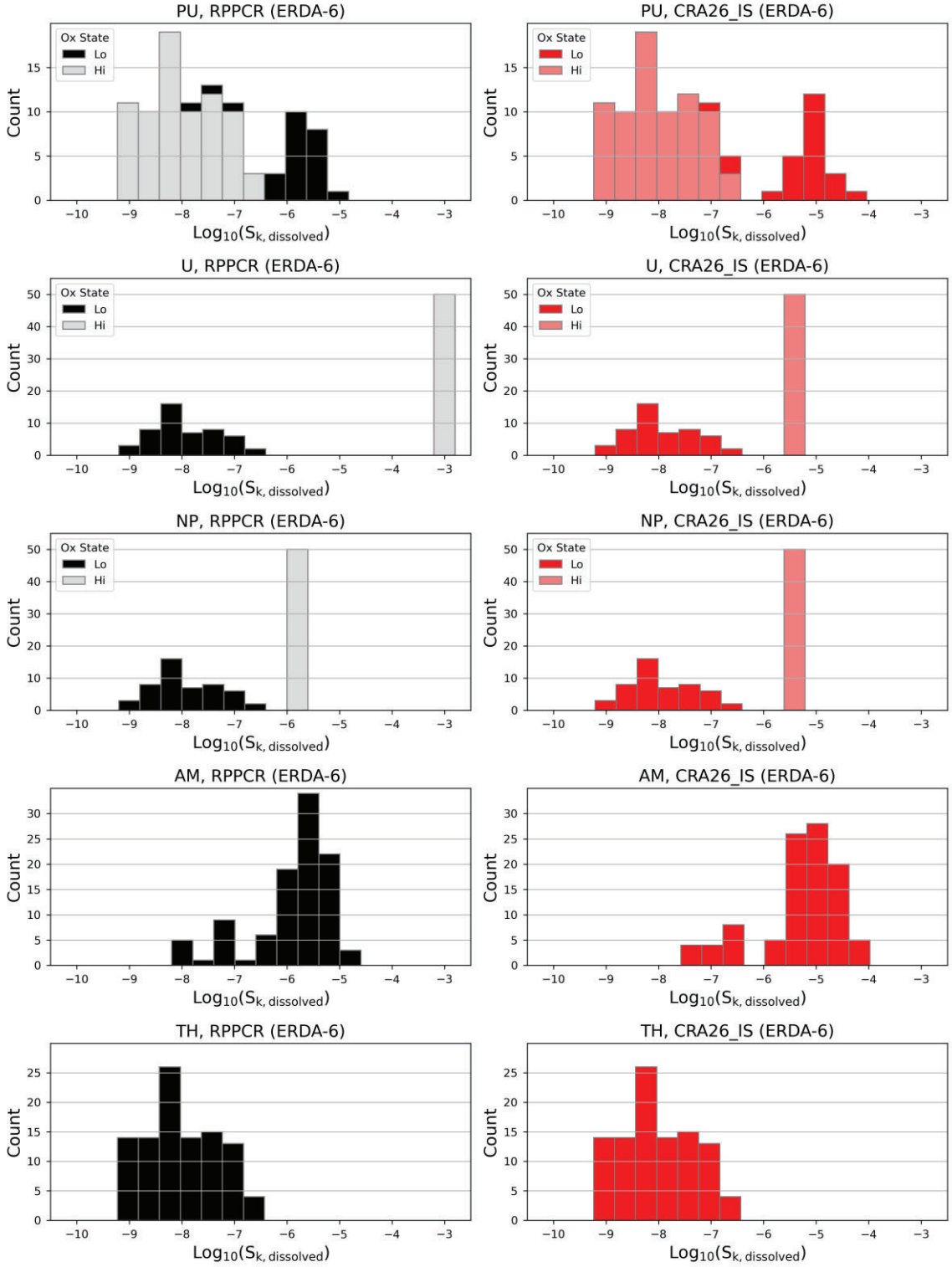


Figure 19. Log_{10} of solubility (Replicate 1, ERDA-6, b = 1)

Information Only

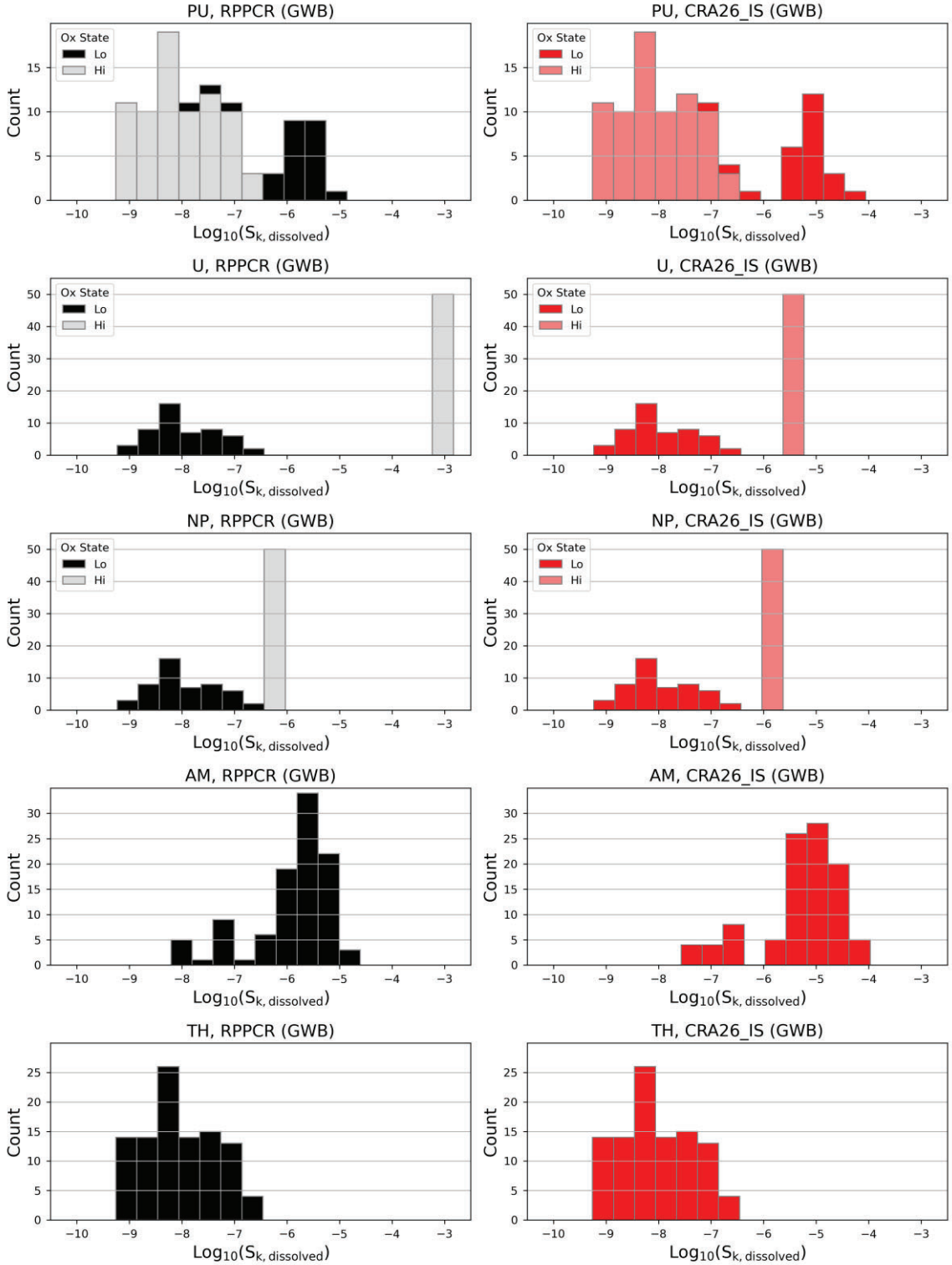


Figure 20. Log_{10} of solubility (Replicate 1, GWB, b = 1)

Information Only

Table 7. Mean solubility in mol/L (Replicate 1, b = 1)

Brine	Analysis	PU	U	NP	AM	TH
ERDA-6	RPPCR	5.64E-07	5.00E-04	9.16E-07	2.68E-06	2.96E-08
ERDA-6	CRA26_IS	2.33E-06	1.52E-06	2.02E-06	1.21E-05	2.90E-08
GWB	RPPCR	5.46E-07	5.00E-04	2.63E-07	2.60E-06	2.75E-08
GWB	CRA26_IS	2.35E-06	1.52E-06	5.03E-07	1.21E-05	2.75E-08

5.2.4 Colloid enhancement parameters

The element mobile concentration limit, S_k, is the sum of solubility and concentrations of actinide aqueous species sorbed to four types of colloids – mineral fragments, intrinsic colloids, humic colloids, and microbial colloids (Eq. 1). Colloid enhancement parameters are introduced to specify the colloid contributions to S_k, as described by Eq. 3. Differences between RPPCR and CRA26_IS colloid enhancement parameters are:

(i) Proportionality constants (for concentration relative to solubility) and cap values for microbial colloids are specified by actinide in the RPPCR (Table 8) and, as recommended by Kaplan et al. (2025), by actinide and oxidation state in the CRA26_IS (Table 9).

(ii) Proportionality constants for humic colloids, which are specified by oxidation state and brine type, are updated for the CRA26_IS (Table 10) by Mariner (2025).

Concentrations associated with mineral fragment and intrinsic colloids are the same for the two analyses, as is the cap for humic colloids. These parameters are specified by actinide (Table 11)

Table 8. PROPMIC (dimensionless) and CAPMIC (mol/L) for the RPPCR

	PU	U	NP	AM	TH
PROPMIC	0.3	0.0021	12.0	3.52	3.1
CAPMIC	1.22×10^{-9}	2.22×10^{-6}	2.33×10^{-6}	9.0×10^{-7}	6.95×10^{-4}

Information Only

Table 9. PROPMIC (dimensionless) and CAPMIC (mol/L) for the CRA26_IS

	PU+3	PU+4	U+4	U+6	NP+4	NP+5	AM+3	TH+4
PROPMIC	2.92	0.3	0.0021	0.0021	12.0	12.0	2.92	3.1
CAPMIC	4.97×10^{-7}	4.07×10^{-9}	9.65×10^{-6}	9.65×10^{-6}	1.52×10^{-7}	1.52×10^{-7}	4.97×10^{-7}	6.95×10^{-4}

Table 10. PHUMSIM and PHUMCIM (dimensionless) for the RPPCR and the CRA26_IS*

	PHUMOX3	PHUMOX4	PHUMOX5	PHUMOX6
PHUMSIM	0.3 (0.2)	0.02 (0.01)	0.00091	0.12
PHUMCIM	0.3 (0.2)	0.01	0.0074	0.51

* RPPCR values, where different to the CRA26_IS, are shown in parentheses.

Table 11. CONCMIN, CONCINT, and CAPHUM (mol/L) for the RPPCR and the CRA26_IS

	PU	U	NP	AM	TH
CONCMIN	2.6×10^{-8}	2.6×10^{-8}	2.6×10^{-8}	2.6×10^{-8}	2.6×10^{-8}
CONCINT	4.3×10^{-8}	1.4×10^{-6}	4.3×10^{-8}	6.7×10^{-7}	4.8×10^{-7}
CAPHUM	1.1×10^{-5}	1.1×10^{-5}	1.1×10^{-5}	1.1×10^{-5}	1.1×10^{-5}

PROPMIC (the proportionality constant for microbial colloids) increases by a factor of about 10 for Pu(III), decreases somewhat for Am(III), and otherwise is unchanged for the CRA26_IS. CAPMIC (the cap value for microbial colloids) increases by a factor of about 400 for Pu(III) in the CRA26_IS. CAPMIC also increases for Pu(IV), U(IV), and U(VI), decreases for Np(IV), Np(V), and Am(III), and remains the same for Th(IV). Humic proportionality constants either increase in the CRA26_IS or are the same as the RPPCR values.

Information Only

5.2.5 Element mobile concentration limits

Histograms of $\log_{10}$ of the element mobile concentration limit, S_k, are shown for each primary actinide in Figure 21. The histograms are for Replicate 1 vectors in the RPPCR and the CRA26_IS, ERDA-6 brine, and minimum brine volume. For Pu, U, and Np, lighter colors indicate counts in the high oxidation state. Similar to the solubility, the element mobilization potentials of U and Np in their higher oxidation states are greater than those in the lower oxidation states, while the element mobilization potentials of Pu(IV) are mostly less than those of Pu(III).

Solubility and colloid contributions are shown as fractions of S_k in Figure 22 and Figure 23, where Pu, U, and Np have been separated into low and high oxidations states. S_k is constant for U and Np in the high oxidation state and Figure 23 uses bar charts to illustrate their fractions. (The uncertainty factor is 0.0 for U(VI) and Np(V). An(VI) baseline solubility is the same for all brine volumes, making S_k for U(VI) constant for all brine volumes. For Np(V), S_k is constant for a given brine volume.)

Comparing Figure 19 and Figure 21, the element mobile concentration limit is seen to span a narrower range than does solubility. In large part this is because the element mobile concentration limit can be no smaller than the sum of mineral fragment and intrinsic colloid-related concentrations. Keeping in mind Eq. 3, the following observations can be made for the individual actinides:

Pu(III): Significant increases in PROPMIC and CAPMIC cause the contribution of microbial colloids to dominate at low values of S_k in the CRA26_IS (Figure 22). In the RPPCR, intrinsic and mineral fragment colloids are the main contributors at small S_k. In both analyses, dissolved ionic species and humic colloids are the largest contributors at large S_k.

Pu(IV): Dissolved ionic species, intrinsic colloids, and mineral fragments are the dominant contributors in both analyses, and their distributions are similar. (Figure 23).

U(IV): Intrinsic colloids dominate in both analyses (Figure 22).

U(VI): The reduction in baseline solubility from 1×10^{-3} mol/L in the RPPCR to 3×10^{-6} mol/L in the CRA26_IS reduces S_k. In the CRA26_IS, dissolved ionic species, humic colloids, and intrinsic colloids are the dominant contributors. In the RPPCR, dissolved ionic species are the dominant contributors (Figure 23).

Np(IV): Intrinsic colloids and mineral fragments dominate at lower values of S_k in both analyses (Figure 22). At higher values of S_k, microbial colloids are the main contributor in the RPPCR. An order of magnitude reduction in CAPMIC reduces the microbial contribution in the CRA26_IS.

Np(V): S_k is dominated by microbial colloid and dissolved ionic species in the RPPCR (Figure 23). A decrease in CAPMIC reduces the microbial contribution in the CRA26_IS, while an increase in baseline solubility enhances the contributions of dissolved ionic species.

Information Only

Am: Intrinsic colloid species dominate at low S_k in both analyses (Figure 23). In the CRA26_IS, microbial colloids contributions decrease somewhat (lower PROPMIC and CAPMIC) while humic colloid contributions increase (higher PHUMOX3).

Th: In both analyses, intrinsic colloids dominate at low S_k (Figure 23). Contributions from dissolved ionic species and microbial colloids grow as S_k increases.

Table 12 lists mean values of S_k for the primary actinides. Mean S_k in both brine types increases in the CRA26_IS for Pu and Am, decreases for U and Np, and is largely unchanged for Th.

Information Only

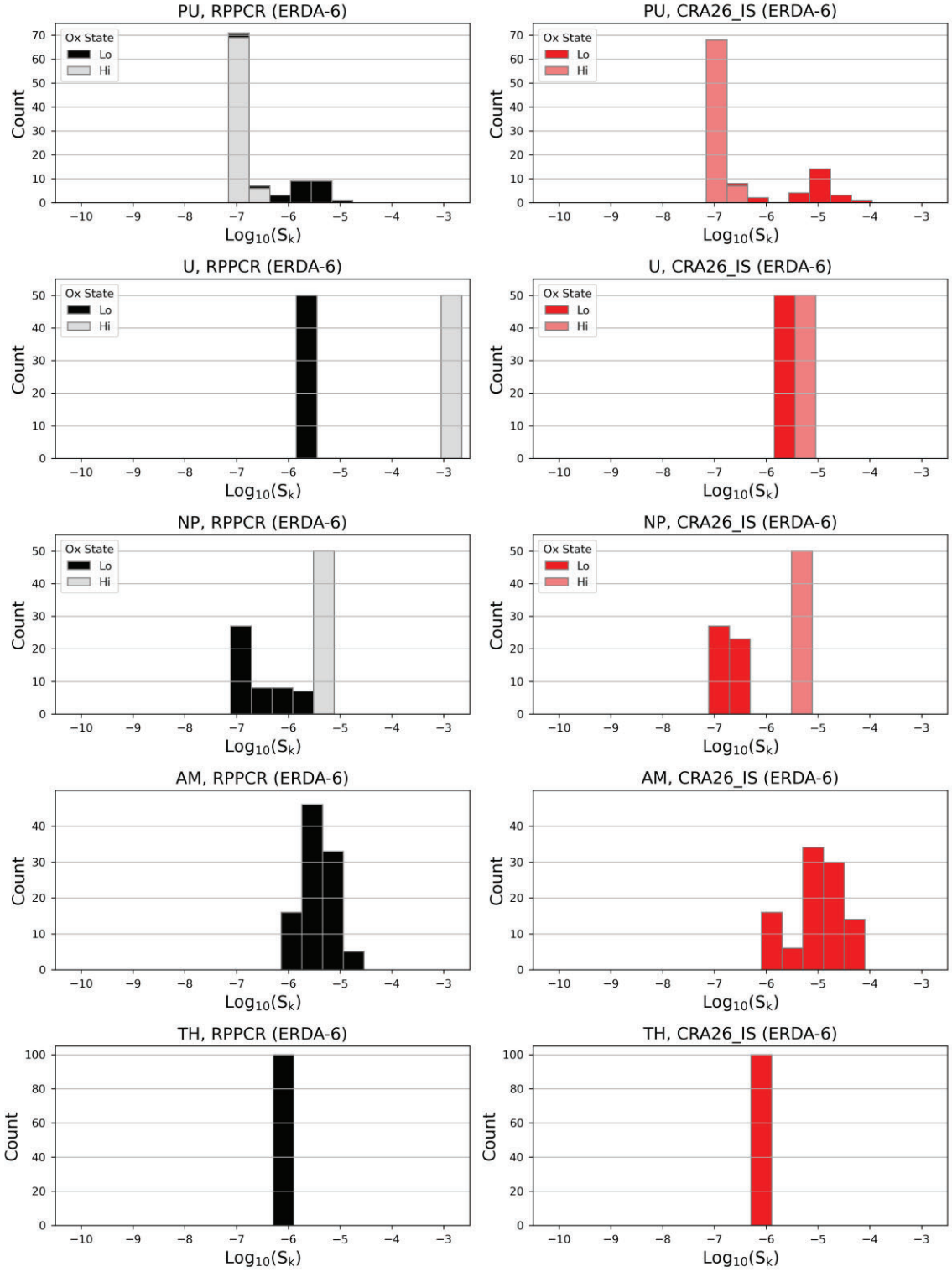


Figure 21. Histograms of Log_{10} of the element mobile concentration limit (Replicate 1, ERDA-6 brine, b = 1)

Information Only

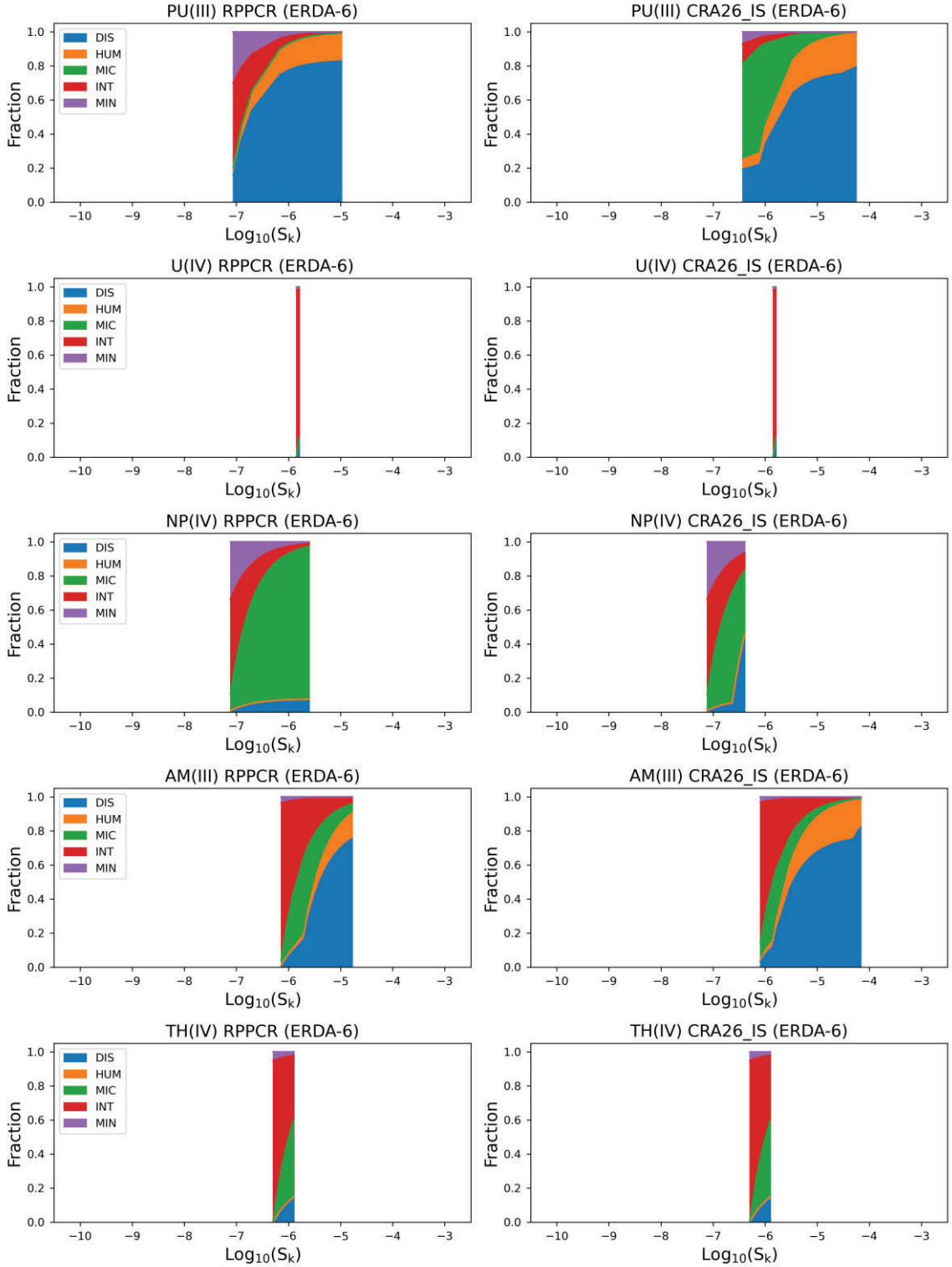


Figure 22. Fractional contributions to the element mobile concentration limit (Replicate 1, ERDA-6 brine, b = 1, low oxidation state for Pu, U and Np)

Information Only

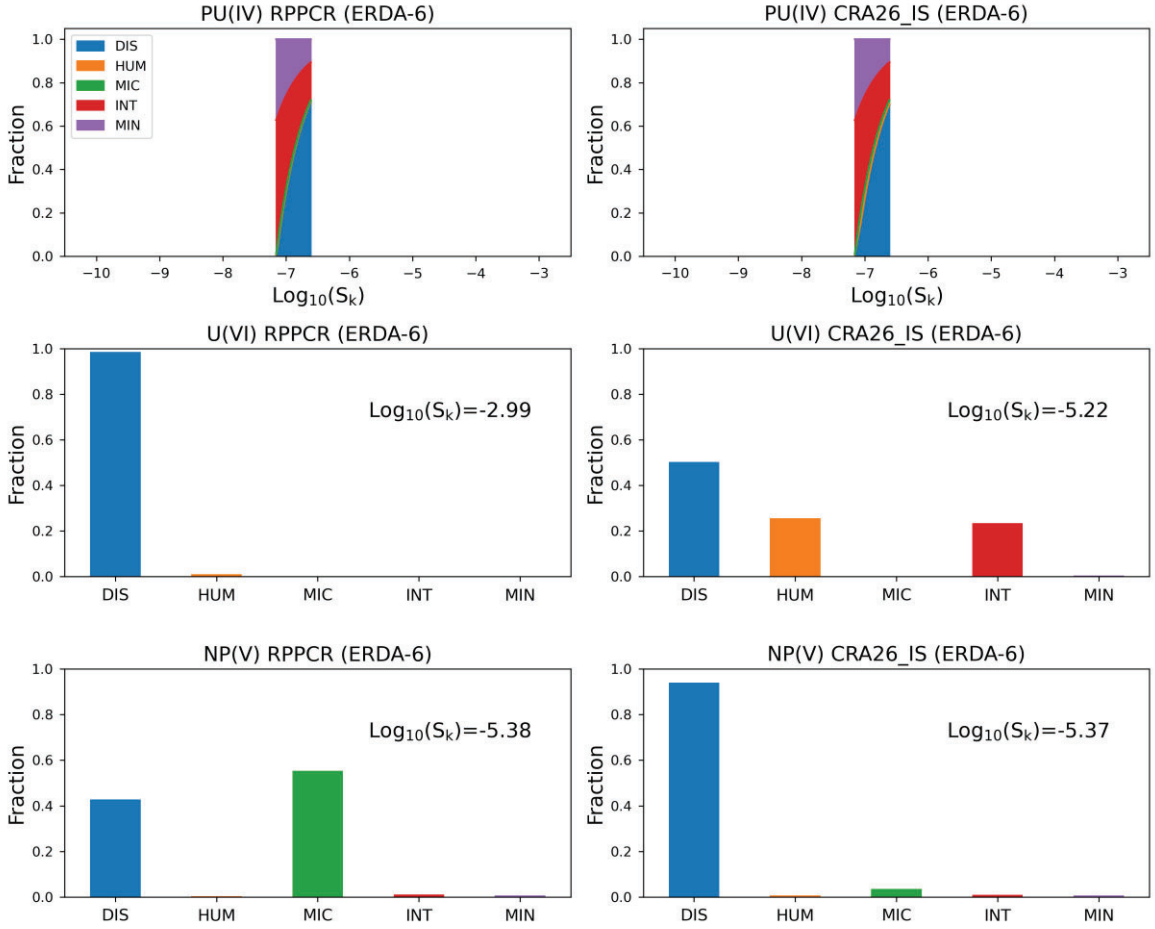


Figure 23. Fractional contributions to the element mobile concentration limit (Replicate 1, ERDA-6 brine, b = 1, high oxidation state for Pu, U and Np)

Table 12. Mean element mobile concentration limits in mol/L (Replicate 1, b = 1)

Brine	Analysis	PU	U	NP	AM	TH
ERDA-6	RPPCR	7.43E-07	5.08E-04	2.35E-06	4.69E-06	6.27E-07
ERDA-6	CRA26_IS	3.20E-06	3.71E-06	2.23E-06	1.66E-05	6.25E-07
GWB	RPPCR	7.21E-07	5.08E-04	1.68E-06	4.59E-06	6.19E-07
GWB	CRA26_IS	3.22E-06	3.12E-06	6.97E-07	1.67E-05	6.19E-07

Information Only

5.2.6 Mobile concentration limits of the lumped radionuclides

PANEL uses Eq. 12 to determine the mobile concentration limit of a lumped radionuclide, $S_{k,j}^{L}$, as the product of the mole fraction, $X_{k,j}^{L}$, and the element mobile concentration limit, S_k, for brine volume multiplier equal to one. Histograms of $\log_{10}(S_{k,j}^{L})$ for Replicate 1 vectors in the RPPCR and the CRA26_IS are plotted in Figure 24. The histograms are simply those for the corresponding actinides in Figure 21 shifted by $\log_{10}(X_{k,j}^{L})$. Figure 10 plots $X_{k,j}^{L}$ for PU238L, U234L, and TH230L. The value of $X_{k,j}^{L}$ is 1.0 for PU239L and AM241L (Eq. 11).

Information Only

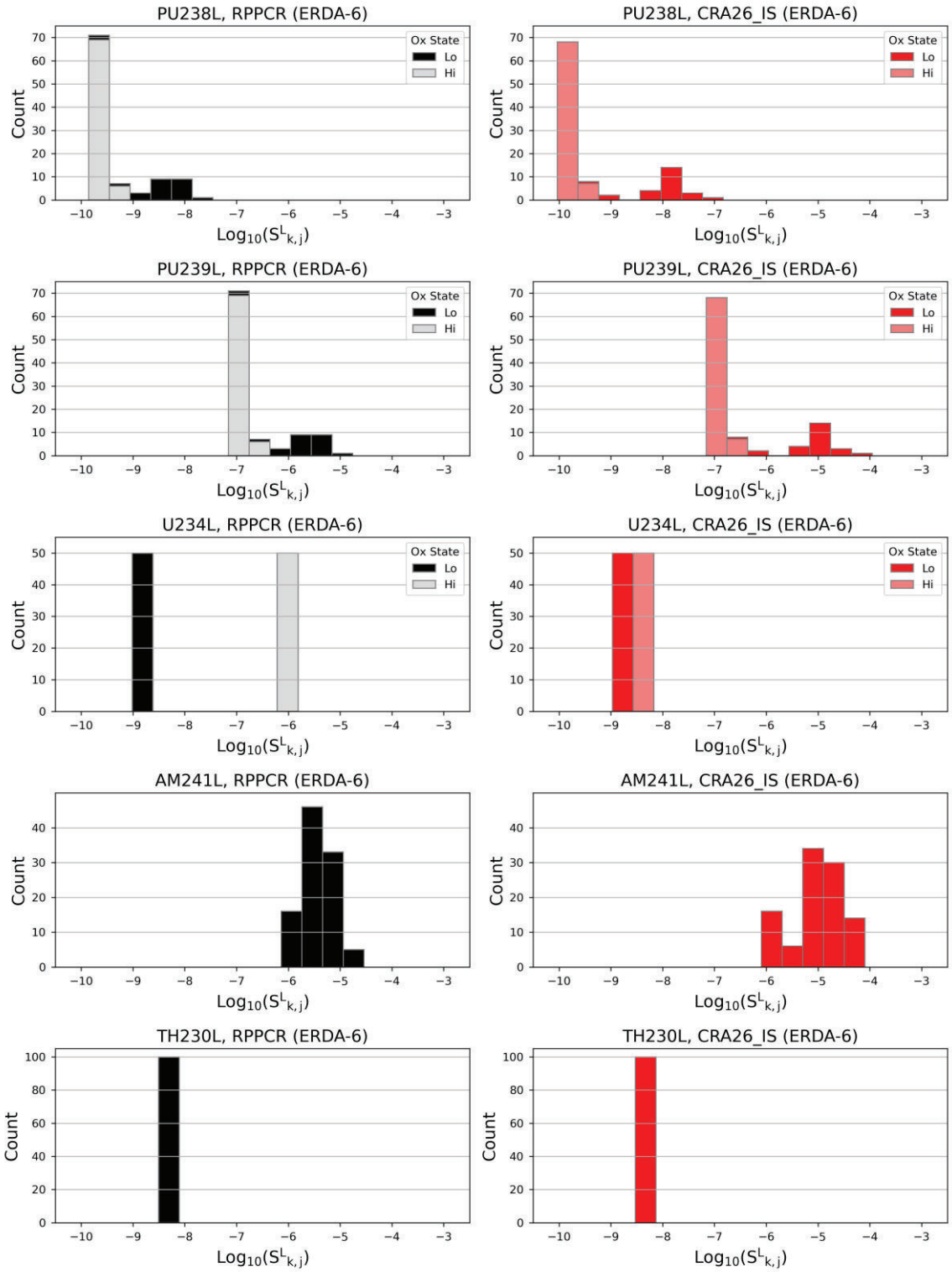


Figure 24. Histograms of Log_{10} of the lumped radionuclide mobile concentration limit (Replicate 1, ERDA-6, b = 1)

Information Only

Table 13 lists mean values of $S_{k,j}^{L}$. Mean $S_{k,j}^{L}$ in both brine types increases in the CRA26_IS for PU238L, PU239L, and AM241L, and decreases for U234L. The mean for TH230L is approximately the same for both brines and both analyses.

Table 13. Mean values of lumped radionuclide mobile concentration limit in mol/L (Replicate 1, b = 1)

Brine	Analysis	PU238L	PU239L	U234L	AM241L	TH230L
ERDA-6	RPPCR	1.48E-09	7.43E-07	3.46E-07	4.69E-06	3.85E-09
ERDA-6	CRA26_IS	4.25E-09	3.20E-06	2.79E-09	1.66E-05	3.62E-09
GWB	RPPCR	1.44E-09	7.21E-07	3.46E-07	4.59E-06	3.80E-09
GWB	CRA26_IS	4.27E-09	3.22E-06	2.35E-09	1.67E-05	3.59E-09

5.2.7 Radionuclide concentrations for DBRs as a function of time

PANEL uses Eq. 6 to determine the concentrations of 26 radionuclides (listed at the beginning of Section 3.1) for a period of 10,000 years starting at repository closure. The sum of the concentrations, $c_{DBR}(t)$, is used in the determination of DBRs (Section 3.1.8).

Figure 25 shows concentration in EPA units/m^3 as a function of time for 9 radionuclides in the RPPCR. The curves plotted are mean values for the 100 vectors of Replicate 1 and for the minimum volume of brine in the waste area, that is, for b=1 in Eq. 6. The 9 radionuclides are constituents of the lumped radionuclides (Table 4).[19] The mean of $c_{DBR}(t)$ for Replicate 1, designated CDBR here, is also shown in Figure 25. The concentrations for the CRA26_IS are shown in Figure 26.

In both Figure 25 and Figure 26, ^{241}Am dominates at early times, while ^{239}Pu and ^{240}Pu become more significant at later times. ^{238}Pu, with a half-life of 87.8 years, decays rapidly. Beyond about 1,000 years, the next largest contributor to CDBR is ^{234}U in the RPPCR and ^{230}Th in the CRA26_IS; however, at these times their mean concentrations are down approximately two orders of magnitude, or more, compared to CDBR in the two analyses. Consequently, this report will focus on ^{241}Am, ^{239}Pu, ^{240}Pu, and DBR concentrations.

Figure 27 compares the mean concentrations of ^{241}Am, ^{239}Pu, and ^{240}Pu, and CDBR, from the previous two figures. The figure shows the mean concentrations in the CRA26_IS are higher than those in the RPPCR. At closure, CDBR in the CRA26_IS is 2.6 times the RPPCR value; at 10,000 years, CDBR in the CRA26_IS is 2.1 times the RPPCR value.

When determining a DBR, code CCDFGF interpolates the concentrations obtained by PANEL for the five brine volume multipliers. A change to DBRMINBV for the CRA26_IS means that CCDFGF will, in general, interpolate between different b-values in the two analyses for a given volume of brine in the waste at the time of an intrusion. Figure 28 compares mean concentrations

[19] ^{241}Pu, also used in lumping, is not regulated and thus cannot be converted to EPA units.

Information Only

of ^{241}Am, ^{239}Pu, ^{240}Pu, and CDBR for the largest brine volume multiplier, that is, b=5. As in Figure 27, mean concentrations are higher in the CRA26_IS.

Radionuclide mobile concentration limit, $S_{k,j}(t)$, is the product of the element mobile concentration limit, S_k, and the mole fraction $X_{k,j}(t)$ (Eq. 4). Inventory at closure, decay, and ingrowth alone determine $X_{k,j}(t)$, meaning it is the same for all simulations, that is, all vectors, in an analysis. The element mobile concentration limit, on the other hand, varies between vectors (Sections 3.1.1 - 3.1.3). For element k, if S_k^{min} and S_k^{max} are the minimum and maximum values of S_k in a replicate, then vectors that realize these values will bound $S_{k,j}(t)$ for the replicate. For Replicate 1 and brine volume multiplier b=1, Figure 29 shows $S_k^{min} \times X_{k,j}(t)$ and $S_k^{max} \times X_{k,j}(t)$ – the black dashed curves in the figure – for ^{241}Am, ^{239}Pu and ^{240}Pu in the two analyses. Note that the bounds span a wider range in the CRA26_IS for all three radionuclides, largely due to S_k extending to higher values for Am and Pu (Figure 21).

The blue curves in Figure 29 are the inventory limits, $I_{k,j}(t)/V_{min}$, for ^{241}Am, ^{239}Pu and ^{240}Pu, with b=1 in Eq. 6. The inventory limits are increased in the CRA26_IS. The figure indicates, for the minimum brine volume, that (i) concentrations of ^{239}Pu and ^{240}Pu are solubility limited for all vectors and at all times in the two analyses; and (ii) ^{241}Am concentrations for a given vector are solubility limited at early times and inventory limited at later times.

Figure 30 plots ^{241}Am, ^{239}Pu and ^{240}Pu concentrations for all 100 vectors of Replicate 1 in the RPPCR and the CRA26_IS, illustrating the behavior just described. The concentrations are the result of implementing Eq. 6 with b=1 and EDA-6 brine. Figure 31 plots $c_{DBR}(t)$ for all vectors of Replicate 1 in the two analyses. The red curves in Figure 30 and Figure 31 are mean concentrations; these were previously shown in Figure 27.

Information Only

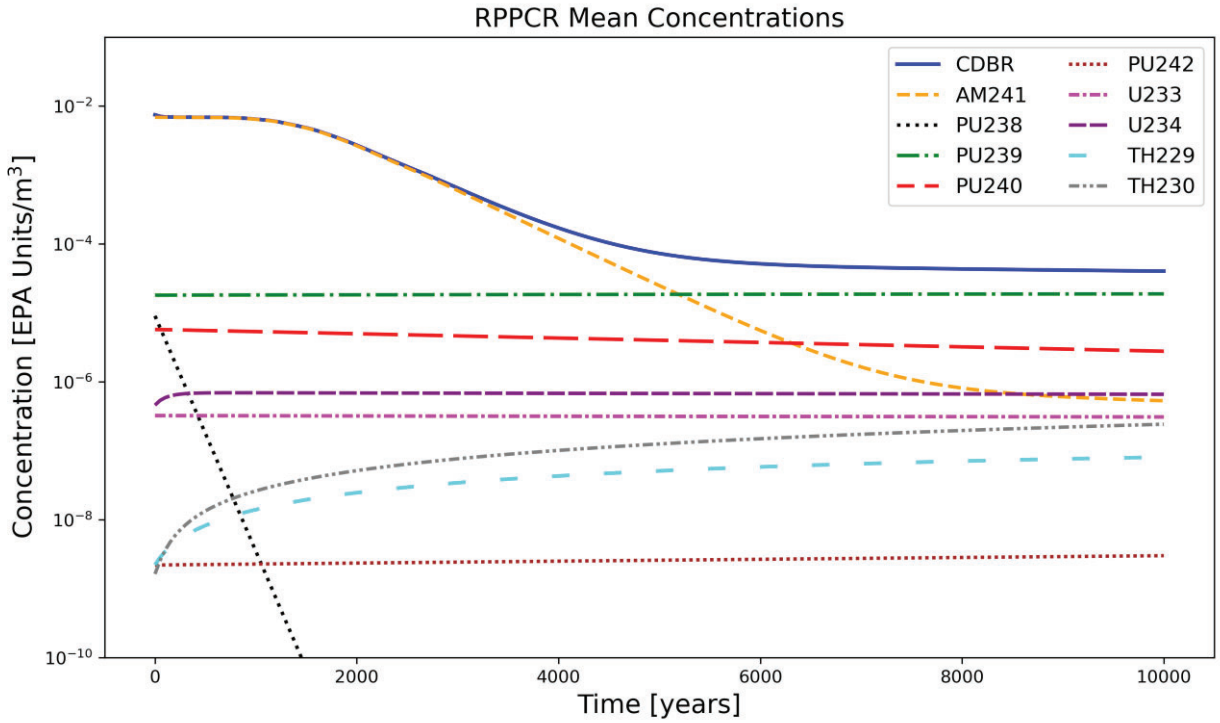


Figure 25. RPPCR mean concentrations versus time (Replicate 1, ERDA-6, b = 1)

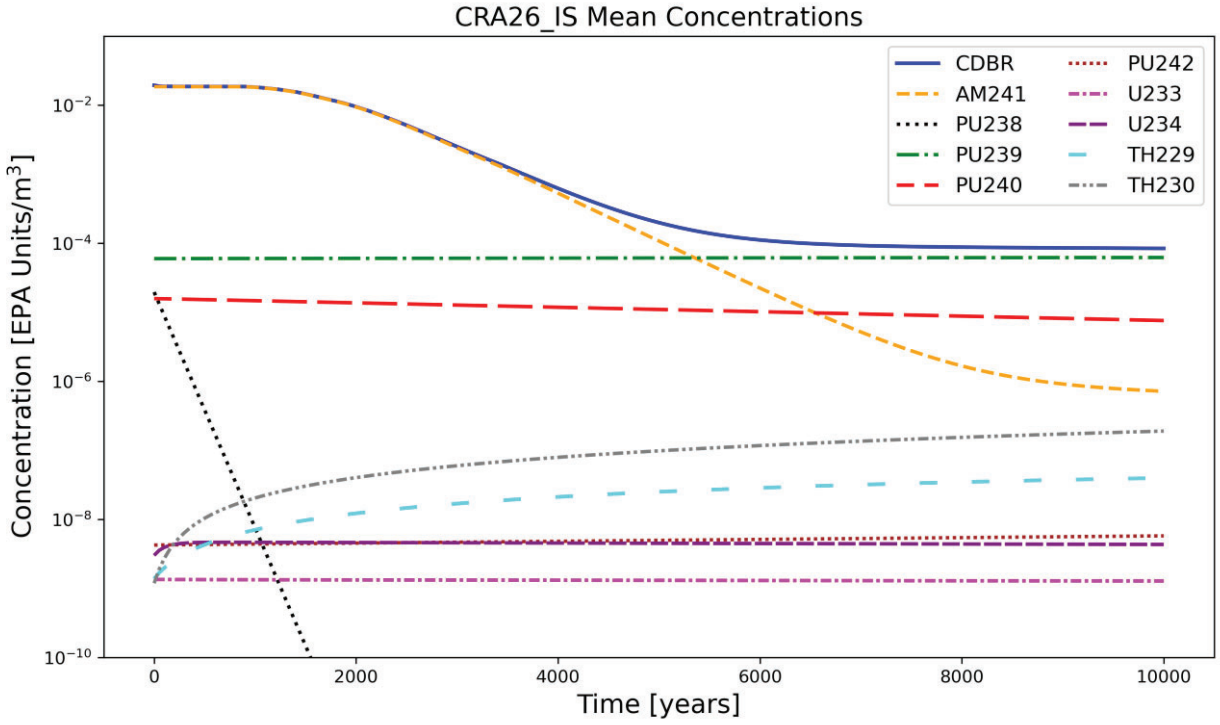


Figure 26. CRA26_IS mean concentrations versus time (Rep. 1, ERDA-6, b = 1)

Information Only

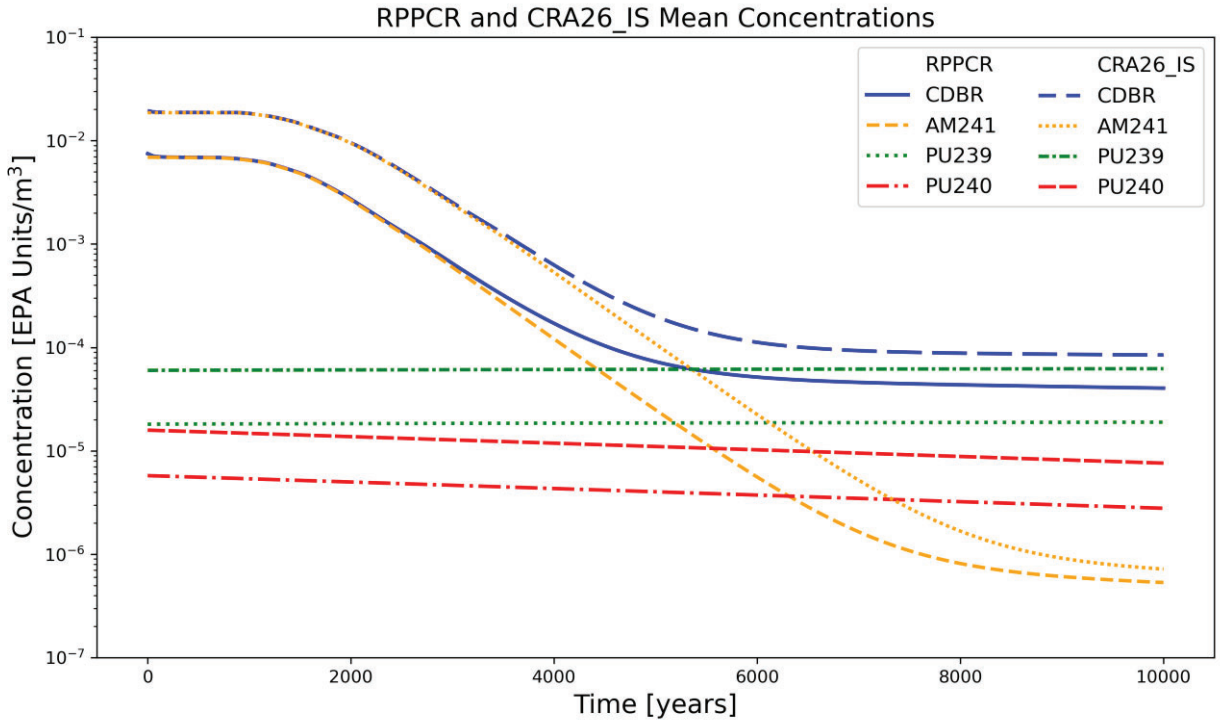


Figure 27. Comparison of mean concentrations (Replicate 1, ERDA-6, b = 1)

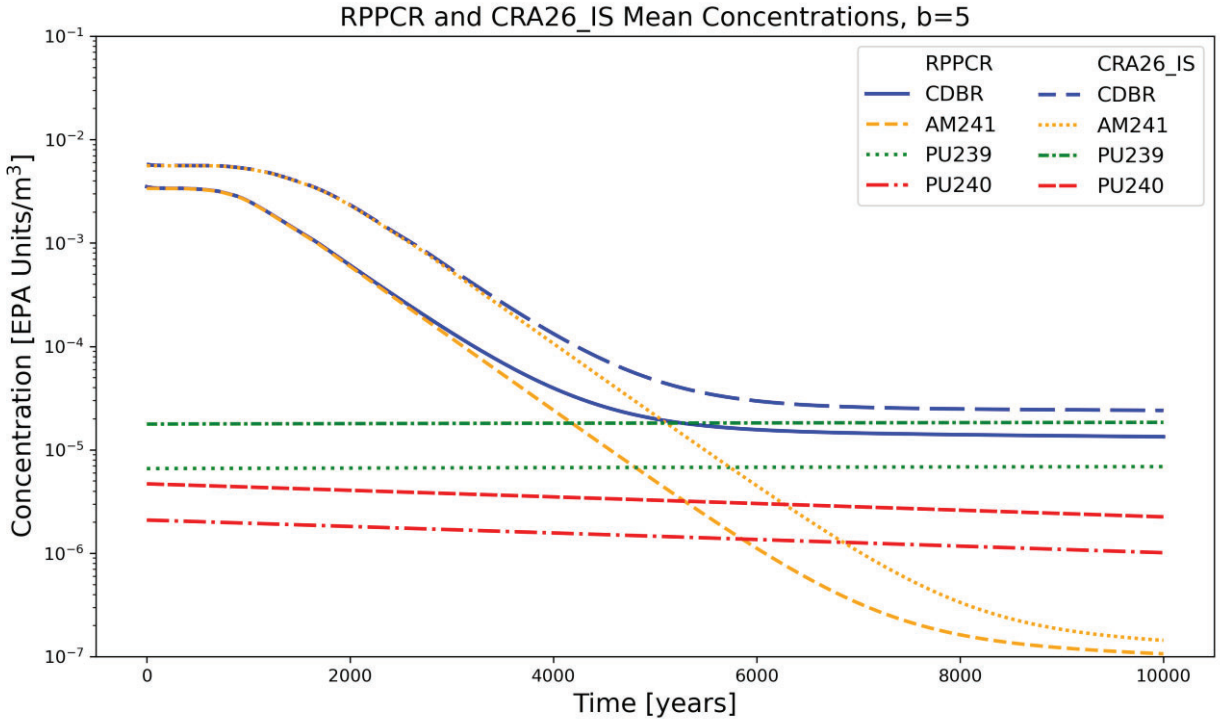


Figure 28. Comparison of mean concentrations (Replicate 1, ERDA-6, b = 5)

Information Only

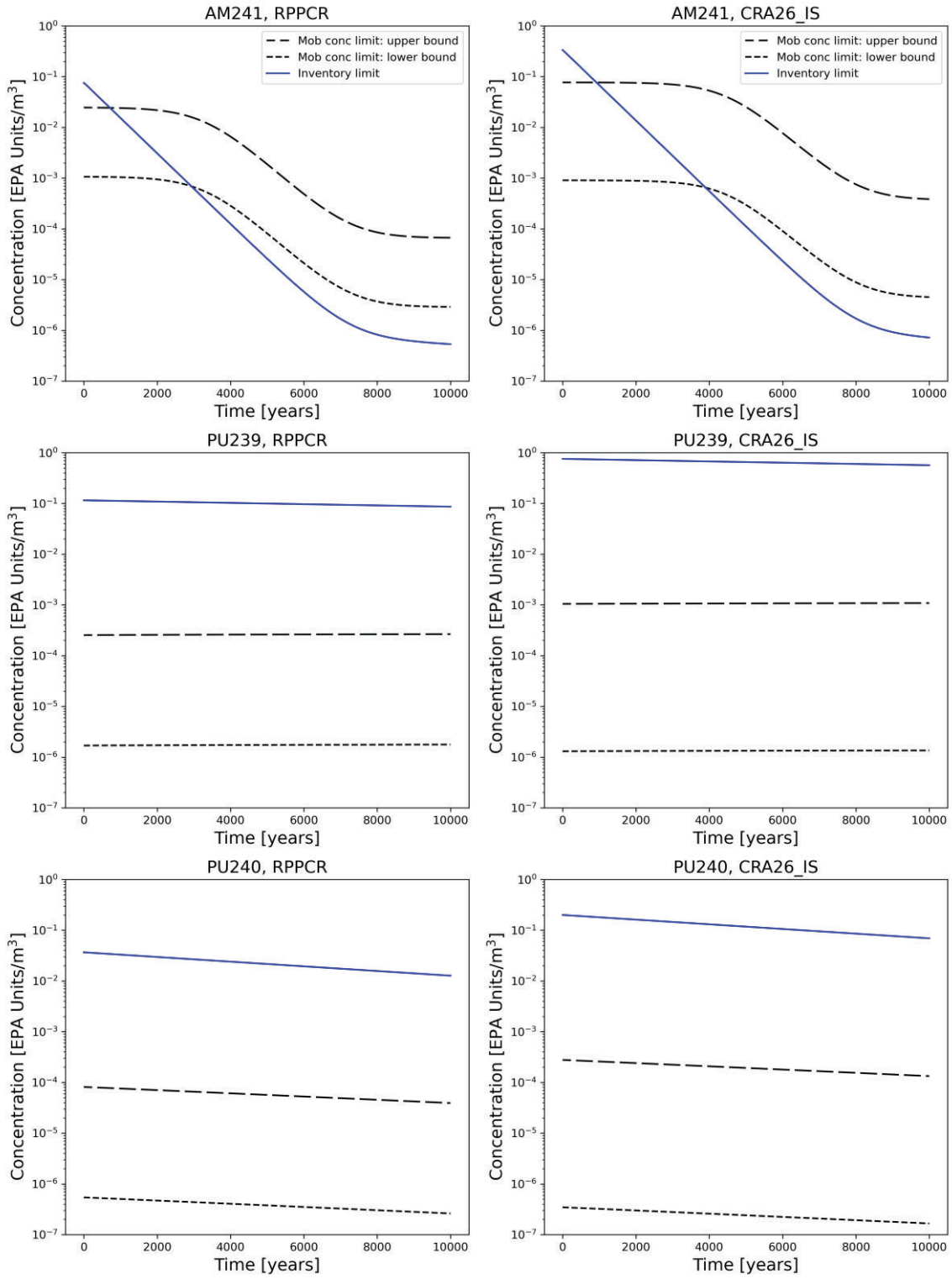


Figure 29. Radionuclide mobile concentration limit bounds and inventory limit (Replicate 1, ERDA-6, b = 1)

Information Only

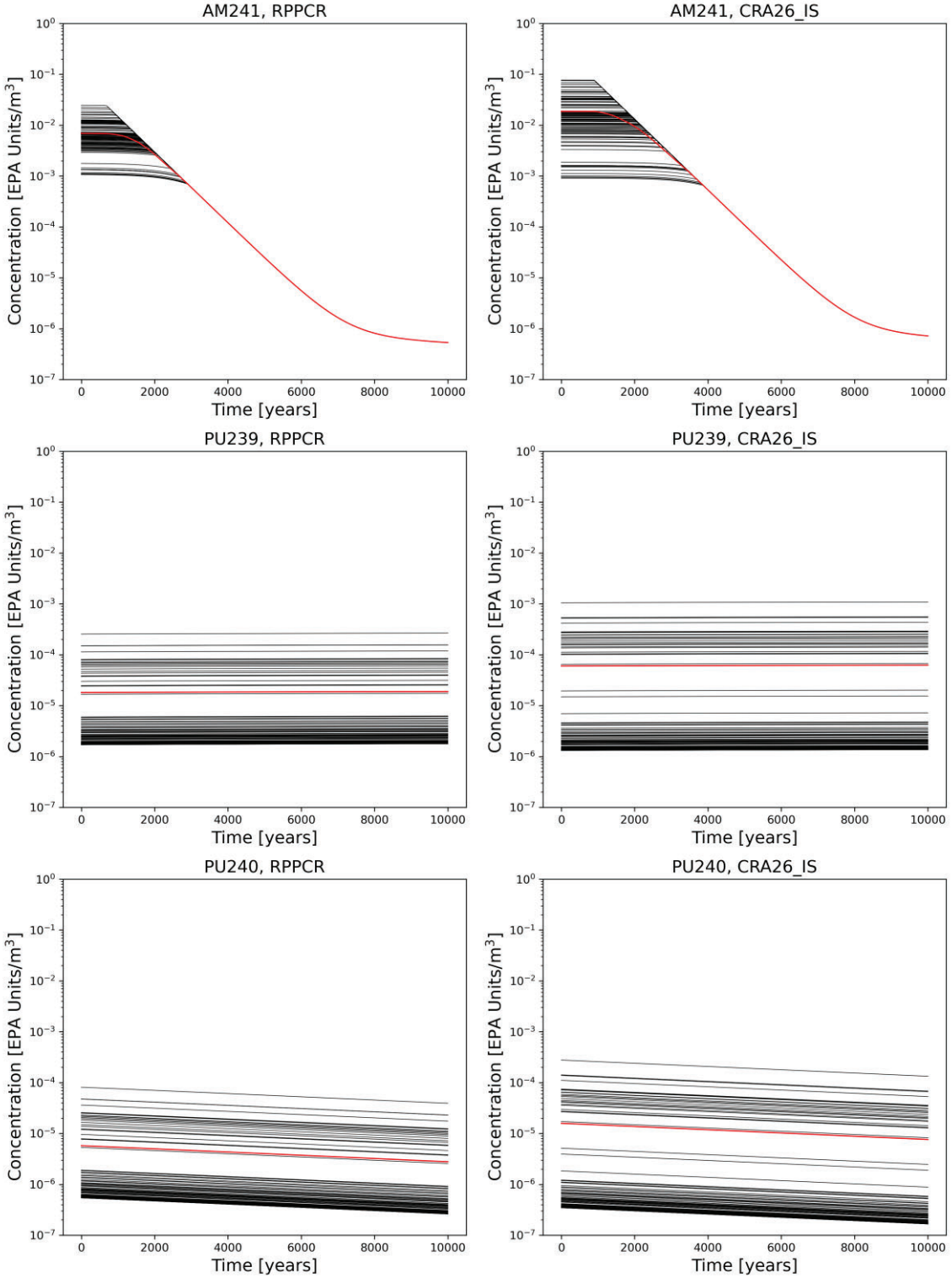


Figure 30. Concentration versus time, all vectors (Replicate 1, ERDA-6, b = 1)

Information Only

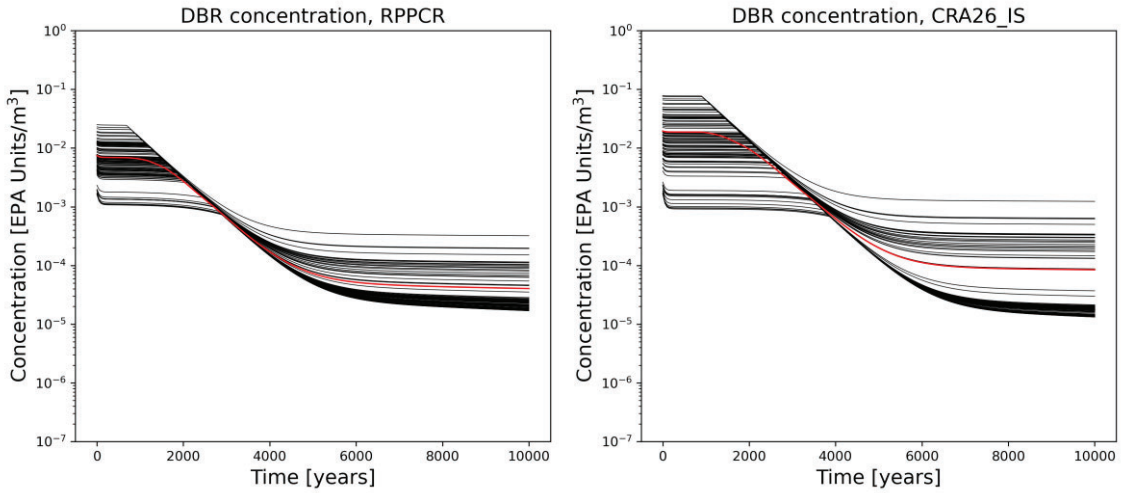


Figure 31. DBR concentration versus time, all vectors (Replicate 1, ERDA-6, b = 1)

Distributions of ^{241}Am, ^{239}Pu, ^{240}Pu, and DBR concentrations are shown at specific times in the box plots in Figure 32-Figure 35.[20] Data for the distributions are obtained by taking vertical cuts through the concentrations in Figure 30 and Figure 31 at the times specified.

[20] In this report the box bottom and top edges indicate the 25th and 75th percentiles, the box interior line indicates the 50th percentile (median), and the green triangle marker indicates the mean. The "whiskers" (the extended vertical lines with horizontal bars) indicate the 2nd and 98th percentiles, while the diamond markers exterior to the bars are discrete outliers (less than the 2nd percentile or greater than the 98th percentile).

Information Only

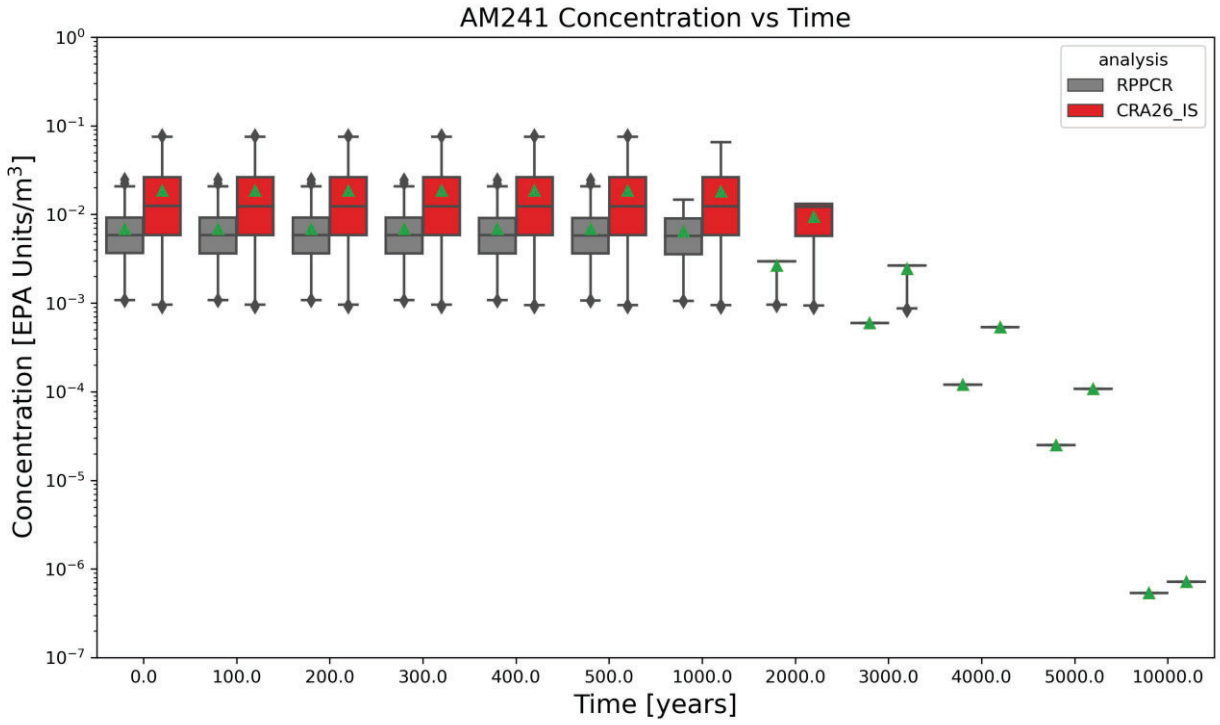


Figure 32. AM241 concentration vs time (Replicate 1, ERDA-6, b = 1)

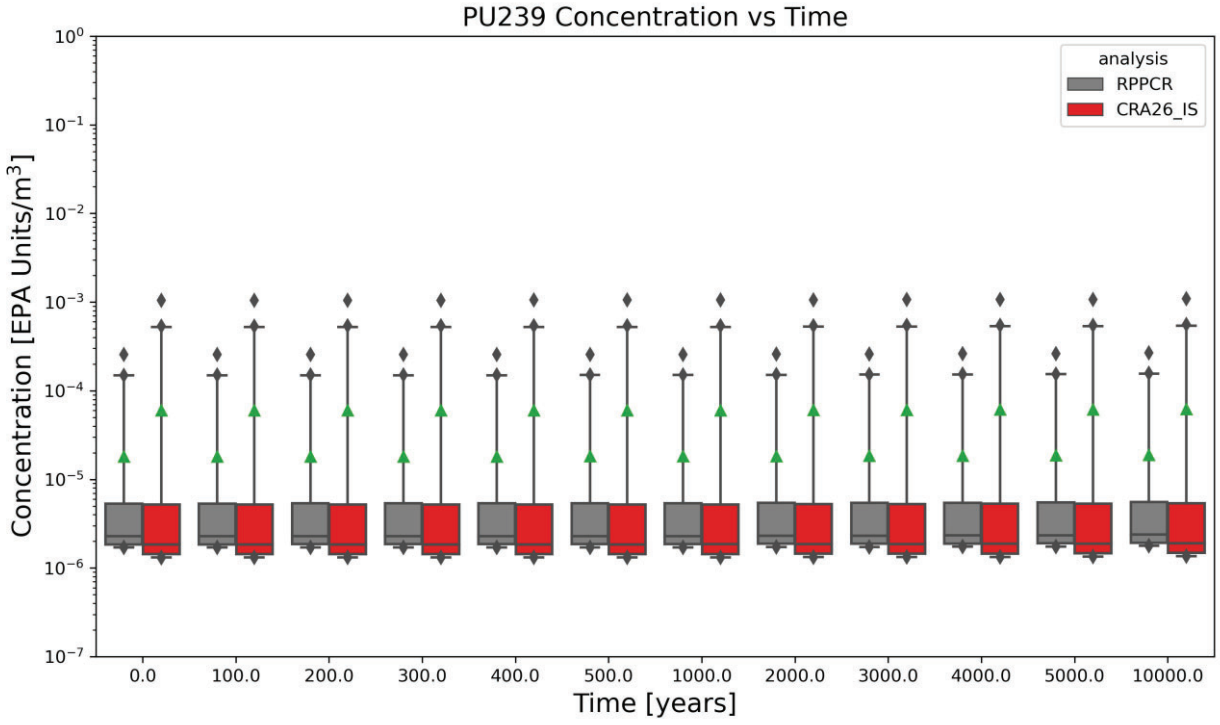


Figure 33. PU239 concentration vs time (Replicate 1, ERDA-6, b = 1)

Information Only

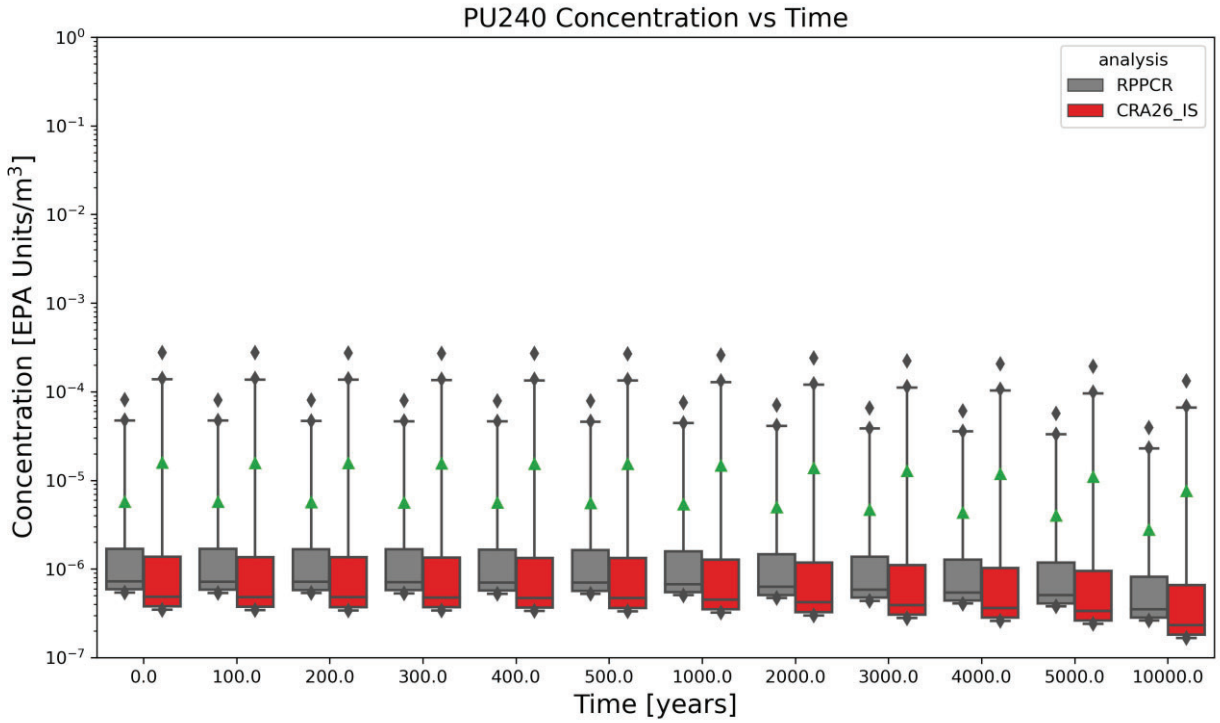


Figure 34. PU240 concentration vs time (Replicate 1, ERDA-6, b = 1)

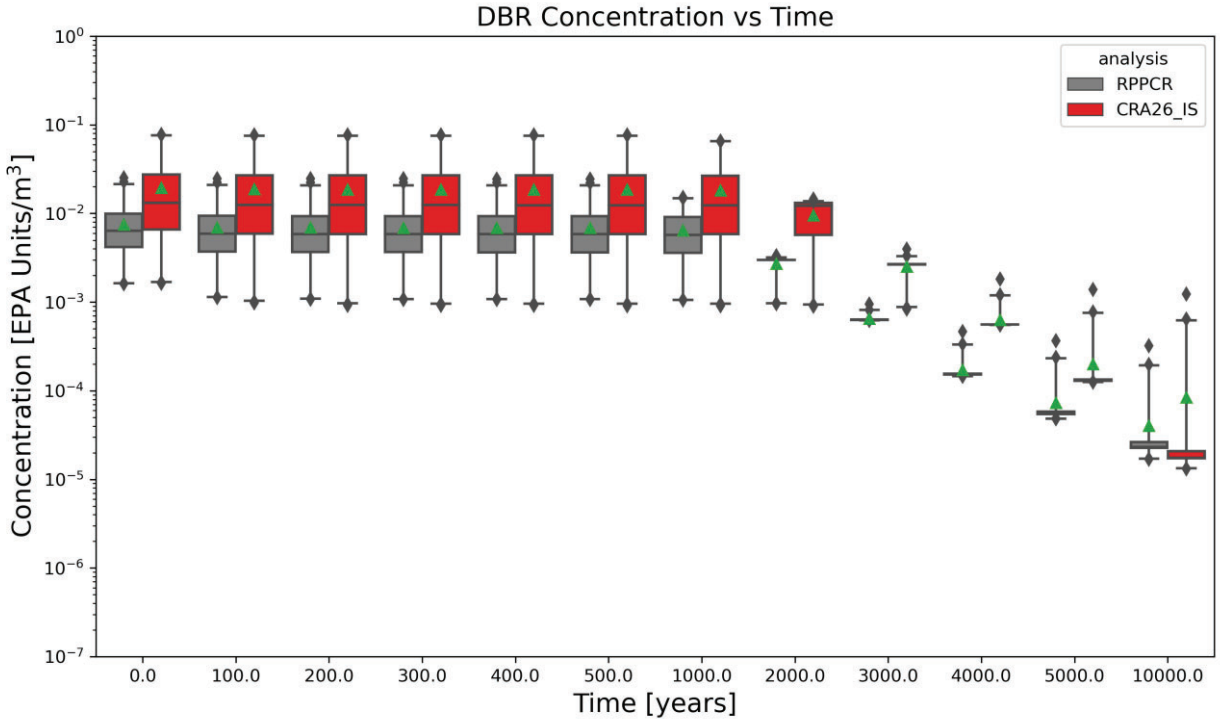


Figure 35. DBR concentration vs time (Replicate 1, ERDA-6, b = 1)

Information Only

5.3 NUTS and PANEL: radionuclide transport

NUTS models transport for the five lumped radionuclides everywhere that BRAGFLO models fluid flow; however, NUTS *to Culebra* transport releases are by far the most significant. PANEL only models *to Culebra* transport releases. NUTS determines *to Culebra* releases for intrusion scenarios 1-5 (Section 4.4). PANEL determines *to Culebra* releases for scenario 6 (Section 3.3). NUTS and PANEL *to Culebra* results are presented together below.

5.3.1 Brine flow to the Culebra

Both NUTS and PANEL require brine flow data as input: cumulative brine discharge up the borehole for PANEL; brine flow rate between grid cells for NUTS. Figure 36 shows cumulative brine discharge up the borehole for all six intrusion scenarios in the RPPCR and the CRA26_IS. Mean, maximum, and median of the cumulative brine flow are given in Table 14. For the figure and the table, brine flow has been accumulated at the intersection of the borehole and MB138; or, for scenario 1,with no intrusion, at the same model grid cell.

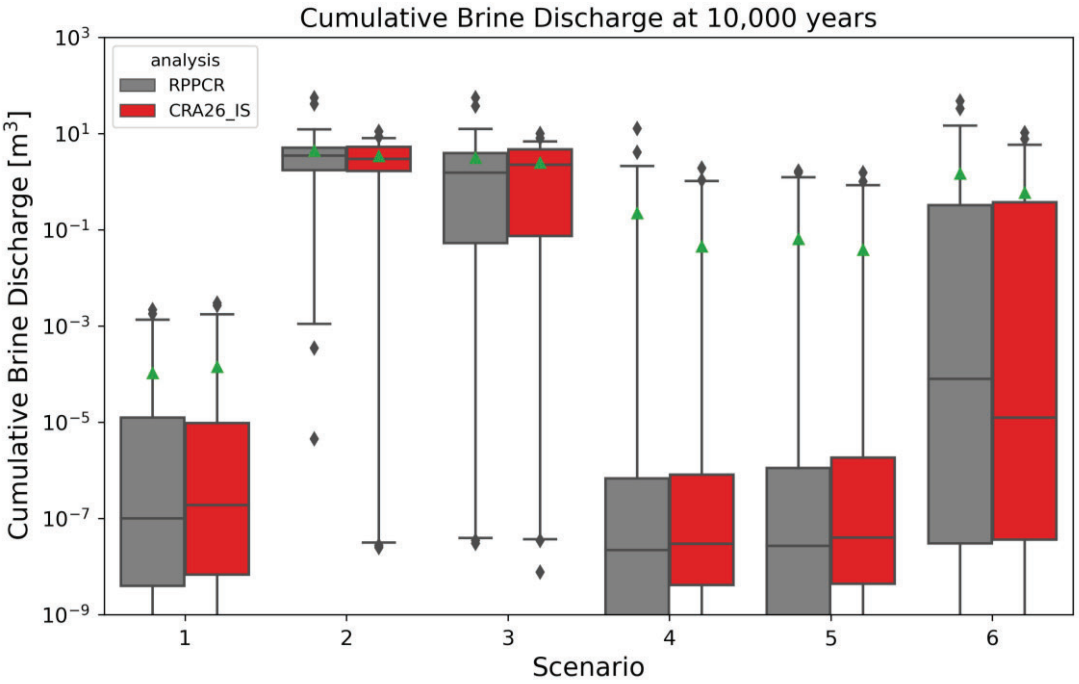


Figure 36. Cumulative brine discharge up the borehole (Replicate 1)

Cumulative brine discharge is largest in scenarios 2, 3 and 6 – the scenarios involving an intrusion into the Castile. Most simulations in scenarios 4 and 5 have cumulative brine discharge less than 1.0×10^{-7} m^3. For scenarios 2-6, mean brine discharge is decreased in the CRA26_IS compared to the RPPCR.

Information Only

Table 14. Mean, maximum and median cumulative brine discharge up the borehole at 10,000 years (Replicate 1)

Scenario	RPPCR mean (m^3)	CRA26_IS mean (m^3)	RPPCR max (m^3)	CRA26_IS max (m^3)	RPPCR median (m^3)	CRA26_IS median (m^3)
1	1.05E-04	1.43E-04	2.16E-03	2.99E-03	9.93E-08	1.89E-07
2	4.44E+00	3.41E+00	5.55E+01	1.10E+01	3.45E+00	2.98E+00
3	3.15E+00	2.48E+00	5.61E+01	9.99E+00	1.54E+00	2.23E+00
4	2.23E-01	4.53E-02	1.26E+01	1.91E+00	2.20E-08	2.98E-08
5	6.50E-02	3.81E-02	1.67E+00	1.55E+00	2.69E-08	4.02E-08
6	1.46E+00	5.94E-01	4.70E+01	1.04E+01	8.02E-05	1.24E-05

5.3.2 NUTS vector screening

NUTS runs SCN (Screening) mode simulations to identify vectors likely to contribute appreciably to transport releases (Section 4.1). Screening mode is run for all vectors and all five NUTS modeling scenarios (Table 5). In a screening simulation, NUTS assigns a tracer concentration of 1 kg/m^3 to brine leaving the waste area. If the cumulative mass of tracer crossing the LWB via the marker beds, or entering the Culebra via the shaft and borehole, exceeds 10^{-7} kg at 10,000 years, then the vector is screened in for NUTS ISO and NUTS INT simulations.

No vector was screened in based on transport through the anhydrite marker beds to the LWB, for any scenario in either analysis. In the RPPCR, the maximum tracer release through the marker beds is 3.6×10^{-8} kg for MB139 at the LWB to the south in scenario 1. In the CRA26_IS, the maximum tracer release through the marker beds is 9.9×10^{-12} kg for MB139 at the LWB to the south in scenario 4.

No vector was screened-in for the release pathway up the shaft to the Culebra. The maximum cumulative tracer discharge up the shaft is less than 1×10^{-40} kg in both the RPPCR and the CRA26_IS, which is below the level of numerical noise in the simulation.

Figure 37 shows cumulative tracer discharges through the borehole to the Culebra and Table 15 lists mean, maximum, and median tracer discharge amounts. Screened-out vectors have been assigned a cumulative tracer discharge of zero, reducing mean values. Boxes marking 25th through 75th percentiles are absent from Figure 37 where less than 25% of vectors are screened in. Discharge values equal to zero fall below the minimum discharge shown in the figure, as do the maximum discharges for scenarios 4 and 5 in the CRA26_IS. Both mean and maximum tracer releases through the borehole to the Culebra are decreased in the CRA26_IS compared to the RPPCR, consistent with reduced brine flow up the borehole.

Table 16 summarizes the number of screened-in vectors. Vectors screened in for scenarios 2-5 are automatically screened in for scenario 1. No vector was screened in based on tracer discharge in the scenario 1 simulation for either analysis.

Information Only

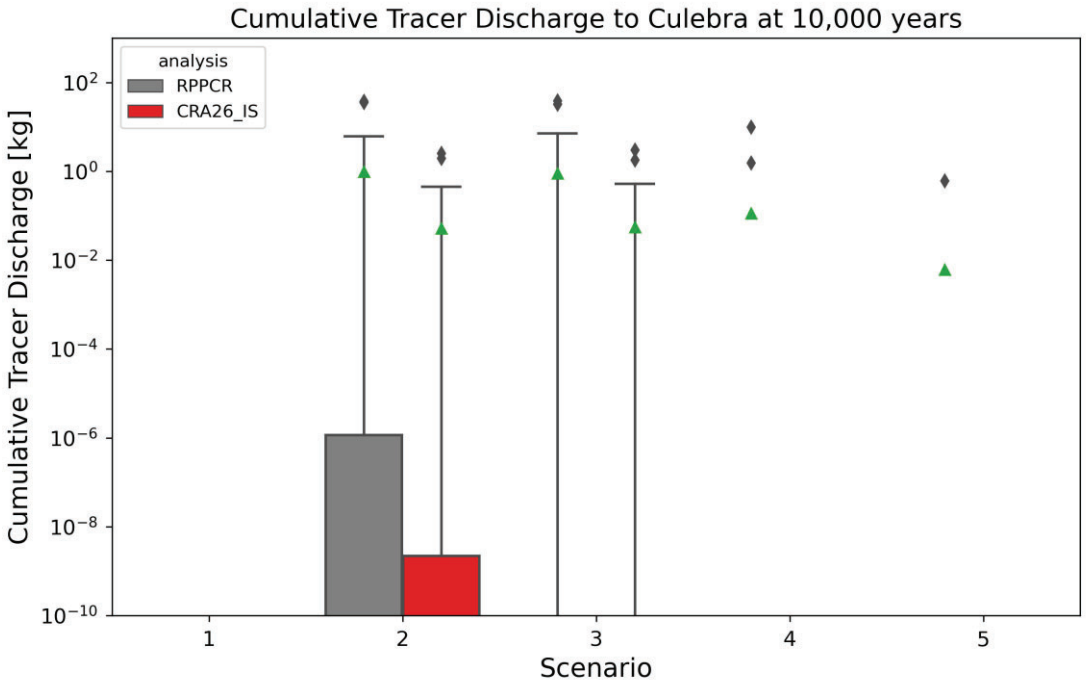


Figure 37. Cumulative tracer releases to the Culebra in kg at 10,000 years (Replicate 1)

Table 15. Mean, maximum and median cumulative tracer releases through a borehole to the Culebra at 10,000 years (Replicate 1)

Scenario	RPPCR Mean (kg)	CRA26_IS Mean (kg)	RPPCR Max (kg)	CRA26_IS Max (kg)	RPPCR Median (kg)	CRA26_IS Median (kg)
1	9.03E-113	5.29E-115	9.03E-111	5.29E-113	0.00E+00	0.00E+00
2	9.72E-01	5.12E-02	3.74E+01	2.52E+00	4.03E-25	3.81E-25
3	8.89E-01	5.48E-02	3.83E+01	2.97E+00	4.45E-38	2.57E-39
4	1.13E-01	8.46E-14	9.79E+00	6.58E-12	0.00E+00	0.00E+00
5	6.09E-03	9.21E-17	6.09E-01	9.21E-15	0.00E+00	0.00E+00

Information Only

Table 16. Number of screened-in vectors

Scenario	RPPCR R1	RPPCR R2	RPPCR R3	RPPCR Total	CRA26_IS R1	CRA26_IS R2	CRA26_IS R3	CRA26_IS Total
1	25	25	23	73	24	21	22	67
2	25	25	22	72	24	20	21	65
3	17	15	19	51	17	13	16	46
4	2	2	1	5	0	1	0	1
5	1	1	1	3	0	0	0	0

5.3.3 Radionuclide releases through the marker beds and up the shaft

Total cumulative releases through the marker beds to the LWB and total cumulative releases up the shaft to the Culebra are summed and plotted for scenarios 1-5 in Figure 38. The sum of cumulative releases along these pathways does not exceed 1×10^{-20} EPA units for any vector in either analysis, which is within the numerical noise of the simulation. Radionuclide discharge through the anhydrite marker beds to the LWB and up the shaft is essentially zero and is not covered further in this report.

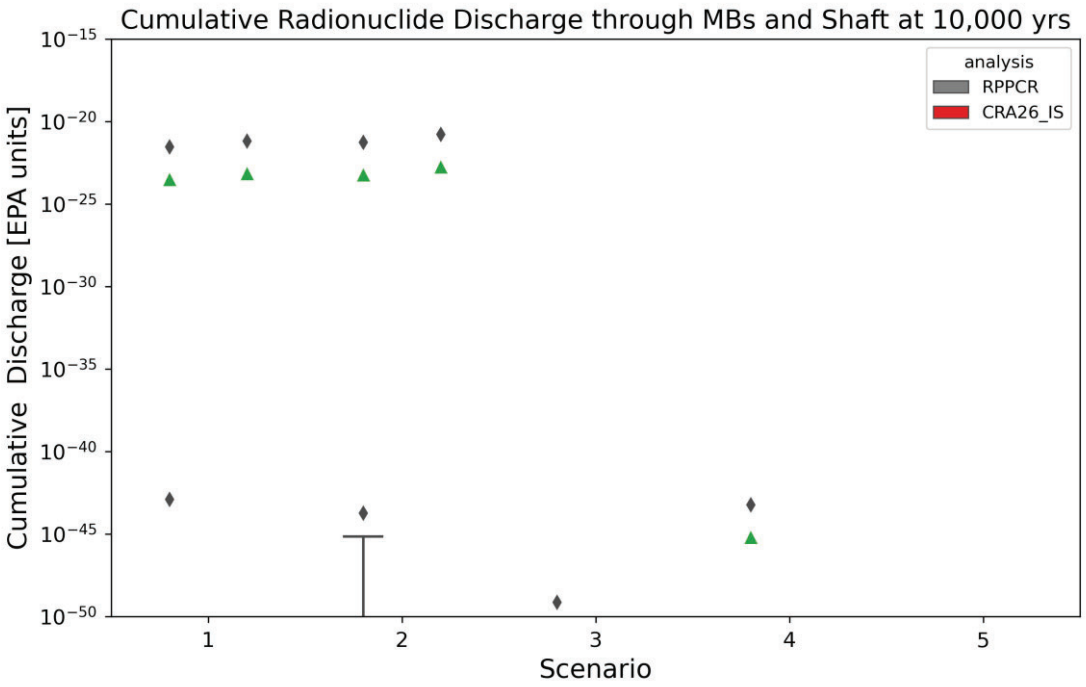


Figure 38. Total cumulative releases through marker beds and shaft at 10,000 years

Information Only

5.3.4 Radionuclide *to Culebra* releases

This section and the next focus on *to Culebra* releases for the BRAGFLO borehole intrusion scenarios. NUTS determines lumped radionuclide *to Culebra* releases for screened-in vectors in BRAGFLO scenarios 2-5. Releases for screened-out vectors are set to zero. PANEL determines individual radionuclide *to Culebra* releases for all vectors in BRAGFLO scenario 6. PANEL then combines the individual radionuclide releases to produce lumped radionuclide *to Culebra* releases. The figures and tables in this section are generated using data from NUTS ISO mode simulations and from PANEL's E2 intrusion at 1,000 years followed by an E1 at 2,000 years.

Figure 39 shows cumulative *to Culebra* releases at 10,000 years for scenarios 2-6, as well as total releases for each scenario – obtained by summing the accumulated releases of all five lumped radionuclides. Screened-out vectors have been included when making the box plots and affect the mean values shown. (Zero values corresponding to screened-out vectors fall below the minimum shown in the figures.) As noted above, boxes marking 25th through 75th percentiles are absent from the plots where less than 25% of vectors are screened in.

AM241L and PU239L are the dominant *to Culebra* releases in both analyses. For scenarios 2-5, the mean cumulative releases of all lumped radionuclides are decreased in the CRA26_IS compared to the RPPCR (Figure 39). In scenario 6, the mean cumulative releases of AM241L, PU238L, and total releases are increased in the CRA26_IS. Scenario 6 has the highest total releases in both analyses.

Decreased mean releases in scenarios 2 and 3 in the CRA26_IS – scenarios with screened-in vectors for Replicate 1 of both analyses – are attributed to reduced brine flow up the borehole (Figure 36). If brine flow up the borehole, $q'_{BF}(\mathbf{x}_C, t)$ in Eq. 21, is reduced then lumped radionuclide concentrations, $c^L_{k,j}(\mathbf{x}_C, t)$ in Eq. 21, may also be reduced if less waste is delivered to the Culebra. (Recall that $\mathbf{x}_C$ is the grid cell location where borehole and Culebra intersect.) Figure 40 shows distributions of $c^L_{k,j}(\mathbf{x}_C, t)$ for scenarios 2 and 3 in the two analyses, indicating reduced mean concentrations in the CRA26_IS. It is also worth noting that waste at the Culebra may be diluted by brine flowing down the borehole – an effect accounted for by NUTS when determining $c^L_{k,j}(\mathbf{x}_C, t)$. Figure 41 shows lumped radionuclide concentrations $c^L_{k,j}(\mathbf{x}_W, t)$, where $\mathbf{x}_W$ is the location where the borehole passes through the center of the waste panel. Mean lumped radionuclide concentrations in the waste are greater than at the Culebra. Figure 41 also shows that the mean concentrations of AM241L, PU239L, and PU238L at $\mathbf{x}_W$ increase in the CRA26_IS, consistent with greater inventory and increased concentration limits.

Increased mean releases of AM241L and PU238L in scenario 6 in the CRA26_IS are attributed to PANEL's simpler transport model (which treats the waste area as a whole), and to increases in inventory and concentration limits.

Mean cumulative releases are listed in Table 17 and maximum releases in Table 18 for the 100 vectors in Replicate 1. Comparing Table 17 with Table 4-10 of Kim (2023a), mean *to Culebra* releases in the RPPCR and the CRA26_IS are down by at least two orders of magnitude compared to the CRA-2019. (RPPCR statistics differ slightly because Kim's are determined from three replicates, rather than one for Table 17.)

Information Only

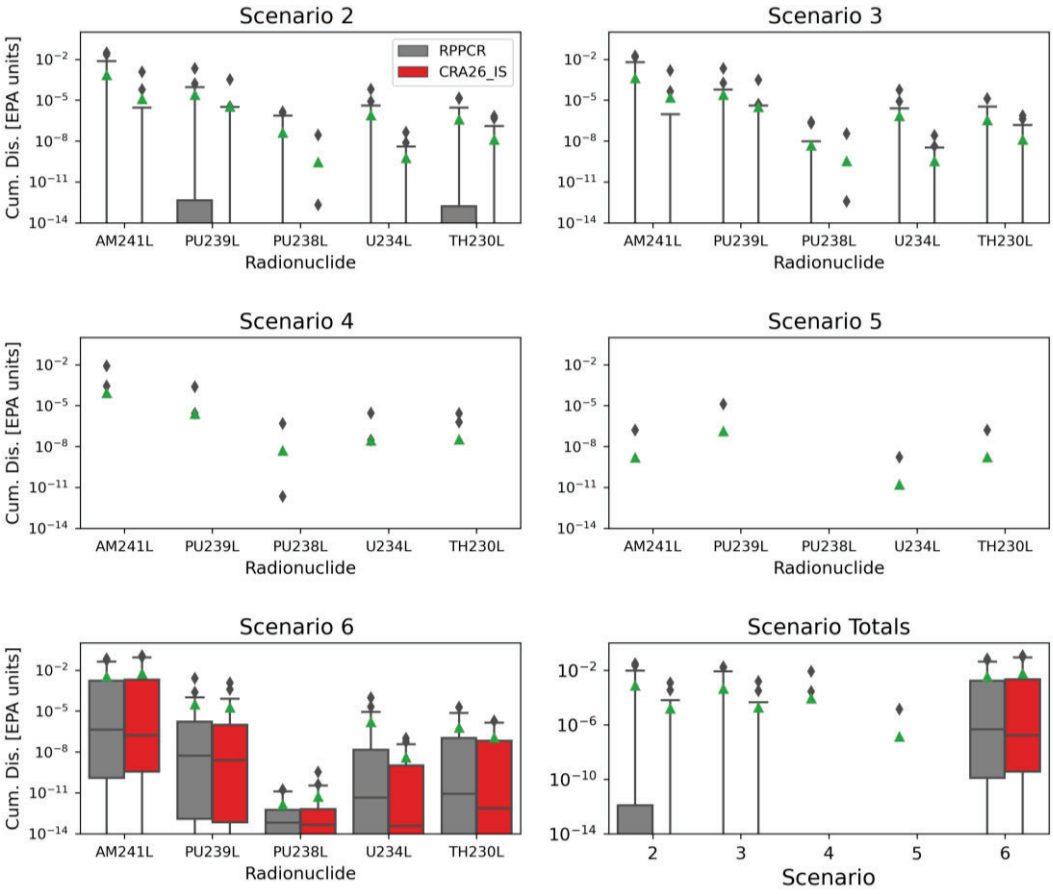


Figure 39. Cumulative lumped radionuclide discharge (Replicate 1)

Information Only

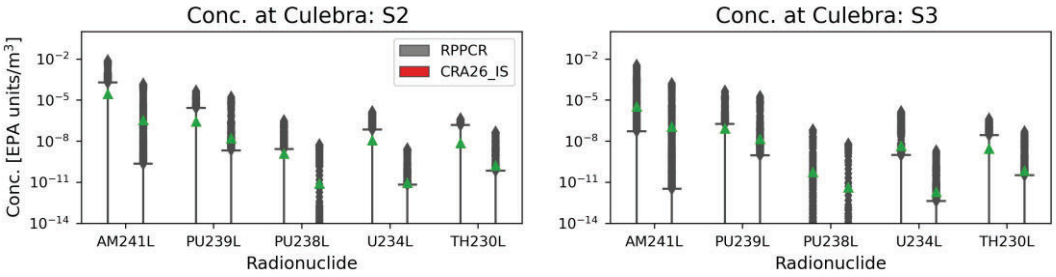


Figure 40. Lumped radionuclide concentrations at the Culebra (Replicate 1)

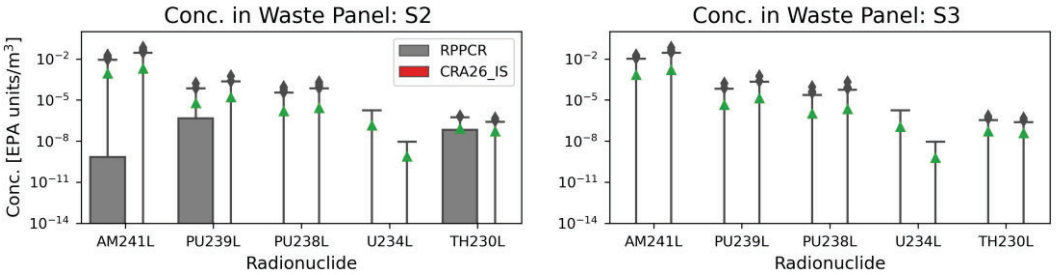


Figure 41. Lumped radionuclide concentrations in the waste (Replicate 1)

Table 17. Mean cumulative lumped radionuclides discharges through a borehole to the Culebra at 10,000 years (EPA units, Replicate 1)

Analysis	Scenario	AM241L	PU239L	PU238L	U234L	TH230L	TOTAL
RPPCR	2	6.99E-04	2.54E-05	4.12E-08	7.69E-07	3.85E-07	7.26E-04
RPPCR	3	4.08E-04	2.44E-05	4.77E-09	6.94E-07	3.50E-07	4.34E-04
RPPCR	4	8.43E-05	2.46E-06	4.90E-09	2.82E-08	3.22E-08	8.69E-05
RPPCR	5	1.58E-09	1.31E-07	2.05E-22	1.65E-11	1.64E-09	1.34E-07
RPPCR	6	3.40E-03	3.19E-05	1.39E-12	1.60E-06	6.23E-07	3.43E-03
CRA26_IS	2	1.23E-05	3.40E-06	2.83E-10	5.71E-10	1.26E-08	1.57E-05
CRA26_IS	3	1.51E-05	3.13E-06	3.46E-10	3.42E-10	1.30E-08	1.83E-05
CRA26_IS	4	0.00E+00	0.00E+00	0.00E+00	0.00E+00	0.00E+00	0.00E+00
CRA26_IS	5	0.00E+00	0.00E+00	0.00E+00	0.00E+00	0.00E+00	0.00E+00
CRA26_IS	6	5.89E-03	1.88E-05	5.34E-12	3.89E-09	1.14E-07	5.91E-03

Information Only

Table 18. Maximum cumulative lumped radionuclide discharges through a borehole to the Culebra at 10,000 years (EPA units, Replicate 1)

Analysis	Scenario	AM241L	PU239L	PU238L	U234L	TH230L	TOTAL
RPPCR	2	2.94E-02	2.09E-03	1.39E-06	6.13E-05	1.42E-05	2.94E-02
RPPCR	3	1.78E-02	2.14E-03	2.60E-07	5.65E-05	1.29E-05	1.79E-02
RPPCR	4	8.16E-03	2.44E-04	4.90E-07	2.79E-06	2.61E-06	8.41E-03
RPPCR	5	1.58E-07	1.31E-05	2.05E-20	1.65E-09	1.64E-07	1.34E-05
RPPCR	6	6.69E-02	2.55E-03	1.75E-11	9.41E-05	1.93E-05	6.70E-02
CRA26_IS	2	1.17E-03	3.32E-04	2.83E-08	4.46E-08	6.61E-07	1.17E-03
CRA26_IS	3	1.47E-03	3.03E-04	3.46E-08	2.61E-08	7.35E-07	1.48E-03
CRA26_IS	4	0.00E+00	0.00E+00	0.00E+00	0.00E+00	0.00E+00	0.00E+00
CRA26_IS	5	0.00E+00	0.00E+00	0.00E+00	0.00E+00	0.00E+00	0.00E+00
CRA26_IS	6	1.14E-01	1.18E-03	3.44E-10	9.90E-08	1.88E-06	1.14E-01

5.3.5 Radionuclide *to Culebra* release histories

The complete history of cumulative *to Culebra* releases for the five lumped radionuclides is plotted for scenarios 2-6 in Figure 42-Figure 46. The red lines in the figures are mean cumulative releases (histories for screened out vectors, which are zeroed, are included in the calculation of the means). For scenarios 4 and 5, only a few vectors in Replicate 1 in the RPPCR and none in the CRA26_IS are screened in (Table 16); hence the small number of histories shown for these scenarios. Figure 47 shows total releases for scenarios 2-6.

For most simulations, the majority of the discharge occurs in the first few hundred years after the borehole plug degrades (plug degradation occurs 200 years after the intrusion). For scenario 6, where an E2 intrusion at 1,000 years is followed by an E1 at 2,000 years, most of the discharges occur after the E1 intrusion. (Some scenario 6 simulations show small discharges occurring prior to the E2 intrusion. PANEL uses the brine discharge up the borehole at MB138 in its scenario 6 transport calculations. The pre-intrusion discharges could be related to brine movement caused by pressure differences between the repository, DRZ, and MB138.)

Information Only

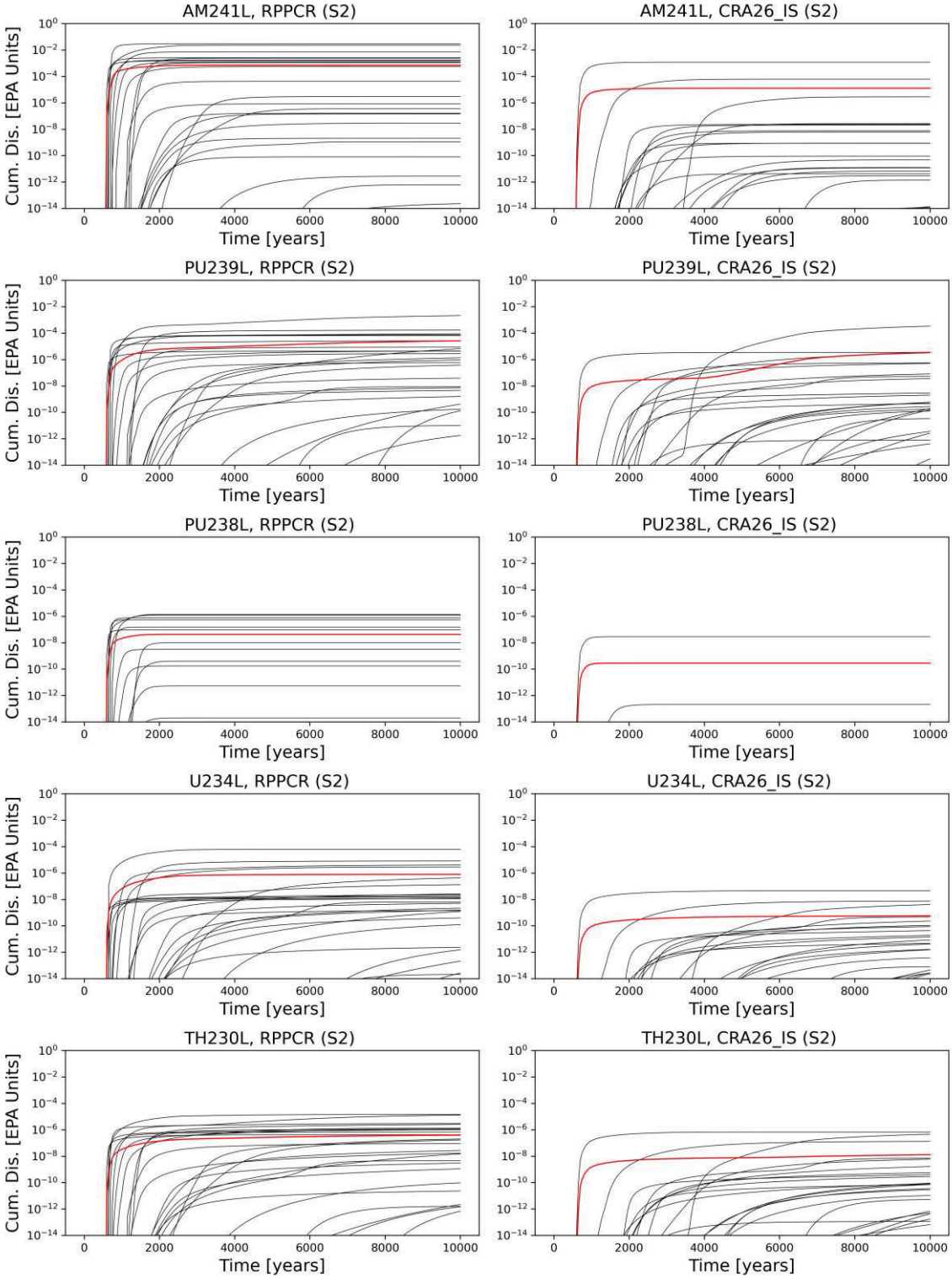


Figure 42. Cumulative radionuclide discharges for Replicate 1 of Scenario 2 vs time

Information Only

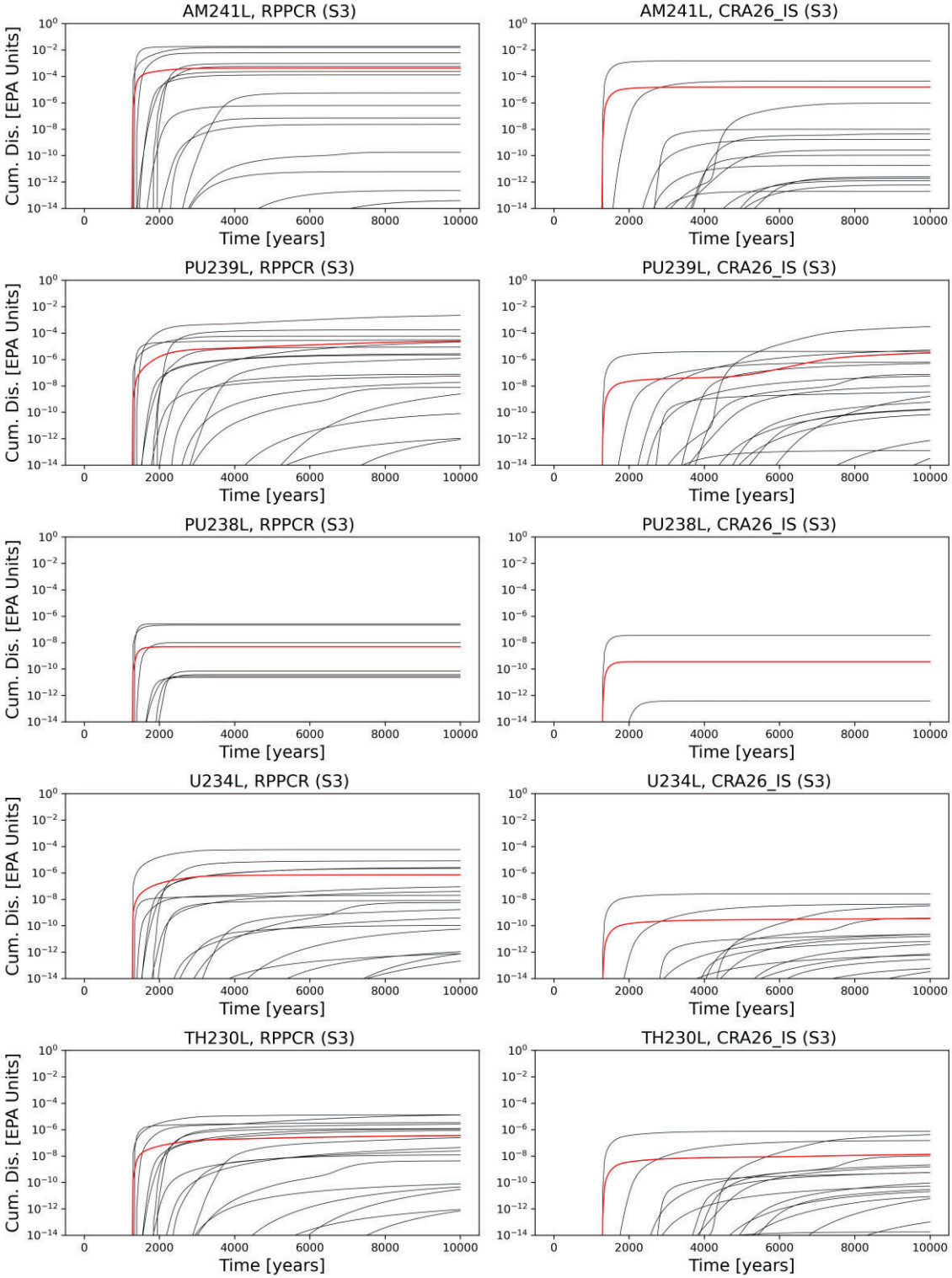


Figure 43. Cumulative radionuclide discharges for Replicate 1 of Scenario 3 vs time

Information Only

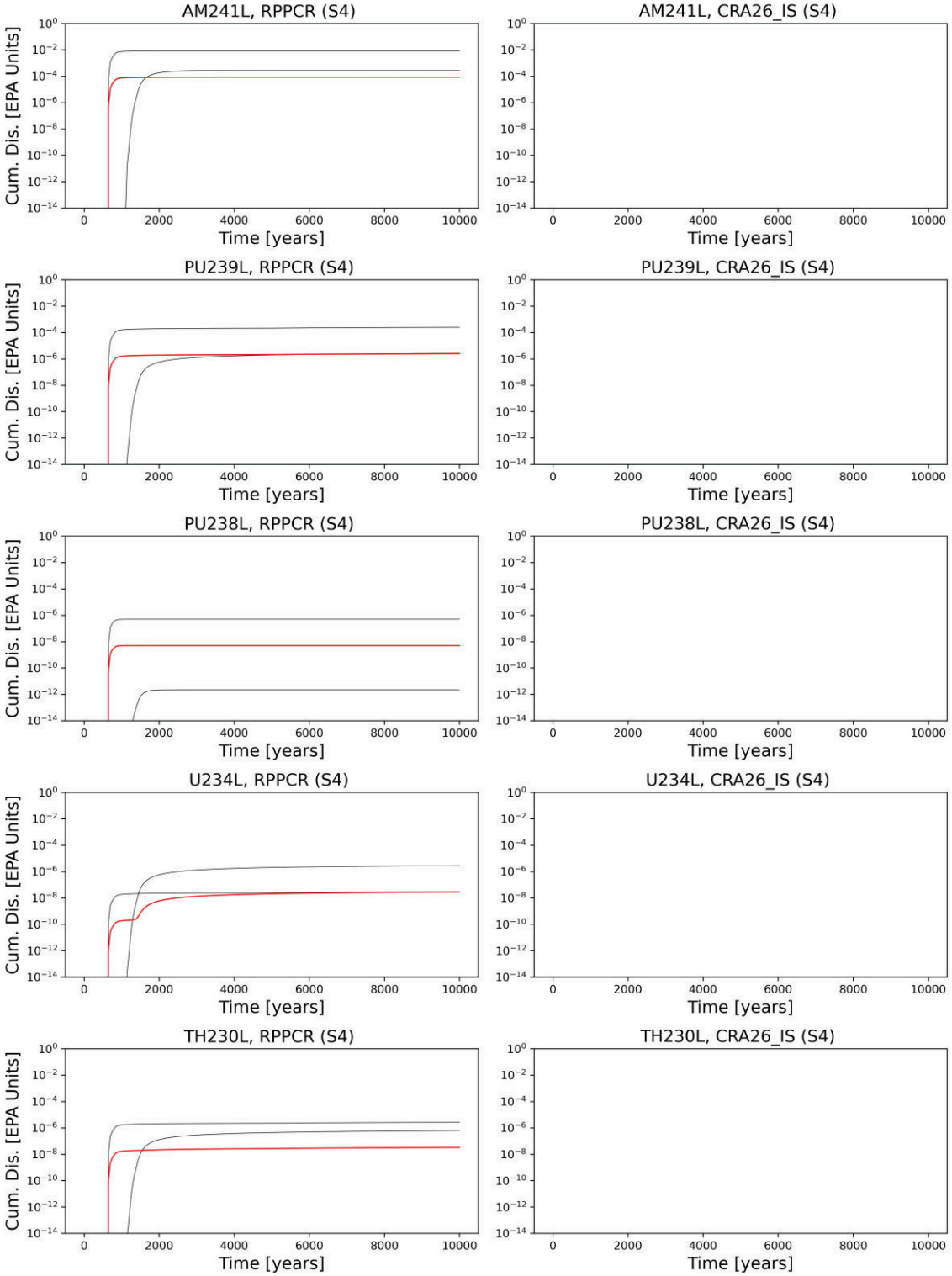


Figure 44. Cumulative radionuclide discharges for Replicate 1 of Scenario 4 vs time

Information Only

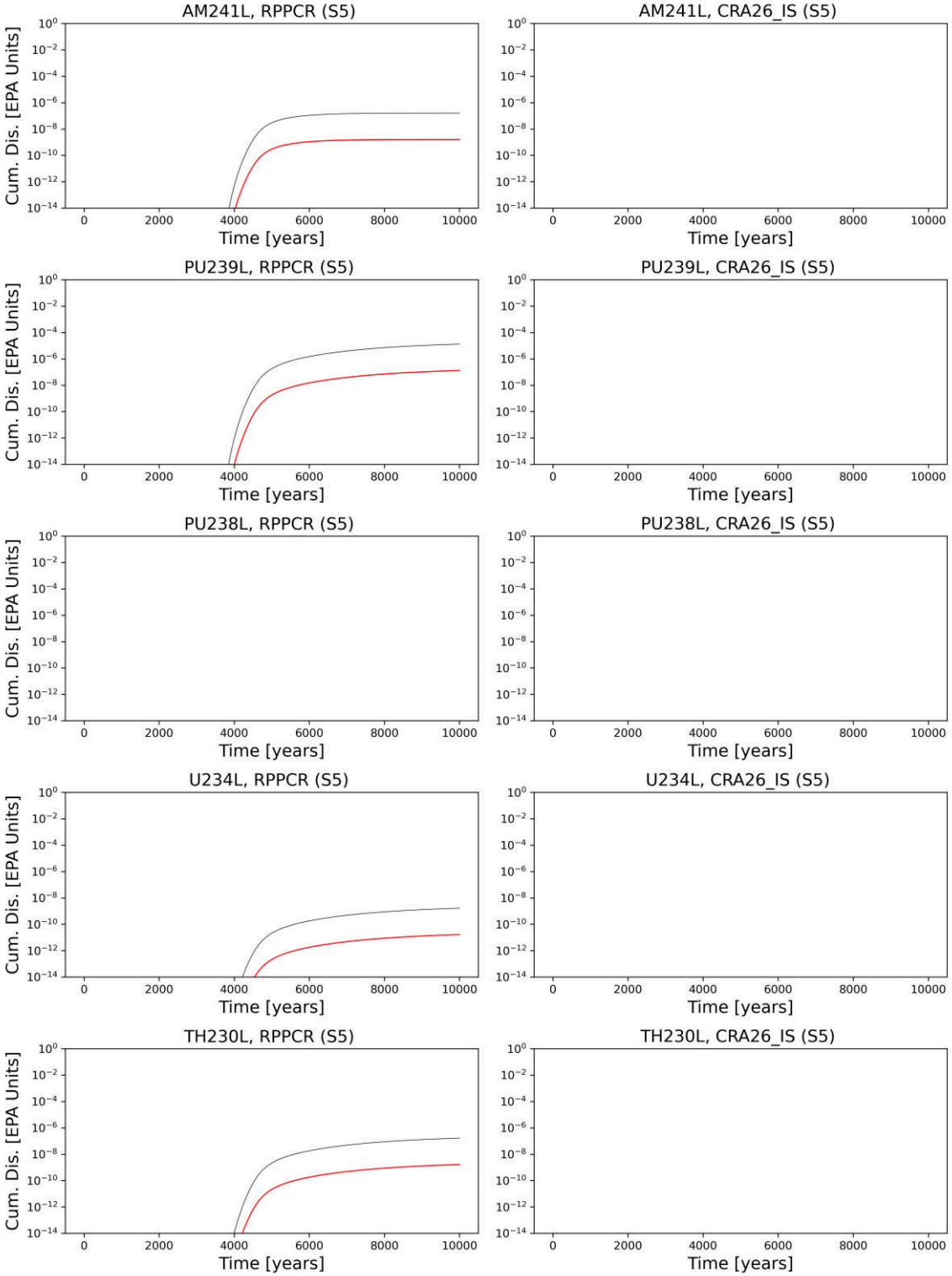


Figure 45. Cumulative radionuclide discharges for Replicate 1 of Scenario 5 vs time

Information Only

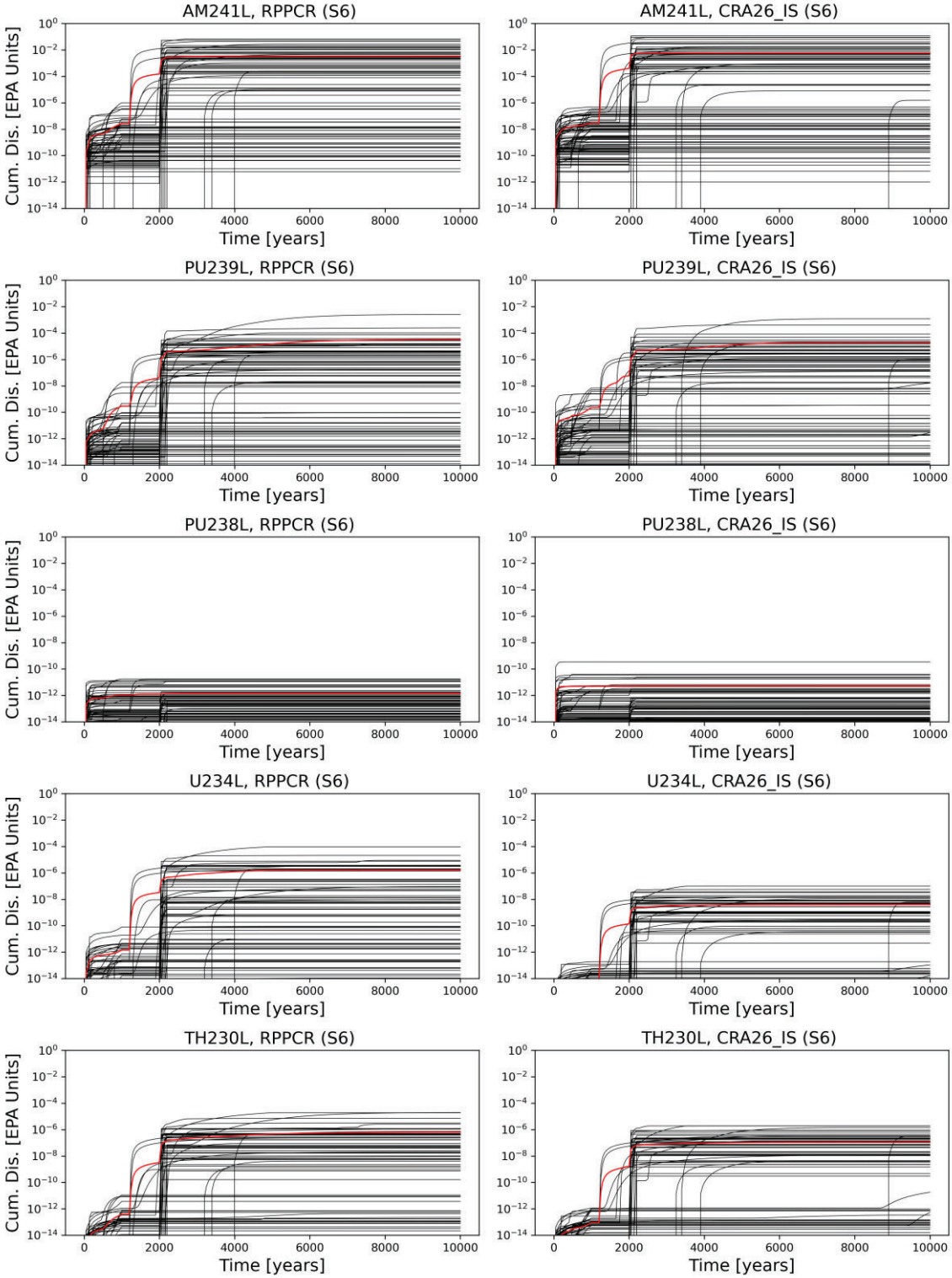


Figure 46. Cumulative radionuclide discharges for Replicate 1 of Scenario 6 vs time

Information Only

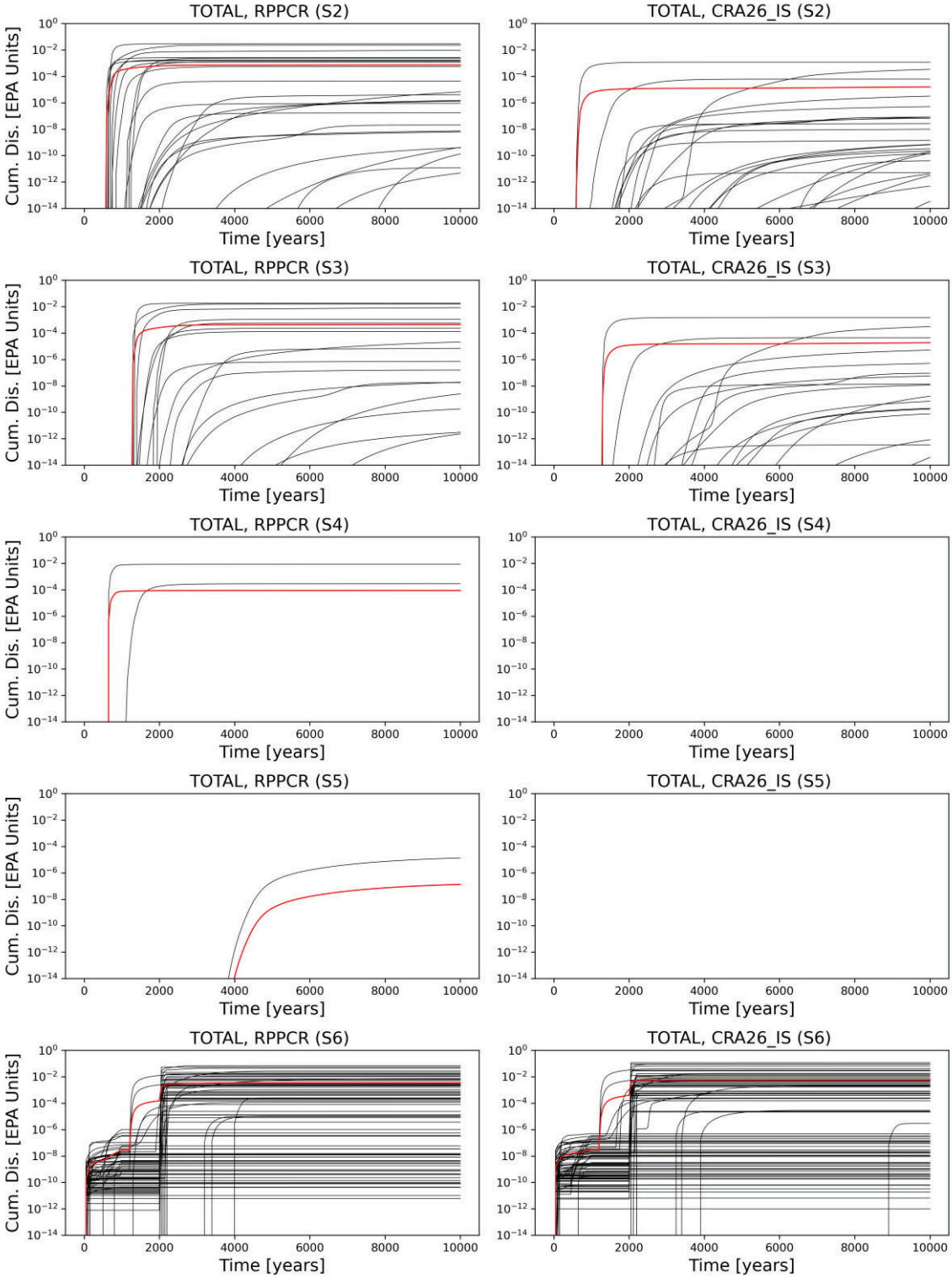


Figure 47. Total cumulative radionuclide discharges for Replicate 1 vs time

Information Only

6.0 SUMMARY

Changes are introduced for the CRA26_IS analysis that impact actinide mobilization and transport in the Salado Formation. Most notably: the repository is reduced in size from 19 panels to 12 panels; radionuclide inventory and WUF value are increased; and actinide solubility in the waste area is increased due to changes in baseline solubility, solubility uncertainty, and colloid enhancement parameters.

Concentrations for use in the determination of DBRs increase in the CRA26_IS when compared to RPPCR concentrations at equivalent brine volume multipliers. It should be noted however that the minimum brine volume in the repository for a DBR to occur is reduced significantly in the CRA26_IS. A consequence is that, for a given volume of brine in the waste area, DBR concentrations may be determined using different brine volume multipliers in the two analyses.

Mean releases to the Culebra in the CRA26_IS decrease for all lumped radionuclides in intrusion scenarios 2-5, compared to the RPPCR. For intrusion scenario 6, mean releases to the Culebra in the CRA26_IS increase for AM241L and PU238L, and decrease for PU239L, U234L, and TH230L, compared to the RPPCR. In both analyses, mean releases to the Culebra are down at least two orders of magnitude compared to the CRA-2019.

Information Only

7.0 REFERENCES

Bollinger, M. 2024. Letter to Ms. L. Veal. Subject: Planned Change Request for the use of Replacement Panels 11 and 12. March 12, 2024. CBFO:ERCD:MG:SV:24-0168. Carlsbad, NM: U.S. DOE, Carlsbad Field Office.

Brunell, S. 2025. Update to CRA-2026 PA Input Parameters Due to Revised WIPP Repository Dimensions. EIMS-0004799007. Carlsbad, NM: Sandia National Laboratories.

Brush, L.H., and J.W. Garner. 2005. Additional Justification of the Insignificant Effect of Np on the Long-Term Performance of the WIPP. Memorandum to D.S. Kessel, February 1, 2005. Sandia National Laboratories, Carlsbad, NM. ERMS 538533.

Day, B. 2025. BRAGFLO Grid Development for CRA-2026. EIMS-0004447000. Carlsbad, NM: Sandia National Laboratories.

Domski, P.S. 2023a. An Update to the WIPP EQ3/6 Database DATA0.FM1 with the Creation of DATA0.FM6. Sandia National Laboratories, Carlsbad, NM. ERMS 579370.

Domski, P.S. 2023b. Prediction of Baseline Actinide Solubilities for the Replacement Panels Planned Change Request (RPPCR) Performance Assessment. Sandia National Laboratories, Carlsbad, NM. ERMS 579503.

Domski, P. 2025a. Prediction of Baseline Actinide Solubilities for the 2026 WIPP Compliance Recertification Application Performance Assessment Interim-State Analysis (CRA-2026 IS). EIMS-0004838025. Carlsbad, NM: Sandia National Laboratories.

Domski, P. 2025b. Parameter Memorandum: Uncertainty Analysis of Actinide Solubilities for the 2026 Compliance Recertification Application (CRA-2026). EIMS-0004447122. Carlsbad, NM: Sandia National Laboratories.

Fox, B., D. Clayton, and T.B. Kirchner. 2009. Radionuclide Inventory Screening Analysis Report for the PABC-2009 (Revision 0). Sandia National Laboratories, Carlsbad, NM. ERMS 551679.

Hansen, C., S. Brunell, B. Day, S. King, and J. Wilgus. 2025. Analysis Plan for the 2026 WIPP Compliance Recertification Application Performance Assessment. AP-214. Carlsbad, NM: Sandia National Laboratories.

Helton, J.C., J.E. Bean, J.W. Berglund, F.J. Davis, K. Economy, J.W. Garner, J.D. Johnson, R.J. MacKinnon, J. Miller, D.G. O'Brien, J.L. Ramsey, J.D. Schreiber, A. Shinta, L.N. Smith, D.M. Stoelzel, C. Stockman, and P. Vaughn. 1998. Uncertainty and Sensitivity Analysis Results Obtained in the 1996 Performance Assessment for the Waste Isolation Pilot Plant. Albuquerque, NM: Sandia National Laboratories. SAND98-0365.

Kaplan, U., Swanson, J., and Kutahyali-Aslani, C. 2025. LANL ACRSP Parameter Recommendations for CRA-2026 Performance Assessment. Revision 1. LCO-ACP-41. Carlsbad, NM: Los Alamos National Laboratory.

Information Only

Kicker, D.C. 2025. Analysis Report for Radionuclide Inventory Screening in the 2026 Compliance Recertification Application Performance Assessment: Interim State Repository, Revision 0. Carlsbad, NM: Sandia National Laboratories.

Kicker, D. and T. Zeitler. 2013. Radionuclide Inventory Screening Analysis for the 2014 Compliance Recertification Application Performance Assessment (CRA-2014 PA). Sandia National Laboratories, Carlsbad, NM. ERMS 559257.

Kim, S. 2013. Analysis Package for Salado Transport Calculations: CRA-2014 Performance Assessment. Sandia National Laboratories, Carlsbad, NM. ERMS 560174.

Kim, S. 2022a. Design Document and User's Manual for PANEL Version 5.02. Sandia National Laboratories, Carlsbad, NM. ERMS 577751.

Kim, S. 2022b. Design Document and User's Manual for NUTS Version 2.08. Sandia National Laboratories, Carlsbad, NM. ERMS 573824.

Kim, S. 2023a. Analysis Report for Actinide Mobilization and Salado Transport in the Replacement Panels Planned Change Request (RPPCR). Carlsbad, NM: Sandia National Laboratories ERMS 57926.

Kim, S. 2023b. Software Problem Report for PANEL Version 5.02. Sandia National Laboratories, Carlsbad, NM. SPR 23-002.

Kim, S. 2024. Addendum to Design Document for PANEL Version 5.03. Sandia National Laboratories, Carlsbad, NM. ERMS 581391.

Kim, S., P. Docherty, D. Kicker, and S. King, 2024. Investigation of Radionuclide Screening on Total Curies versus Potentially Mobilized Curies. Sandia National Laboratories, Carlsbad, NM. Milestone TSPA-24-06. ERMS 581503.

King, S. 2025. Area for RH waste disposal for the interim state CRA-2026 PA calculation. EIMS-0004801801. Carlsbad, NM: Sandia National Laboratories.

Knerr, R. 2020. Letter to Ms. Lee Ann B. Veal, U.S. Environmental Protection Agency, subject: "Planned Change Request for Alternative Panel Closure Locations for Panels 1 and 2," Carlsbad, NM: U.S. DOE, Carlsbad Field Office.

Leigh, C., and J. Trone. 2005. Calculation of Radionuclide Inventories for Use in NUTS in the Performance Assessment Baseline Calculation Revision 0. ERMS 539644. Sandia National Laboratories. Carlsbad, NM.

Mariner P. 2025. CRA-2026 IS updates to the WIPP humic colloids models for An(III) and An(IV). EIMS-0004838142. Carlsbad, NM: Sandia National Laboratories.

Popielak, R. S., R. L. Beauheim, S. R. Black, W. E. Coons, C. T. Ellingson, and R. L. Olsen. 1983. Brine reservoirs in the Castile formation, Waste Isolation Pilot Plant, Southeastern New Mexico. U. S. Department of Energy, Carlsbad, NM. TME 3153.

Reed, D.T., J.S. Swanson, J.F. Lucchini, and M.K. Richmann. 2013. Intrinsic, Mineral, and Microbial Colloid Enhancement Parameters for the WIPP Actinide Source Term. Los Alamos National Laboratory; Carlsbad, NM. LCO-ACP-18, LA-UR-13-20858.

Information Only

Sarathi, R.S. 2019. Analysis Package for Actinide Mobilization and Salado Transport in the 2019 Compliance Recertification Application Performance Assessment (CRA-2019 PA). Sandia National Laboratories, Carlsbad, NM. ERMS 571371.

Shinta, A. A. 1997. User's Manual for NUTS, Version 2.05. Sandia National Laboratories, Albuquerque, NM. ERMS 246002.

Stockman, C., A. Shinta, and J. Garner. 1996. Analysis Package for the Salado Transport Calculations (Task 2) of the Performance Assessment Analysis Supporting the Compliance Certification Application. Sandia National Laboratories, Albuquerque, NM. ERMS 422314.

U.S. Department of Energy (U.S. DOE). 1996. Title 40 CFR Part 191 Compliance Certification Application for the Waste Isolation Pilot Plant (October). Carlsbad, NM: Carlsbad Area Office. DOE/CAO-1996-2184.

U.S. DOE. 2019. Title 40 CFR Part 191 Compliance Recertification Application for the Waste Isolation Pilot Plant. DOE/WIPP-19-3609. U.S. Department of Energy, Waste Isolation Pilot Plant, Carlsbad, NM: Carlsbad Field Office.

U.S. DOE. 2024. Annual Transuranic Waste Inventory Report – 2024. DOE/TRU-24-3425.0. Carlsbad, NM: U.S. DOE, Carlsbad Field Office.

U.S. Environmental Protection Agency (U.S. EPA). 1998. 40 CFR Part 194: Criteria for the Certification and Recertification of the Waste Isolation Pilot Plant's Compliance with the Disposal Regulations: Certification Decision. Federal Register, vol. 63 (May 18, 1998): 27354 – 27406.

U.S. EPA. 2006. "Technical Support Document for Section 194.24: Evaluation of the Compliance Recertification – Actinide Source Term and Culebra Dolomite Distribution Coefficient Values." EPA Air Docket A 98-49, Item II B1-3. Washington, DC: U.S. Environmental Protection Agency Office of Air and Radiation.

Van Soest, G. 2025. Interim State Performance Assessment Inventory Report-2024. Revision 0. INV-IPA-24. Carlsbad, NM: Los Alamos National Laboratory.

Ward, A. 2025. Performance Assessment Inventory for Analysis of a 12-Panel Repository Configuration. Letter to Bill McInroy. March 18, 2025. CBFO:ERCD:AW:RS:25-0197. Carlsbad, NM: Department of Energy Carlsbad Field Office.

Information Only

Sandia National Laboratories is a multimission laboratory managed and operated by National Technology & Engineering Solutions of Sandia, LLC, a wholly owned subsidiary of Honeywell International Inc., for the U.S. Department of Energy's National Nuclear Security Administration under contract DE-NA0003525. This research is funded by WIPP programs administered by the Office of Environmental Management (EM) of the U.S. Department of Energy.







Information Only